

# Development of press forming techniques for thermoplastic composites

Investigation of a multiple step forming approach

Francisco Saraiva

MSc Thesis in Aerospace Engineering  
Structural Integrity & Composites





# Development of press forming techniques for thermoplastic composites

Investigation of a multiple step forming approach

by

Francisco Saraiva

to obtain the degree of Master of Science  
at the Delft University of Technology,  
to be defended publicly on Friday March 17, 2017 at 01:30 PM.

Student number: 4413725  
Thesis committee: Ir. J. Sinke, TU Delft, Supervisor  
Dr. ir. R. C. Alderliesten, TU Delft, Chairman  
Dr. ir. O. K. Bergsma, TU Delft  
Dr. ir. J. M. J. F. van Campen, TU Delft

An electronic version of this thesis is available at <http://repository.tudelft.nl/>.



# Summary

Thermoplastic composites are very attractive for aerospace structures due to their high specific strength and stiffness, enhanced toughness and high temperature resistance. One of the manufacturing methods used to produce thermoplastic composite parts is press forming. Press formed parts typically have constant thickness and fibre orientation. However, composite parts may be optimized by tailoring the stiffness and strength, thereby reducing structural weight. In this thesis, the processing techniques for this manufacturing method were developed by investigating the feasibility of a multiple step forming approach for the production of parts with variable thickness and fibre orientation. This manufacturing approach was proven from both a formability and structural integrity viewpoints. By using an efficient blankholder system with clamps and springs, thermoplastic composite laminates can be multiple step formed into three-dimensional shapes with no occurrence of visual forming defects such as wrinkling, fibre buckling or ply folding. Furthermore, good quality bonds can be achieved between laminates formed and co-consolidated in different steps. To achieve a high degree of bonding between GF/PEI composite laminates, the co-consolidation process window was estimated to be between 270°C and 300°C. The use of a post-consolidation stage in a hot press was needed to improve the degree of bonding between co-consolidated laminates formed in different steps, which led to very long production cycle times. For future research, the maximum temperature limit of the metal mould should be increased and tooling active cooling mechanisms must be incorporated to allow the mould to be rapidly cooled down, thereby decreasing production cycle times. With these implementations, a better insight on the feasibility of the process in an industrial environment may be gained.



# Contents

List of Figures	vii
List of Tables	xi
List of Acronyms	xiii
List of Symbols	xv
<b>1 Introduction</b>	<b>1</b>
1.1 Research Questions	4
1.2 Thesis Outline	4
<b>2 Literature Review</b>	<b>5</b>
2.1 Deformation Mechanisms	6
2.1.1 <i>Intra-ply shear</i>	6
2.1.2 <i>Fibre straightening</i>	7
2.1.3 <i>Inter-ply slippage</i>	7
2.1.4 <i>Tool-ply slippage</i>	8
2.1.5 <i>Resin percolation</i>	9
2.1.6 <i>Transverse squeeze flow</i>	9
2.2 Process variants	9
2.2.1 <i>Matched die forming</i>	9
2.2.2 <i>Rubber forming</i>	10
2.2.3 <i>Diaphragm forming</i>	11
2.3 Formability of thermoplastic composites	12
2.4 Process induced deformations	13
2.5 Effects of stamping in material mechanical and physical properties	14
2.6 Discussion	15
<b>3 Design of the Experimental Setup</b>	<b>17</b>
3.1 Experimental setup assemblies	18
3.1.1 <i>Rig</i>	18
3.1.2 <i>Blankholder</i>	19
3.1.3 <i>Press assembly</i>	20
3.2 Design choices and considerations of the press assembly	21
3.2.1 <i>Extension cylinder</i>	22
3.2.2 <i>Top mounting plate</i>	22
3.2.3 <i>Rubber mould and rubber mould box</i>	22
3.2.4 <i>Metal mould</i>	25
3.2.5 <i>Constraining blocks</i>	25
3.2.6 <i>Bottom mounting plate</i>	26
3.2.7 <i>Heating plate</i>	27
3.3 Overview of the press assembly	31
<b>4 Multiple Step Forming of GF/PEI Woven Composite Laminates</b>	<b>33</b>
4.1 Experimental Procedure	34
4.1.1 <i>Materials and blank preparation</i>	34
4.1.2 <i>Press Forming</i>	35
4.1.3 <i>Temperature measurements</i>	37
4.1.4 <i>Microscopy</i>	37

4.2	Results and Discussion . . . . .	38
4.2.1	Temperature curves . . . . .	38
4.2.2	Forming behaviour . . . . .	43
4.2.3	Demonstrator . . . . .	48
4.2.4	Microscopy. . . . .	49
4.3	Summary . . . . .	50
<b>5</b>	<b>Mode I Interlaminar Fracture Toughness of Co-Consolidated GF/PEI Composites</b>	<b>51</b>
5.1	Experimental Procedure . . . . .	53
5.1.1	Preconsolidated laminates . . . . .	53
5.1.2	Co-consolidated laminates . . . . .	54
5.1.3	Specimen preparation . . . . .	55
5.1.4	Microscopy. . . . .	56
5.2	Methodology . . . . .	57
5.2.1	Orthogonal array experiment. . . . .	57
5.2.2	Double Cantilever Beam tests . . . . .	58
5.2.3	Statistical analysis . . . . .	60
5.3	Results and Discussion. . . . .	62
5.3.1	DCB test results . . . . .	62
5.3.2	ANOM results . . . . .	65
5.3.3	ANOVA results . . . . .	66
5.3.4	Interaction plots . . . . .	66
5.4	Summary . . . . .	69
<b>6</b>	<b>Multiple step forming and post-consolidation of GF/PEI composite laminates</b>	<b>71</b>
6.1	Experimental Procedure . . . . .	72
6.1.1	Materials and blank preparation . . . . .	72
6.1.2	Multiple step forming process. . . . .	72
6.1.3	Post-consolidation process . . . . .	73
6.1.4	Specimen preparation . . . . .	75
6.2	Results and Discussion. . . . .	76
6.2.1	DCB test results . . . . .	76
6.2.2	Qualitative analysis of post-consolidated formed shape. . . . .	77
6.3	Summary . . . . .	78
<b>7</b>	<b>Conclusions and Recommendations</b>	<b>79</b>
<b>A</b>	<b>Designing an orthogonal array experiment</b>	<b>83</b>
<b>B</b>	<b>Statistical methods - Analysis of Means and Analysis of Variance</b>	<b>85</b>
B.1	Analysis of means (ANOM) . . . . .	85
B.2	Analysis of variance (ANOVA) . . . . .	86
<b>C</b>	<b>Double Cantilever Beam Test Data and Load-Displacement Curves</b>	<b>89</b>
C.1	Preconsolidated Specimens . . . . .	89
C.2	Co-consolidated Specimens Run 1. . . . .	91
C.3	Co-consolidated Specimens Run 2. . . . .	93
C.4	Co-Consolidated Specimens Run 3 . . . . .	94
C.5	Co-Consolidated Specimens Run 4 . . . . .	95
C.6	Co-Consolidated Specimens Run 5 . . . . .	96
C.7	Co-Consolidated Specimens Run 6 . . . . .	97
C.8	Co-Consolidated Specimens Run 7 . . . . .	98
C.9	Co-Consolidated Specimens Run 8 . . . . .	100
C.10	Co-Consolidated Specimens Run 9 . . . . .	101
C.11	Post-consolidated specimens from multiple step formed shape . . . . .	102
C.12	Preconsolidated specimens from new material . . . . .	103
	<b>Bibliography</b>	<b>105</b>

# List of Figures

1.1	Boeing 787 material structural weight distribution [1]	1
1.2	Comparison of thermoset and thermoplastic polymer structures [3]	2
1.3	Tandem press line configuration [8]	3
1.4	Multiple step forming approach for the manufacturing of a variable thickness part	3
2.1	Stages of the press forming process [11]	5
2.2	Intra-ply shear in fabric layer [12]	6
2.3	Intra-ply shear in UD plies [9]	7
2.4	Process window of 90° bends [23]	10
2.5	Schematic explanation of the balance between the apparent intra-ply (IR), frictional (FR), and bending (BR) rigidity of the plies [35]	12
3.1	Overview of experimental setup	18
3.2	(a) Rig with integrated IR-panels, ventilation system, moving frame, (b) rail and glass plates used to protect IR-lamps	19
3.3	(a) Blankholder holding the laminate through springs and crocodile clamps and (b) loaded into the moving frame of the rig	20
3.4	Overview of the press assembly	20
3.5	Exploded view of the press assembly (obs: rubber mould not depicted)	21
3.6	Top mounting plate	22
3.7	Rubber mould and the existing gaps with respect to the metal mould	23
3.8	Material rupture upon forming with high clamping pressures [20]	24
3.9	Schematic representation of mould closing sequence	24
3.10	Laminate deformations [34]	24
3.11	Metal mould	25
3.12	Constraining block preventing metal mould from being released from mounting plate	26
3.13	Metal mould constrained by blocks and rubber pads	26
3.14	(a) Schematic and (b) real representation of metal strips acting as stoppers	26
3.15	Guiding Pins	27
3.16	Insulating block around metal mould	27
3.17	Heating plate with five heating elements	28
3.18	Heating plate cavities to insert thermal switches	29
3.19	Schematic representation of electrical circuit integrated in the heating plate	29
3.20	Technical representation of electrical circuit integrated in the heating plate	29
3.21	Power controller	30
3.22	Overview of press assembly	31
3.23	Guiding pins fixed to the top mounting plate and M12 bolts used to fix the bottom press assembly to the press	32
4.1	Layup schematic representation	34
4.2	Consolidation temperature and pressure profiles of GF/PEI laminate	34
4.3	Blank cutting layout	35
4.4	Press forming stages and indication of laminate and moulds' temperatures	36
4.5	Thermocouples instrumented at the bottom surface of the metal mould and at the center of the laminate to be formed in the first step	37
4.6	Data acquisition system and thermocouple instrumented on the side wall of the rubber mould	37
4.7	Experimental run n°1 & Forming step n°1 - Laminate and moulds' temperature curves	38
4.8	Heat sources during the consolidation stage of a press forming process	39

4.9	Experimental run n°2 & Forming step n°1 - Laminate and moulds' temperature curves .	40
4.10	Experimental run n°3 & Forming step n°1 - Laminate and moulds' temperature curves .	41
4.11	Experimental run n°3 & Forming step n°2 - Interface and moulds' temperature curves .	41
4.12	Experimental run n°4 & Forming step n°1 - Laminate and moulds' temperature curves .	42
4.13	Experimental run n°4 & Forming step n°2 - Interface and moulds' temperature curves .	42
4.14	Blank springback and release from the mould in experimental runs 1 and 2 . . . . .	44
4.15	Blanks formed in 1 <sup>st</sup> forming step on runs 3 and 4 . . . . .	44
4.16	Larger corner radii at the two edges of the formed shape . . . . .	45
4.17	Constraint of rubber mould's sides in order to reduce non-uniform pressure distributions . . . . .	45
4.18	Multiple step formed shape with 2 <sup>nd</sup> blank co-consolidated to 1 <sup>st</sup> blank . . . . .	46
4.19	Forming scenario A, where blank doesn't make contact with metal mould's surface during forming . . . . .	46
4.20	Forming scenario B, where blank makes contact with metal mould's surface during the entire forming process . . . . .	46
4.21	Run 3 - Multiple step formed shape with (a) no visual forming defects, but (b) with very weak bond . . . . .	47
4.22	Demonstrator part after (a) 1 <sup>st</sup> and (b) 2 <sup>nd</sup> forming steps, showing accurate dimensional control and alignment with respect to the mould . . . . .	48
4.23	Demonstrator part manufactured via three forming steps . . . . .	48
4.24	Cross-sections of co-consolidated flanges in runs (a) 3 and (b) 4 (10x magnification), showing no evidence of an interface between co-consolidated laminates . . . . .	49
5.1	Three modes of loading a delamination: (a) opening, (b) shearing and (c) tearing [60] . .	51
5.2	Longitudinal tensile failure in SBS test specimen . . . . .	52
5.3	Layup of 14-ply laminate with Kapton film inserted at the midplane . . . . .	53
5.4	Temperature and pressure profiles of GF/PEI preconsolidated specimens . . . . .	53
5.5	Production sequence of 14-ply co-consolidated plates with (a) lay up and consolidation of 7-ply laminate, (b) stacking of two 7-ply preconsolidated laminates with (c) a Kapton insert at the interface . . . . .	54
5.6	Co-consolidation run 3 - Programmed temperature and pressure profiles . . . . .	55
5.7	Co-consolidation run 3 - Measured temperature . . . . .	55
5.8	Specimen cutting layout . . . . .	55
5.9	Excess adhesive after post-curing . . . . .	56
5.10	DCB specimen configuration . . . . .	56
5.11	(a) DCB test load-displacement curve and (b) delamination resistance curve showing higher $G_{IC}$ propagation values than initiation values . . . . .	58
5.12	Area under load-displacement curve of DCB tested specimen . . . . .	59
5.13	(a) Schematic and real (b) representations of the variable $t$ . . . . .	60
5.14	DCB test results of preconsolidated and co-consolidated laminates . . . . .	62
5.15	Thickness results for preconsolidated and co-consolidated laminates . . . . .	63
5.16	Microscopy cross-sections of 14-ply preconsolidated laminate at 320°C with large areas of fibre-fibre contact at the midplane interface (2.5x magnification) . . . . .	64
5.17	Microscopy cross-sections of 14-ply co-consolidated laminate at 270°C with small areas of fibre-fibre contact at the midplane interface (2.5x magnification) . . . . .	64
5.18	Microscopy cross-sections of 14-ply co-consolidated laminate at 300°C with large areas of fibre-fibre contact at the midplane interface (2.5x magnification), but possibly lower than preconsolidated laminates' . . . . .	64
5.19	$G_{IC}$ VIS vs Time, Temperature and Pressure scatter plots . . . . .	65
5.20	Main effects plots for $G_{IC}$ VIS output . . . . .	65
5.21	Interaction plots for $G_{IC}$ VIS output . . . . .	67
5.22	Main effects plots for thickness output . . . . .	68
6.1	Multiple step forming process followed by a post-consolidation step . . . . .	71
6.2	Blank cutting layout . . . . .	72

---

6.3	Kapton films placed on the sidewalls of the laminate formed in the first step in order to create a crack and enable the production of specimens for DCB testing . . . . .	73
6.4	(a) Formed shape placed and fixed on the metal mould and then (b) submitted to a post-consolidation process by closing the moulds and applying temperature and pressure . . . . .	74
6.5	Post-consolidation process - Programmed temperature, pressure and time profiles . . . . .	74
6.6	Measured temperature curves during the post-consolidation process . . . . .	75
6.7	Specimen cutting layout from post-consolidated formed shape . . . . .	75
6.8	DCB test results of preconsolidated and post-consolidated laminates . . . . .	76
6.9	Thickness of preconsolidated and press formed post-consolidated laminates . . . . .	77
6.10	Formed shape (a) before and (b) after performing a post-consolidation process . . . . .	77
7.1	Potential multiple step forming production cycle, with short consolidation times in each forming step, and a final consolidation step with cooling under pressure . . . . .	80
7.2	Mould concept with two materials connected through springs or pneumatic pistons, allowing fast cooling and heating rates . . . . .	81
C.1	Load-displacement curves of preconsolidated specimens . . . . .	90
C.2	Load-displacement curves of co-consolidated specimens run 1 . . . . .	92
C.3	Load-displacement curves of co-consolidated specimens run 2 . . . . .	93
C.4	Load-displacement curves of co-consolidated specimens run 3 . . . . .	94
C.5	Load-displacement curves of co-consolidated specimens run 4 . . . . .	95
C.6	Load-displacement curves of co-consolidated specimens run 5 . . . . .	96
C.7	Load-displacement curves of co-consolidated specimens run 6 . . . . .	97
C.8	Load-displacement curves of co-consolidated specimens run 7 . . . . .	99
C.9	Load-displacement curves of co-consolidated specimens run 8 . . . . .	100
C.10	Load-displacement curves of co-consolidated specimens run 9 . . . . .	101
C.11	Load-displacement curves of specimens taken from post-consolidated multiple step formed shape . . . . .	102
C.12	Load-displacement curves of preconsolidated specimens from new material roll . . . . .	103



# List of Tables

2.1	Inter-ply slippage dependence on $T$ , $P$ and $v$ . . . . .	8
2.2	Tool-ply slippage dependence on $T$ , $P$ and $v$ at $T > T_m$ . . . . .	9
3.1	Constituent components of the press assembly . . . . .	21
4.1	Parameters used in forming experiments . . . . .	35
4.2	Demonstrator manufacturing parameters . . . . .	37
5.1	Co-consolidation L9 orthogonal array experiment . . . . .	57
5.2	$G_{IC}$ VIS results . . . . .	60
5.3	ANOVA results for $G_{IC}$ VIS output . . . . .	66
5.4	ANOVA results for thickness output . . . . .	68
6.1	Multiple step forming process parameters . . . . .	73
A.1	Co-consolidation L9 orthogonal array experiment . . . . .	84
B.1	$G_{IC}$ VIS results . . . . .	85
B.2	ANOVA results for $G_{IC}$ output . . . . .	88
C.1	DCB test results of preconsolidated specimens . . . . .	89
C.2	DCB test results of co-consolidated specimens run 1 . . . . .	91
C.3	DCB test results of co-consolidated specimens run 2 . . . . .	93
C.4	DCB test results of co-consolidated specimens run 3 . . . . .	94
C.5	DCB test results of co-consolidated specimens run 4 . . . . .	95
C.6	DCB test results of co-consolidated specimens run 5 . . . . .	96
C.7	DCB test results of co-consolidated specimens run 6 . . . . .	97
C.8	DCB test results of co-consolidated specimens run 7 . . . . .	98
C.9	DCB test results of co-consolidated specimens run 8 . . . . .	100
C.10	DCB test results of co-consolidated specimens run 9 . . . . .	101
C.11	DCB test results of specimens taken from post-consolidated multiple step formed shape . . . . .	102
C.12	DCB test results of preconsolidated specimens from new material roll . . . . .	103



# List of Acronyms

<b>8HS/PPS</b>	An 8-harness satin woven fabric glass fibre reinforced polyphenylene sulfide composite material
<b>ANOM</b>	Analysis of means
<b>ANOVA</b>	Analysis of variance
<b>CAD</b>	Computer aided design
<b>CF/PEI</b>	Carbon fibre/polyetherimide composite material
<b>CF/PEEK</b>	Carbon fibre/polyether ether ketone composite material
<b>CNC</b>	Computer numerically controlled
<b>CTE</b>	Coefficient of thermal expansion
<b>DCB</b>	Double Cantilever Beam
<b>DOF</b>	Degree of freedom
<b>FEM</b>	Finite element modelling
<b>GF/PEI</b>	Glass fibre/polyetherimide composite material
<b>GTSS</b>	Grand Total Sum of Squares
<b>ILSS</b>	Interlaminar shear strength
<b>IR</b>	Infra-red
<b>MBT</b>	Modified Beam Theory method for strain energy release rate calculation
<b>PEI</b>	Polyetherimide thermoplastic polymer
<b>PID</b>	Proportional-integral-derivative control system
<b>PPS</b>	Polyphenylene sulfide thermoplastic polymer
<b>SBS</b>	Short Beam Shear
<b>SS</b>	Sum of squares
<b>SSR</b>	Solid state relay
<b>TP</b>	Thermoplastic polymer matrix system
<b>TS</b>	Thermoset polymer matrix system
<b>UD</b>	Unidirectional



# List of Symbols

$\alpha_R$	Coefficient of thermal expansion across the fibres [ $^{\circ}\text{C}^{-1}$ ]
$\alpha_T$	Coefficient of thermal expansion along the fibres [ $^{\circ}\text{C}^{-1}$ ]
$\delta$	Load point displacement [mm]
$\mu$	Friction coefficient
$\theta$	Tool angle [ $^{\circ}$ ]
$\tau_{yield}$	Interlaminar yield shear stress [Pa]
$\tau_{steady\ state}$	Interlaminar steady state shear stress [Pa]
A	Crack area [ $\text{mm}^2$ ]
a	Crack length in DCB test specimens [mm]
$a_0$	Initial crack length in DCB test specimens [mm]
b	Crack width in DCB test specimens [mm]
$\text{DOF}_{exp}$	Degrees of freedom in a matrix experiment
$\text{DOF}_f$	Degrees of freedom needed to describe a factor effect
$\text{DOF}_{required}$	Degrees of freedom required in the experiment
$\text{DOF}_{two-way\ interaction}$	Degrees of freedom for each two way interaction
F	Large displacement correction factor
$F_{prac}$	F-ratio calculated experimentally
$F_{table}$	Tabulated F-ratio
G	Strain energy release rate [ $\text{KJ}/\text{m}^2$ ]
$G_I$	Strain energy release rate for mode I opening load case [ $\text{KJ}/\text{m}^2$ ]
$G_{IC}$	Mode I interlaminar fracture toughness [ $\text{KJ}/\text{m}^2$ ]
h	Specimen thickness [mm]
L	Specimen length [mm]
P	Applied load [N]
$\text{SS}_{time}$	Variance due to time
$\text{SS}_{temperature}$	Variance due to temperature
$\text{SS}_{pressure}$	Variance due to pressure
$\text{SS}_{error}$	Variance due to experimental error
T	Temperature [ $^{\circ}\text{C}$ ]
t	Parameter used in large displacement correction factor [mm]

$T_m$	Melting temperature [°C]
$T_g$	Glass transition temperature [°C]
$T_{\text{forming}}$	Forming temperature [°C]
$U$	Strain energy [J]
$v$	Stamping velocity [m/s]
$x$	Number of control factors in a designed experiment
$y$	Number of levels of each control factor in a designed experiment

# Introduction

With the current need for reducing fuel consumptions and the carbon footprint in the aerospace industry, reducing aircraft structural weight has become one of the main priorities. Both primary structural elements, such as wings and fuselages, and secondary structures are being re-designed from the baseline and commonly used aluminium alloys to composite materials. The most recent examples are the Boeing 787 [1] and the Airbus A350 [2], where composite materials make up about 50 % of the overall structural weight.

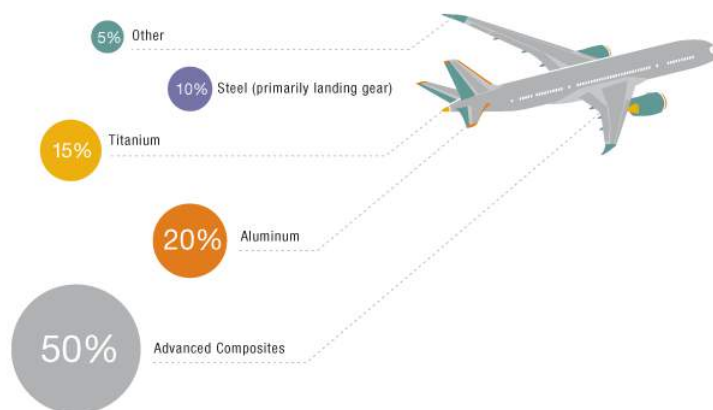


Figure 1.1: Boeing 787 material structural weight distribution [1]

Composite materials consist of high-performance fibre reinforced polymers. The continuous fibres provide the stiffness, high strength and load carrying capabilities, while the polymer matrix holds them together and provides local stress transfer from one fibre to another. Fibres may consist of E-glass, S-glass, Kevlar, boron, carbon, etc. Matrix materials cover a wide range of thermoset (epoxy, polyester, phenolics) and thermoplastic resins (PEI, PPS, PP, PEEK).

Due to its earlier implementation, most of the matrix systems used in composite structures consist of thermoset (TS) resins. Thermosets consist of a resin and curing agent, which form a low viscosity liquid when mixed. This liquid cures as a result of externally applied heat or an internally generated reaction, thus forming a highly crosslinked network polymer (see Figure 1.2). For better material properties (i.e. low void content, higher degree of compaction, better resin impregnation), curing is typically carried at high temperature pressurized ovens (i.e. autoclaves). Autoclave cycles are very time consuming and they represent great manufacturing costs, thus making the high volume production of thermoset based composite structures a challenge.

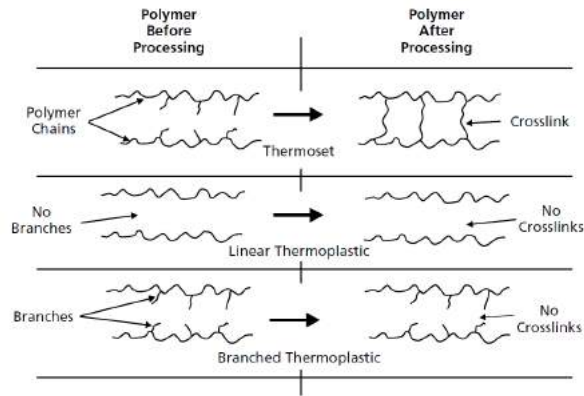


Figure 1.2: Comparison of thermoset and thermoplastic polymer structures [3]

In the early 80's, however, thermoplastic (TP) composites have been introduced and anticipated to gradually increase the number of structural applications in the aerospace industry [4]. Thermoplastics are linear or branched polymers (see Figure 1.2) which become liquid upon the application of heat. Due to the molecular structure of these polymers, these materials have several features which make their application promising, such as:

- Ability to re-melt and be welded
- Cost and time-effective manufacturing processes
- Fire retardancy properties
- Higher toughness and out-of-plane properties
- Higher chemical resistance
- Recyclability

The economical feasibility of thermoplastic composites has been repeatedly demonstrated in several studies and proved to outperform aluminium and thermoset composite design counterparts. Examples of parts where the cost-effectiveness has been demonstrated are landing gear doors, ribs and floor panels [5].

One of the common manufacturing processes used to produce thermoplastic composite parts is press forming. Parts such as ribs, brackets, clips and stiffeners have been manufactured through this method [6]. Thermoplastic composite press formed parts typically have constant thickness and constant fibre orientation. Tailoring the stiffness and strength by locally varying the thickness and fibre orientation is a technique which is currently not being implemented and that could potentially lead to optimized and lighter designs.

This method of optimizing structural performance and reducing weight has been successfully applied in the automotive industry, where metal tailor-made blanks with variable thickness, are press formed. This represents a weight-saving strategy in the sense that the thickness is intentionally increased at load intensive regions, but at the less loaded regions the thickness is decreased [7].

In the automotive industry, a variant of the press forming process, the tandem press line, is also widely applied. In this process, multiple presses are placed next to each other and each one performs a specific forming or punching operation, as shown in Figure 1.3. Thus, before the final shape of the product is obtained, the initial flat sheet is submitted to a sequence of forming steps.

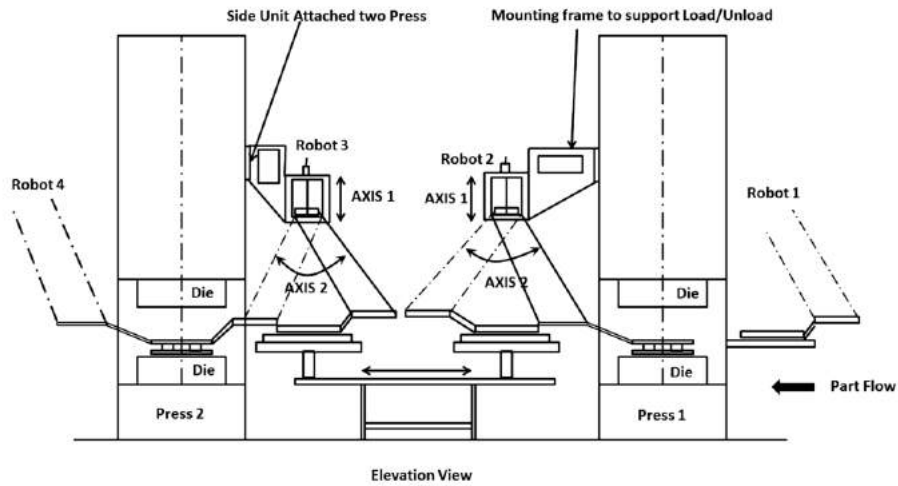


Figure 1.3: Tandem press line configuration [8]

In this research, the feasibility of a multiple step forming approach for the production of tailored thermoplastic composite parts will be investigated. The process consists on producing tailored parts by forming multiple blanks in different forming steps. Only one die set is used, opposed to the tandem press line variant, and instead of performing multiple forming operations on the same blank, a new blank is formed and co-consolidated to the blank(s) formed in the previous step(s). Thus, in each forming step, a new feature (i.e. local reinforcement, thickness step) is added to the part being manufactured. A schematic representation of the process is presented in the following figure:

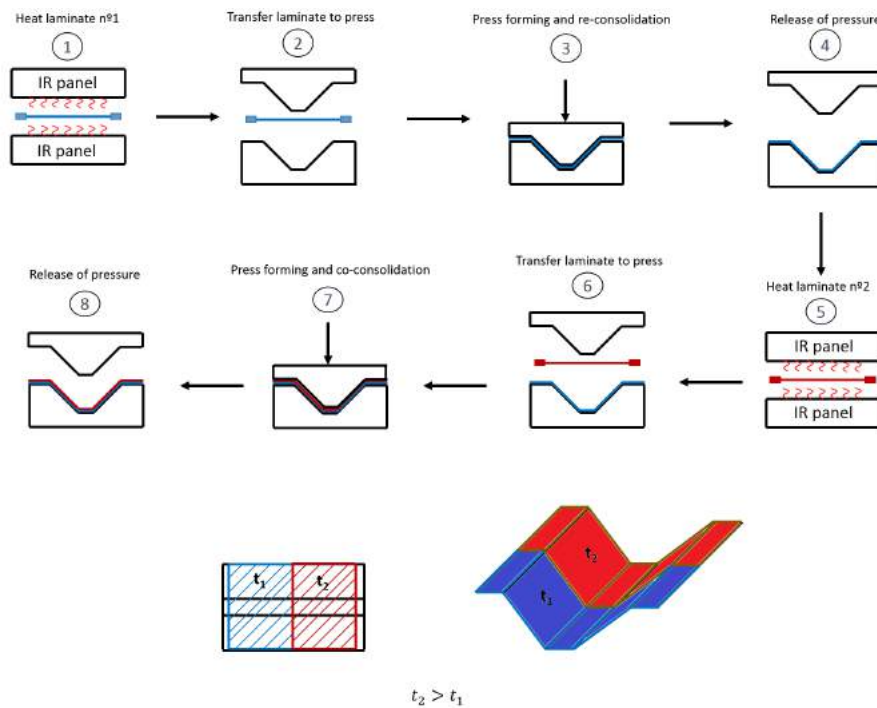


Figure 1.4: Multiple step forming approach for the manufacturing of a variable thickness part

## 1.1. Research Questions

There are significant differences between the press forming process for metals and thermoplastic composites. In press forming thermoplastic composites, blanks must be heated above the melting temperature ( $T_m$ ) or glass transition temperature ( $T_g$ ) of the polymer matrix before being formed. Moreover, formed blanks are submitted to a consolidation stage under pressure after forming to restore the material's pristine mechanical and physical properties. Due to these processing features, the feasibility of the multiple step forming approach must be proven by analysing other types of phenomena. This leads to the formulation of research questions, the answers to which will provide an indication on the feasibility of this manufacturing concept.

The main research question of this thesis can then be formulated as: *Is the multiple step forming approach feasible and could it potentially be applied in an industrial environment?* This research question can then be split into different sub-questions:

1. Is it possible to form laminates in different steps into three-dimensional shapes without visual forming defects?
2. Is it possible to achieve a good quality bond between formed and co-consolidated laminates in different steps? If so, what temperatures are needed?
3. What is the influence of co-consolidation temperature, pressure and time on the bond quality of co-consolidated laminates?

## 1.2. Thesis Outline

In the next chapter, a literature review on the topic of press forming of thermoplastic composites will be provided. In Chapter 3, the design of the experimental setup, which was used to carry out multiple step forming experiments throughout this thesis, will be explained. Chapter 4 will present the conditions at which the multiple step forming approach in GF/PEI composites becomes feasible from a formability standpoint. Chapter 5 then provides the influence of processing parameters (temperature, time and pressure) on the quality of co-consolidated bonds and establishes a feasible processing window. In Chapter 6 the results obtained in Chapter 5 will be used to prove the feasibility of the multiple step forming approach. Finally, the report is concluded in Chapter 7, where the main conclusions of this work and recommendations for future research will be provided.

# 2

## Literature Review

Press forming is a fast, repeatable and cost effective thermoplastic composites manufacturing process [9]. The process starts with a preconsolidated laminate, which is heated above the  $T_m$  of the polymer matrix, if semi-crystalline, or above the glass transition temperature,  $T_g$ , if amorphous. Once the forming temperature,  $T_{forming}$ , of the laminate is reached, it is transferred to the press, usually via an automated transfer system. Laminate transfer from oven to press can also be performed manually, provided that the time between removal from the oven and pressing is such that the temperature of the laminate doesn't drop below the forming temperature.

When the laminate is in the forming station, it is formed into the shape of the mould. The forming process can be **isothermal** or **non-isothermal**. In a **non-isothermal** process, the laminate is drawn into the mould and cools down after making contact with the mould surface. The material then re-consolidates by applying pressure and time. Pressure is removed when temperature drops below a certain level (usually the matrix recrystallization temperature). Non-isothermal processes are often used in materials with lower reinforcement volume fraction or with forms that require lower consolidation pressures, such as commingled and powder impregnated TP composite laminates [10]. The process is also attractive for applications where higher void contents are acceptable, such as in the automotive industry.

In an **isothermal** process, the tool is pre-heated above  $T_m$  or  $T_g$  of the polymer matrix and consolidation pressure is applied while temperature is held constant at this level. Pressure is maintained during the cooling process of the mould and removed when temperature drops below a pre-established value. Parts with excellent consolidation quality (<1% void content) can be obtained through this method. However, this comes with the cost of longer process cycles times and the need to heat up the mould after every forming cycle.

After the consolidation stage, parts are removed from the mould and cooled to room temperature by free surface convection. A subsequent trimming operation is usually necessary to obtain the final shape of the product. A schematic representation of the process is illustrated in the following figure:

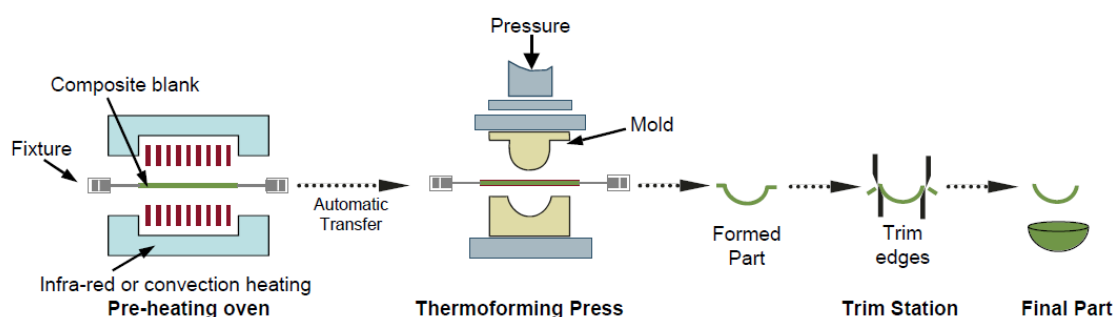


Figure 2.1: Stages of the press forming process [11]

The main advantages of the process are:

- Short cycle times compared to processes such as hand-layup and autoclave consolidation
- Ability to produce single and double curved shapes
- Both UD's and woven fabrics can be formed
- Possibility for automation

In this literature review, some of the most important findings and best practices related to the press forming process of thermoplastic composites will be presented and summarized.

## 2.1. Deformation Mechanisms

Composite materials are formed through the conjugation of different mechanisms, which can be enumerated as follows:

1. Intra-ply shear
2. Fibre straightening
3. Fibre elongation
4. Inter-ply slippage
5. Tool-ply slippage
6. Resin percolation
7. Transverse squeeze flow

### 2.1.1. Intra-ply shear

Intra-ply shear, or Trellis effect, occurs when the material is subjected to in-plane shear and it consists on the rotation of fibres within a ply. This mechanism is the main responsible for allowing a composite material to be formed into a three-dimensional shape. A representation of this effect in a fabric layer is shown in the following figure:

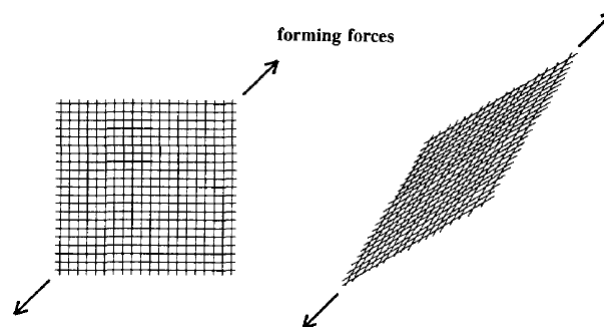


Figure 2.2: Intra-ply shear in fabric layer [12]

The extent at which the fibres can rotate is limited, so they don't always end up coinciding with the loading direction. When fibres reach the limit at which they cannot rotate any more it's said that the crossover angle reaches its minimum allowable value, or commonly designated as locking angle. If the locking angle is reached and the load keeps increasing, shear wrinkling occurs, one of the most frequently reported defects when forming composite parts into three-dimensional shapes.

In UD plies, intra-ply shear is characterised by the parallel movement of the fibres through the thickness (1-3 plane), in the transverse direction (2-3 plane) or along the surface plane (1-2 plane) [9], as shown in the following figure:

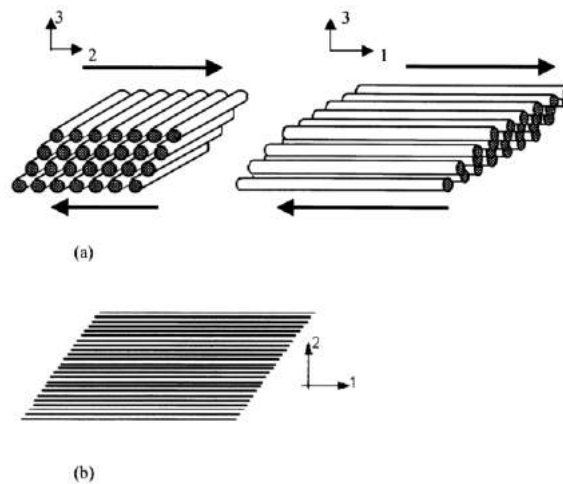


Figure 2.3: Intra-ply shear in UD plies [9]

Methods of characterizing intra-ply shear behaviour under processing temperatures have been developed for fabric and UD materials. The two most common methods of characterizing this deformation mechanism in fabrics are the bias-extension and picture frame tests. The two tests have been compared by Harrison et al [13] and it was suggested that the deformation mechanisms occurring in picture frame tests resemble better the forming behaviour of the material during stamp forming than bias extension tests. However, bias extension tests provide quick and more reliable materials' locking angle.

The shear behaviour is extremely dependent on the shear rate and temperature. The higher the shear rate, the stiffer the material behaves and the sooner it wrinkles, whereas the opposite effect is expected when temperature increases. Performing tests at elevated temperatures and at different shear rates is particularly interesting for thermoforming. The material behaviour at these conditions can be fitted into a model and subsequently used as an input in forming simulations to predict process induced defects during the design phase of a manufacturing process [14].

Intra-ply shear characterisation of UD plies is more cumbersome. It has been a topic of research for many years, where several attempts to fully and reliably characterize this mechanism have been made. It was the work of Haanappel et al [15] that introduced a reliable test method capable of characterising the longitudinal shear mechanism, which consists on using torsion bar specimens with a close to square cross section. The test proved to offer good results in the small strain regime, but more reliable methods need to be investigated for large strains.

### 2.1.2. Fibre straightening

Straightening of fibres is another deformation mechanism taking place in the plane of a ply and it only occurs if fibres are not fully stretched before forming. In fabrics, where fibre bundles are interlaced with some degree of curvature, the curvature reduces after stretching, thus increasing the mechanical properties in the loading direction. However, curvature in the perpendicular direction will increase, thus leading to a reduction in mechanical properties in this direction [12].

### 2.1.3. Inter-ply slippage

Inter-ply slippage is the movement of the individual plies relative to each other and it is the primary mechanism when forming single curved shapes. The phenomenon has been studied and characterised by several authors [12, 16–18]. The sliding of fibres relative to each other depends on matrix viscosity, fibre orientation, temperature, normal pressure and pull-out speed. It is also agreed among different publications that this deformation mechanism is only initiated once a yield shear stress is exceeded. After exceeding this stress, slippage continues at a stationary stress level.

Ply slippage occurs at the resin interlayer. The interlayer has an elasto-viscoplastic behaviour in the sense that below the yield point the behaviour is linear elastic and at the steady state regime it is dependent on the shear rate. It is also plastic because deformation is irreversible. On the basis of this

behaviour, the yield shear stress ( $\tau_{yield}$ ), steady state shear stress ( $\tau_{steady\ state}$ ) and friction coefficient ( $\mu$ ) at the ply-ply interface depend on parameters such as temperature, pressure and pulling velocity ( $v$ ) (representative of the stamping velocity). For non-axial interfaces (i.e. interfaces where fibres from adjacent plies don't have the same orientation) these dependencies are characterised as follows:

Table 2.1: Inter-ply slippage dependence on  $T$ ,  $P$  and  $v$

	$\tau_{yield}$ & $\tau_{steady\ state}$	$\mu$
$T \uparrow$ (constant $v$ and $P$ )	$\downarrow$	$\downarrow$
$v \uparrow$ (constant $T$ and $P$ )	$\uparrow$	$\uparrow$
$P \uparrow$ (constant $T$ and $v$ )	$\uparrow$ slightly	$\downarrow$

For axial interfaces, where fibres of adjacent plies are oriented in the same direction, fibres can penetrate and go from one resin rich layer to the other, thus increasing inter-ply slip resistance. As a result,  $\tau_{yield}$  and  $\tau_{steady\ state}$  in axial interfaces are higher than in non-axial interfaces at the same processing conditions (i.e.  $T$ ,  $P$  and  $v$ ).

With this knowledge, some guidelines can be formulated in order to avoid defects, such as debonding or fibre buckling, when forming single curved shapes:

- The interface between layers must have a sufficiently high temperature for the resin to have low viscosity,  $\tau_{yield}$  and  $\tau_{steady\ state}$
- It is recommendable to have lower forming speeds to promote inter-ply slippage and avoid fibre buckling at the corners
- Avoid adjacent plies from having the same fibre orientation
- In the initial stages of forming, high temperatures are needed to promote inter-ply slippage and low normal pressures are recommended to avoid roving interlocking

#### 2.1.4. Tool-ply slippage

In a press forming process, load transfer between the material and the tool is made by friction. Friction between the laminate and the tool affects the way the laminate deforms. Moreover, the friction coefficient is dependent on deformation rate, temperature, pressure, fibre orientation and surface texture [19].

Similarly to inter-ply slippage, a yield stress has to be overcome in order to initiate ply slipping relative to the tool. Opposed to ply-ply slippage, the yield and steady state shear stresses increase as temperature increases (for  $T > T_m$ ). The same applies for the friction coefficient. For higher temperatures, matrix viscosity decreases and the thickness of the resin rich layer reduces, causing more fibres to come into contact with the tool, thereby increasing Coulomb friction [18]. A distinction can be made between rubber and metal moulds in the sense that metal-ply friction is much lower. Furthermore, release agents are usually much more effective in metal surfaces because they tend to reduce much more the friction coefficient than in rubber surfaces.

Relations between the tool-ply shear stress and the friction coefficient have been established among several authors. In the following table, some of these relations for temperatures greater than  $T_m$  are provided:

Table 2.2: Tool-ply slippage dependence on  $T$ ,  $P$  and  $v$  at  $T > T_m$ 

	$\tau_{steady\ state}$	$\mu$
$T \uparrow$ (constant $v$ and $P$ )	$\uparrow$	$\uparrow$
$v \uparrow$ (constant $T$ and $P$ )	$\uparrow$	$\uparrow$
$P \uparrow$ (constant $T$ and $v$ )	$\uparrow$	$\downarrow$

For temperatures below  $T_m$ , the friction coefficient and steady state shear stress increase as the temperature decreases. This is because there are no fibres penetrating the resin rich layer at this temperature range and therefore the stresses and friction are controlled by matrix viscosity. Moreover, for the same processing conditions ( $P$ ,  $T$  and  $v$ ) and at  $T > T_m$ , tool-laminate shear stresses and friction coefficient are lower than interlaminar ones. Based on this behaviour, large scale interlaminar deformations during mould closing should be done at high temperatures, but improved final conformation (after large scale interlaminar deformations) may be achieved at intermediate temperatures, where tool-laminate friction is lower.

### 2.1.5. Resin percolation

Resin percolation occurs during the consolidation stage of the laminate and it is defined as the transverse flow of resin along the fibres. This flow allows the plies to bond together, so it affects significantly the consolidation and mechanical performance of the material. If resin percolation is not sufficient, consolidation quality will be negatively affected and voids will remain in the material.

### 2.1.6. Transverse squeeze flow

Transverse squeeze flow is also more relevant during the consolidation process and it only occurs in UD plies [9]. It consists of the sideways fibre motion when a normal pressure is applied and the motion of the fibres is induced by the matrix flow. This effect does not occur in woven fabrics because transverse flow is restricted by the weave.

## 2.2. Process variants

The three most common variants of the press forming process are matched die, rubber and diaphragm forming. The features of these variants and the behaviour of thermoplastic composite materials when formed using these different processes will be described in the next sections.

### 2.2.1. Matched die forming

Matched die forming is the most common variant of TP composites press forming. The process uses matched metal dies to form a laminate and ensures good surface quality and well defined details in both sides of the product. Male and female dies can be heated to maintain a uniform temperature distribution during the process. The process enables the generation of highly localized pressures. However, non-uniform pressure distributions can result in resin flow to lower pressure spots and non-uniform thickness distributions. Another disadvantage of the process lies in the fact that tools have to be precisely manufactured and very low tolerances are required.

Extensive research on the material behaviour and consolidation quality in laminates formed with matched dies has been conducted by Hou [20–26]. In references [20–22], hemispherical shapes were formed using different materials, with different fibre architecture. In [20], GF/PEI woven fabric laminates were press formed into hemispherical shapes using matched metal dies. The most relevant findings of this work are enumerated as follows:

- When no tension is applied in the blank, severe wrinkling is pronounced at the flange of the hemispherical part
- The higher the ratio of initial laminate area and final sphere surface area, the more buckling occurs at the flange

- The thinnest section occurs on the apex of the hemisphere due to the high localized consolidation pressures
- Thickness distributions were the same in warp and weft directions, but in the  $\pm 45^\circ$  directions thickening was more pronounced in the edges

Opposite to the trends observed in [20], in [21] it was found that thickness distribution after forming a hemisphere with a UD composite is independent of the angle at which it is measured. Hou [22] also analysed local strains in relation to different fibre orientation directions in hemispherical press formed shapes. In this work, strain distributions along the warp, weft and  $\pm 45^\circ$  directions were determined and the following trends were observed:

- Local strains in the  $\pm 45^\circ$  directions are much higher than in the warp and weft directions
- In the  $\pm 45^\circ$  directions, local strain increases from the apex to the edges of the hemisphere
- Local strain decreases from the apex to the edges of the sphere in warp and weft directions. Maximum strain in these directions occur at the apex of the hemisphere due to high local tensile forces

$90^\circ$  bend stamp forming experiments were also performed using matched metal moulds [23]. It was concluded that if low stamping velocities and pressures are applied, fibres may buckle. Moreover, at too high stamping velocities, or at too high stamping pressures, severe thinning may occur in the bend region. This allowed the author to qualitatively establish a process window, as illustrated in the following figure:

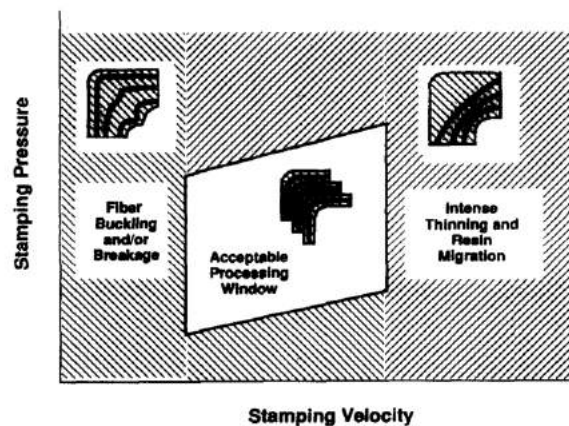


Figure 2.4: Process window of  $90^\circ$  bends [23]

Finally, a consolidation model able to determine what are the required holding times, temperatures and applied pressures in order to produce high quality components was developed in [24]. This model was then successfully applied in the manufacturing of aileron ribs and hinges [25, 26]. Increasing mould temperatures contributed to void content reductions and increase in flexural stiffness and strength.

### 2.2.2. Rubber forming

In the rubber forming process, one mould is made of rubber (usually elastomeric material), whose flexibility allows it to conform into the metal tool under high pressures. The rubber mould is usually pre-shaped, so it resembles the shape of the metal mould. It has the ability to produce complex shapes and generating more uniform pressure distributions compared to matched-metal die forming. Moreover, the rubber mould can compensate for thickness variations and adapt its shape during the forming process [12].

Relevant parameters that should be taken into account when choosing the rubber are:

1. Coefficient of friction

2. Hardness
3. Coefficient of thermal expansion
4. Temperature resistance

The hardness determines whether certain details can be reproduced. Soft rubbers can more easily reproduce details, such as sharp corners, than hard rubbers. The coefficient of friction plays a role in the material tool-ply shear forming behaviour. Higher frictions hinder slippage between rubber and composite, thereby affecting full conformation of the material into the shape of the mould. The ability to form corners also reduces with an increase in friction. The use of lubricants is possible but they often affect the mechanical properties of the composite material. The use of a lubricant that doesn't affect the mechanical properties needs to be investigated [27]. The coefficient of thermal expansion influences the pressure distribution during the consolidation stage. At a high temperature, the rubber expands and may get stuck during forming. As a result, full mould closure may not be achieved and a lot of regions in the laminate may not experience consolidation pressure. Finally, temperature resistance is extremely important. Laminates forming temperatures can go up to 400°C and metal moulds are usually heated to high temperatures in order to achieve good consolidation quality.

Despite soft rubbers having better ability to reproduce details than harder ones, they may experience barrelling effects during forming, thereby introducing a lot of friction and higher risk of clamping itself in the female metal mould. Therefore, the hardness of the rubber must be controlled and carefully chosen. For complex geometries, soft rubber moulds should be used but barrelling effects must be absent. For low complexity products, a harder rubber can provide higher stability but it should be able to conform into the shape of the solid tool and reproduce details.

### 2.2.3. Diaphragm forming

In the diaphragm forming process, a composite laminate is placed over a mould in between two diaphragms and the setup usually goes into an autoclave to be heated, formed, consolidated and cooled down. The first stage of the process involves heating the laminate and the diaphragms above the matrix  $T_m$ . Then, the increased air pressure in the autoclave is responsible for drawing the material into the mould. After forming and consolidation at constant temperature, the material is cooled down under pressure. One unique feature of the process is that hydrostatic pressure is applied [28].

High complexity products with detailed contours, excellent surface finish, uniform thickness, good consolidation quality and fibre placement control can be produced [28, 29], hence the reason why the process has found its way especially in aerospace applications, where production volumes are relatively small. Another advantage is that highly localized pressures and stresses are absent due to the isothermal and hydrostatic nature of the process.

The main disadvantages of the process are the limited formability of the expensive diaphragms, their non-re-usability and the long cycle times. This is mainly due to the low forming rates and the time-consuming heating and cooling cycles. However, the very low forming rates result in a relief of internal stresses, which is beneficial for the part's performance.

Processing parameters and conditions in diaphragm forming have been investigated by O'Brádaigh et al [28, 29] and Keane et al [30]. Some of the main findings of the studies performed by O'Brádaigh et al are enumerated as follows:

- Increased laminate thickness leads to more shear wrinkling and an increase in diaphragm stiffness leads to the alleviation of shear wrinkling
- High ratios of lay-up area and formed area result in severe wrinkling. This effect is more prone to occur when using female tools
- Hemispherical parts produced in female tools lead to larger thickness variations than in male tools

In the work developed by Keane [30], the influence of layup and matrix morphology on the forming behaviour was analysed. The following outcomes of his work are enumerated as follows:

- Quasi-isotropic lay-ups have to be formed at much lower forming rates in order to prevent wrinkling because these laminates develop much higher shear stresses during forming

- Amorphous composites lead to less spring-in compared to semi-crystalline composites. The volume change of amorphous composites is smaller during the solidification, thus resulting in less distortion
- Spring-in increases when the number of  $0^\circ$  plies decreases and when forming takes place in male moulds

### 2.3. Formability of thermoplastic composites

The formability of thermoplastic composites largely depends on the type of fibre reinforcement and layup. In 1998, de Luca et al [31] numerically and experimentally investigated the forming behaviour of both UD and woven fabric laminates with different layups by using a double-dome mould geometry. Results showed that quasi-isotropic laminates comprised of woven fabric plies have less wrinkles than UD quasi-isotropic laminates when formed into the same geometry. Moreover, woven fabric cross-ply laminates showed no wrinkling, opposed to the small amount of wrinkling found in quasi-isotropic ones, thus revealing the lower ability of quasi-isotropic laminates to be formed into three-dimensional shapes.

In 2010, Haanappel [32] compared the formability of two UD laminates, one cross-ply and the other one quasi-isotropic, by using a doubly curved mould shape. Trends were the same as the ones de Luca et al found for woven fabrics. Whereas cross-ply layups have almost no wrinkles, quasi-isotropic laminates show severe wrinkling.

In more recent and detailed studies of Haanappel [33–35], the deformation behaviour of UD and woven fabrics was characterised and quantified. The UD/PEEK material showed concentrated shear strain regions in doubly curved regions and very low shear strain values compared to the 8HS/PPS material, which showed highly concentrated shear strains with much higher values than UD/PEEK. This suggests that the UD/PEEK material has a very limited intra-ply shearing capability, which results in more pronounced wrinkling effects. The 8HS/PPS material, on the other hand, shows significant intra-ply shearing behaviour which tends to suppress wrinkling.

Finally, Haanappel [35] claimed that the resulting deformation mechanism “is determined by the balance between apparent frictional (FR), intra-ply (IR) and bending rigidities (BR) of the laminate”. If more than two fibre orientations are present and there is no out-of-plane deformations, in-plane deformations of the plies are always accompanied with inter-ply slippage. This is illustrated in Figure 2.5 (b). If the summation of intra-ply and apparent frictional rigidity is higher than the bending rigidity, wrinkling will occur (c). On the other hand, if the bending rigidity is higher than the summation of frictional and intra-ply rigidities, significant shearing will occur and wrinkles will be suppressed.

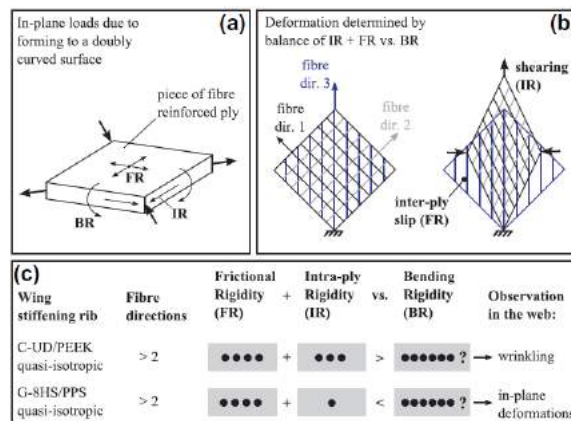


Figure 2.5: Schematic explanation of the balance between the apparent intra-ply (IR), frictional (FR), and bending (BR) rigidity of the plies [35]

## 2.4. Process induced deformations

Process-induced deformations are frequently reflected on the spring-in effect. Spring-in is defined as a reduction of the enclosed angle in bend regions and it arises from the high processing temperatures and subsequent cooling of the material during processing. Due to the difference between the in-plane and out-of-plane coefficient of thermal expansion (CTE) of the composite material, residual stresses develop, which lead to deformations and distortions, namely spring-in behaviour.

This kind of distortions may cause problems during assembly, since deviations between the as-designed and as-manufactured forms lead to low dimensional control, increased costs and more time consuming assembly processes. Therefore, process induced deformations not only affect the specification of tolerance levels for assembly but also the tooling design, the choice of process parameters and material configuration.

Accurate tooling design becomes extremely important in order to prevent unwanted geometries, mainly for aerospace applications where tolerances are typically very small. Tool angles must be compensated for spring-in phenomena, whose magnitude depends on:

- Lay-up configuration
- Processing temperature
- Stamping pressure
- Stamping velocity
- Tool radius
- Part thickness
- Mould angle
- Fibre and matrix CTE

Analytical models and simulation strategies have been developed to provide accurate angle reduction predictions. The most simplistic model, suggested by Zahlan and O'Neill [36], claims that the angle difference is given by:

$$\Delta\theta = (\alpha_R - \alpha_T)\theta\Delta T \quad (2.1)$$

Where  $\theta$  is the bend angle,  $\Delta T$  is the reduction of temperature between stamping and removal of the part, and  $\alpha_R$  and  $\alpha_T$  are the CTE's across and along the fiber direction respectively. However, more accurate prediction methods have been developed and applied by other authors [37–40].

In [37], a spring-in model developed by Jain and Mai [41, 42] was successfully used to assist tooling design for the manufacturing of a thermoformed aileron rib. Furthermore, it was observed that higher residual stresses occur at higher processing temperatures. Therefore, despite higher temperatures providing better impregnation and lower void content, an optimum processing temperature must be selected such that it does not induce any defects such as cracking or delaminations.

In the work carried out by Salomi et al [38], the spring-in behaviour of a TP composite material shaped into a U shape in an autoclave was studied. The experimental data was then compared with the predictions made from Radford and Rennick's adapted model [43]. Differences between the experimental data and the model were observed and attributed to the existence of fibre distortion at the corners, fibre misalignments and wrinkling. The existence of such defects increases the CTE through the thickness direction of the material. As a result, the model was modified to account for this effect. The modified model resulted in a better agreement with experimental data. Finally, the effects of tool radius on the spring-in angle were analysed. Higher spring-in angles for smaller inner tool radii were reported.

In the work developed by Han et al [39], an effective finite element simulation strategy was established to predict the process induced deformation of a carbon fibre reinforced PPS thermoformed 90° bend angle. Experimental results showed that, for the same layup, the spring-in angle increases as the moulding temperature increases. Moreover, because the out-of-plane shrinkage is much higher than the in-plane shrinkage, a  $[(\pm 45)/(0/90)/(\pm 45)]_s$  layup shows larger deformations compared to a

[(0,90)/(±45)/(0,90)]<sub>s</sub>. The predomination of fibres along the length of the part in the later hinders the out-of-plane contraction.

Finally, Brauner et al [40] analysed process-induced deformations in TP composite laminates and correlated final part geometries of 90° L-angle brackets with processing parameters. A thermal and mechanical analysis simulation method, which included the crystallization behaviour of the matrix, was also used to predict the spring-in angle. Spring-in angle was predicted by computing thermally and chemically induced strains, which are the main responsible for process-induced deformations. Results showed that the material surface tends to early acquire higher relative crystallinity values, contrarily to the midplane where the material is more viscous. This phenomenon induces various material properties inside the composite, which result in residual stresses and induced deformations. A spring-in angle of 3.6° was observed in the finite element model, which was in agreement with the experimental result of 3.7°. Differences can be explained by fibre misalignments or irregular fibre volume fractions.

## 2.5. Effects of stamping in material mechanical and physical properties

Press forming processes may introduce changes in matrix distribution, fibre orientation, degree of crystallinity and void content, which subsequently affect the mechanical properties. The effect of forming temperature on the mechanical properties of diaphragm formed CF/PEEK composites was investigated by O'Brádaigh et al [44]. Results showed that there's an optimum temperature range of 360-390 °C that increases the flexural failure load. Laminates formed in this temperature range also have more uniform matrix impregnation, whereas laminates formed at higher temperatures revealed some polymer degradation. Laminates formed at lower temperatures showed several regions with dry fibres.

In the study performed by Manson et al [45], high cooling rates upon forming decreased the degree of crystallinity of the polymer and increased the void content. Annealing processes proved to be effective in increasing the degree of crystallinity, but showed negligible influence on healing defects created during the cooling stage of the press forming cycle, such as micro-cracks, high void content and fibre buckling.

The effect of forming temperature on the fracture toughness of CF/PEEK composites was studied by Jar et al [46]. It was found that both mode I and mode II fracture toughness of laminates formed between 380-400 °C are considerably higher than the ones formed at 360 °C. Further increase in temperature did not seem to increase properties. The main reason for an increase in properties is the improvement of the fibre-matrix interfacial strength.

The effect of applied pressure during cooling of CF/PEEK composites on modes I and II fracture toughness and flexural strength was also studied by Beehag and Ye [47]. It was found that, while differences in the flexural strength and mode I fracture toughness were minimal for applied pressures above 2 bar, mode II fracture toughness increases with a higher cooling pressure.

Finally, the study carried out by Wakeman et al [48] concluded that tool temperature and consolidation pressure have an important effect on the void content and flexural strength of the material. The increase in these parameters result in lower void contents and enhanced mechanical properties.

## 2.6. Discussion

This review has shown that press formed parts are often prone to process induced defects such as fibre buckling, voids, intense thinning and shear wrinkling. The latter is very common when forming quasi-isotropic laminates into three-dimensional and complex shapes, specially in UD laminates. This kind of defects are often difficult to mitigate and sometimes a lot of trial and error runs are performed until a feasible manufacturing solution is found. The most advanced dedicated FEM packages, such as ANIFORM, are able to predict some of these defects but such software packages require knowledge of the material properties at processing temperatures (i.e. Young's modulus, viscosity, etc) and the material behaviour in intra-ply, inter-ply and tool-ply shear.

Thereby, in order to ease the production of more complex parts, with complex features and layups, a novel approach must be taken: the multiple step forming approach. The main potential advantages of the method are the ability to produce variable thickness parts, with tailored stiffness and strength, and the ability to suppress shear wrinkling defects in parts with quasi-isotropic layups. For instance, a part with a  $[(0/90) (45/-45)]_s$  layup could be obtained by forming four layers in four different steps.

One of the main challenges facing this approach is to guarantee a good quality bond between two laminates formed in different steps. Another possible issue might be one laminate sticking to the other when being formed over it, thereby hindering the inter-ply slippage mechanism. In this thesis the feasibility of the multiple step forming approach will be investigated by trying to overcome and solve these issues. Before providing the findings of experimental studies, the design of the experimental setup will be explained in the next Chapter.



# 3

## Design of the Experimental Setup

An important feature of the experimental setup is versatility. The setup should be able to press form different materials with different melting and/or glass transition temperatures, introduce different deformation mechanisms in the material and the mould must be able to be heated to high temperatures, sufficiently above the glass or melt temperature of the polymer. The latter is important because tooling temperature is a key parameter in achieving good consolidation quality and preventing microstructural defects such as delaminations or porosities [48]. Moreover, given that one of the limiting factors of the multiple step forming approach may be the poor co-consolidation quality achieved between laminates formed in different steps, it becomes essential to study the effect of different co-consolidation temperatures in the quality of the process.

The experimental setup should also offer process repeatability and reproducibility. A repeatable process ensures that results can be easily replicated by simply adjusting and setting the processing parameters to a given configuration. This is particularly important to validate results by means of more than one observation. The setup should also contain some degree of reproducibility, which ensures that experimental results are not too dependent on the person who is operating it.

Finally, the designed system should be safe to operate. The press forming process of thermoplastic composites involves multiple stages susceptible to hazards. Heating the material in an infra-red (IR) oven, heating the metal mould, preventing misalignments between moulds and handling electrical components are tasks that involve risks which may potentially lead to accidents. As a result, safety aspects were addressed during the design process and safety features were accordingly implemented to prevent accidents and damage from occurring.

### 3.1. Experimental setup assemblies

The experimental setup consists of:

1. 21 ton pneumatic press
2. Rig with integrated infra-red oven, shuttle transfer system and ventilation system
3. Blankholder
4. Press assembly with integrated soft-hard tool set, heating plate and other mechanical components (further explained in section 3.1.3)

In the following figure, an overview of the experimental setup is provided:

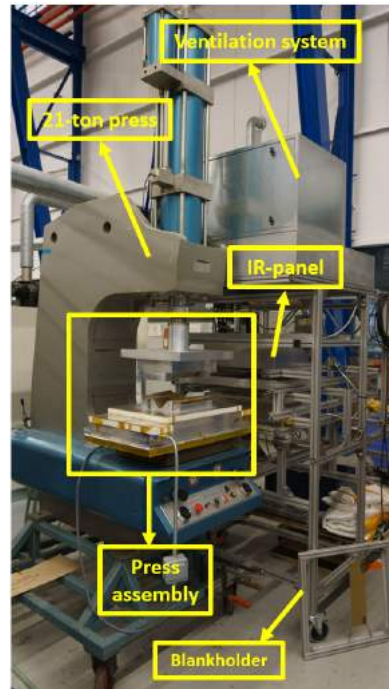


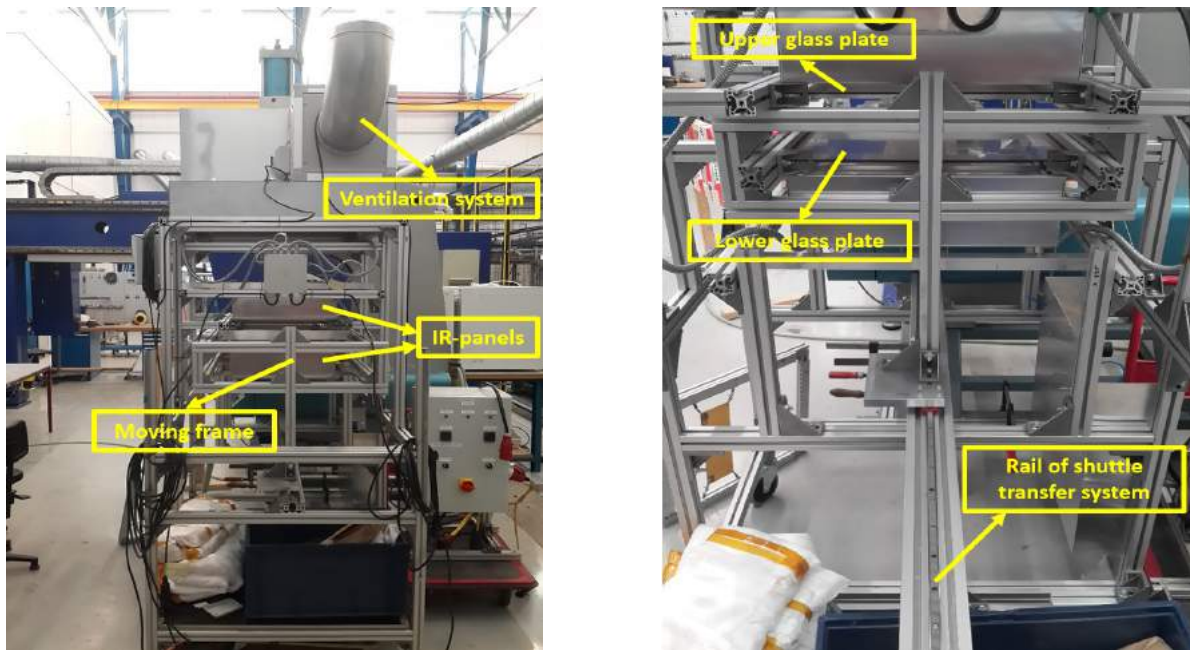
Figure 3.1: Overview of experimental setup

#### 3.1.1. Rig

The rig represents one of the most important constituents of the experimental setup. It contains a shuttle transfer system, consisting of a frame supported on a rail, responsible for quickly transporting the laminate to the press. It is an essential feature of the setup, since low transferring speeds may cause the laminate to fall below its  $T_{\text{forming}}$  and lose its ability to conform into the mould geometry. The transfer system was manually driven and consisted of a frame supported over a rail.

The IR oven consisted of two IR panels symmetrically positioned with respect to the laminate in order to heat the material evenly on both surfaces. The distance between the IR panels and the laminate was small so that the material could reach its  $T_{\text{forming}}$  and heating times could be reduced. It was also convenient to place the IR panels as close as possible to the forming station so that transferring times could be reduced and laminate temperature drops prior to stamping could be minimized. To protect the infra-red lamps, two glass plates were used. The lower glass plate prevents the laminate being heated from making contact with the lamps of the lower IR-panel in case of excessive sagging or falling. The upper glass plate mainly prevents the lamps of the upper IR-panel from making contact with solid particles.

Finally, on top of the rig there was a ventilation system to filter fumes released by the laminate in case of overheating. An overview of the rig and its integrated components is given in the following figure:



(a) Front view of the rig

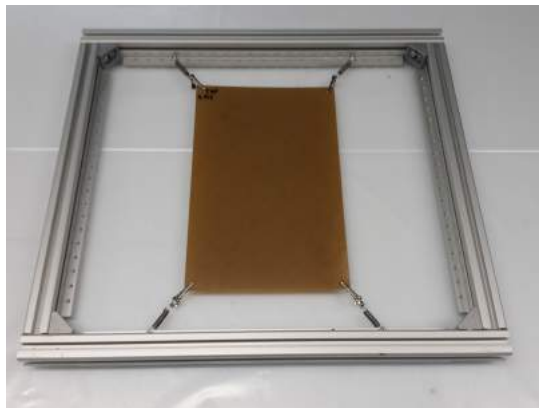
(b) Rail used to move frame and glass plates used to protect infra-red lamps

Figure 3.2: (a) Rig with integrated IR-panels, ventilation system, moving frame, (b) rail and glass plates used to protect IR-lamps

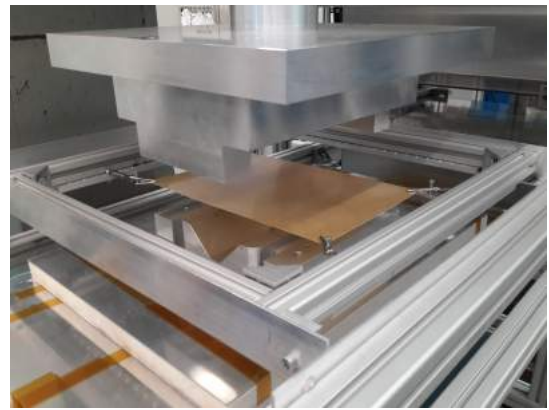
### 3.1.2. Blankholder

The main function of the blankholder is to hold and exert tension in the laminate being formed. The tension exerted by the springs helps mitigating shear wrinkling defects during forming and prevents the laminate from sagging too much while being heated in the IR oven. Excessive sagging may lead to non-uniform temperature distributions in the laminate and to laminate crushing into the tooling when being transported to the forming station.

The designed blankholder (see Figure 3.3a) consists of a compact frame with holes inserted all around in order to allow springs with crocodile clamps to be placed in different locations and to allow the position of the laminate with respect to the tooling to be changed. Crocodile clamps are effective due to the relatively high clamping force they can exert, which in turn prevents the laminate from being released from the blankholder and falling while being heated. In a press forming cycle, the blankholder is loaded into the moving frame of the rig (see Figure 3.3b), which then travels to the IR oven to heat the laminate and then back to the forming station to perform the forming operation.



(a) Blankholder frame



(b) Blankholder loaded into the moving frame of the rig

Figure 3.3: (a) Blankholder holding the laminate through springs and crocodile clamps and (b) loaded into the moving frame of the rig

### 3.1.3. Press assembly

The press assembly is the most complex of the experimental setup. The main components of this setup are the male rubber and female metal moulds, mounted on the top and bottom halves of the press, respectively. Additional components, such as mounting plates, insulating blocks, constraining blocks and a heating plate were also incorporated. Most of the components were designed using CAD software SOLIDWORKS and subsequently manufactured in CNC milling and turning machines. The rubber mould, on the other hand, was casted into the matching shape of the metal mould. It was also contained in a "box", hereinafter designated as rubber mould box, to prevent it from bulging out and tearing under high consolidation pressures. A schematic representation of the press assembly is illustrated in the following figure:

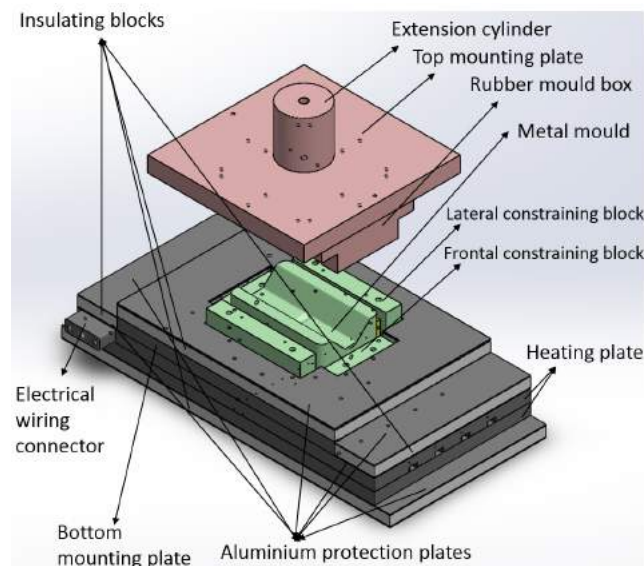


Figure 3.4: Overview of the press assembly

The top half of the setup is made of an extension cylinder, top mounting plate, rubber mould box and rubber mould (not shown in the figure). The bottom half consists of a more complex assembly made of multiple components, among which the metal mould and the heating plate. In the next section, a more detailed explanation of every component installed on the press will be provided.

### 3.2. Design choices and considerations of the press assembly

Before a detailed explanation of the function of each component is provided, an exploded view of the designed system is depicted in Figure 3.5. Enumerated components are then described in Table 3.1.

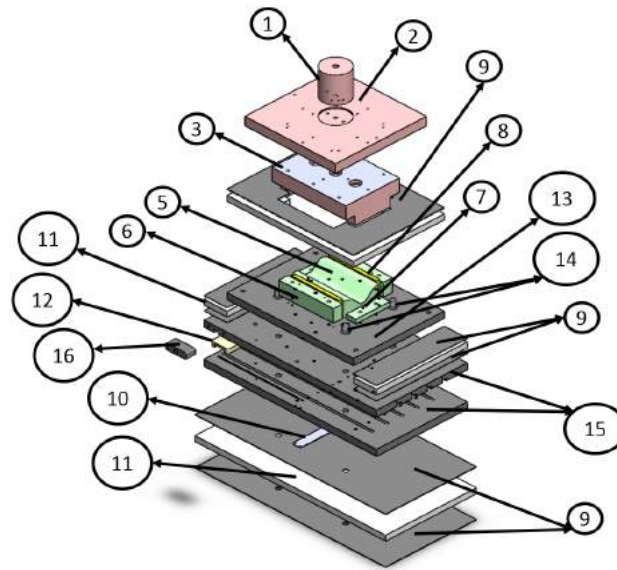


Figure 3.5: Exploded view of the press assembly (obs: rubber mould not depicted)

Table 3.1: Constituent components of the press assembly

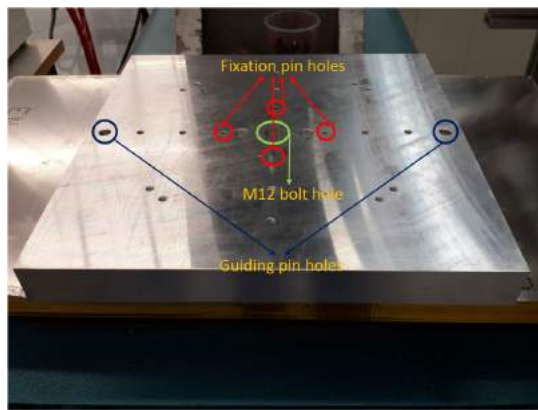
Category	Component	Qty.	Material	N°
Top half	Extension cylinder	×1	Aluminium	1
	Top mounting plate	×1	Aluminium	2
	Rubber mould box	×1	Aluminium	3
	Rubber mould	×1	Bi-component silicone	4
Bottom half	Metal mould	×1	Aluminium	5
	Lateral constraining block	×2	Aluminium	6
	Frontal constraining block	×2	Aluminium	7
	Rubber pads	×4	Bi-component silicone	8
	Protection plate	×7	Aluminium	9
	Cover plate	×1	Aluminium	10
	Insulating block	×4	Marinite I	11
	Insulating connector	×1	Marinite I	12
	Bottom mounting plate	×1	Aluminium	13
	Ring	×4	Aluminium	14
	Heating plate	×1	Aluminium	15
	Electrical wiring connector	×1	Aluminium	16

### 3.2.1. Extension cylinder

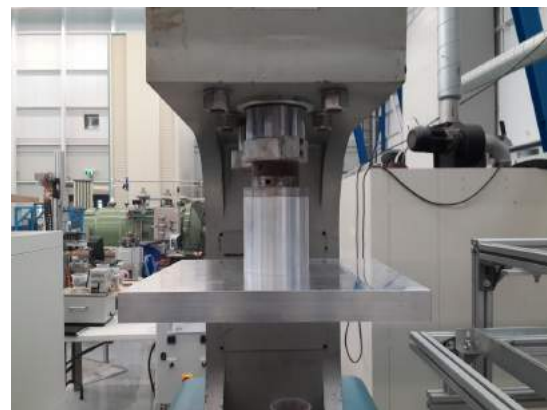
The extension cylinder is mounted on the upper part of the press and its main function is to decrease the distance and time the press has to travel during a forming operation. The distance between the top mould and the laminate becomes smaller, so does the time between the moment the laminate is transferred to the press and the moment it starts being formed. A short time between transferring and pressing a laminate is desired to avoid its temperature from dropping too much. If temperature drops significantly, defects such as out-of-plane fibre buckling [23, 49] caused by the inability of plies to slip with respect to each other [12, 16–18] may occur.

### 3.2.2. Top mounting plate

The top mounting plate is joined to the extension cylinder and its function is to mount the rubber mould box. The mounting plate is designed such that the rubber mould box can be mounted into two different positions perpendicular to each other, thus providing some freedom in the way moulds can be fixed. The plate also contains two holes to fix the guiding pins, used to align the upper and lower moulds. Finally, fixation pins are used to guarantee full alignment between the moulds. In Figure 3.6a, four fixation pin holes are marked in red. The holes used for the insertion of the guiding pins and the M12 bolt, used to fix the plate to the extension cylinder, are marked in purple and green respectively. Figure 3.6b depicts the plate connected to the extension cylinder.



(a) Top mounting plate with fixation pin holes, guiding pin holes and hole to join extension cylinder



(b) Top mounting plate joined to extension cylinder

Figure 3.6: Top mounting plate

### 3.2.3. Rubber mould and rubber mould box

In this setup, the use of a soft-hard die set is preferred due to the flexibility of the rubber which allows it to adapt and accommodate to thickness changes. This feature is extremely important as it is one of the main objectives of this project to investigate the feasibility for manufacturing variable thickness parts via multiple forming steps. Moreover, despite generating rougher surfaces and increasing the friction with respect to the composite material, thereby hindering tool-ply slip deformation mechanisms [19], a rubber mould presents other advantages such as:

- Laminates with multiple thicknesses and shapes with variable thickness can be formed
- A rubber mould doesn't require any external heating. Due to its high specific heat and low thermal conductivity, the rubber mould does not extract a lot of heat from the laminate being formed
- Relatively low cost

The material that was used to produce the mould was a bi-component silicone rubber that vulcanizes at room temperature. The main features that make this rubber adequate for this research are:

1. High accuracy in reproducing small details
2. High tear strength
3. Resistance to high temperatures (up to 200 °C when operating continuously and 300 °C for shorter durations)
4. High elongation at break (350%)

Note that the high temperature resistance is one of the most important features of this rubber. During forming cycles, the rubber makes contact with laminates at high forming temperatures, which in case of GF/PEI is around 320°C. Moreover, the metal mould is also heated to temperatures up to 240°C, so during the consolidation stage of the process the temperature of the laminate and the rubber mould will tend to this value.

During the consolidation stage under pressure and constant temperature, the rubber tends to expand due to its flexibility. Therefore, it becomes necessary to encase the rubber mould in a stiff metal box able to contain the high pressures and prevent it from bulging out and damaging.

In order to prevent the rubber mould from getting stuck due to barrelling effects [12], it is also wise to create sufficiently large gaps between the rubber and metal mould, as depicted in Figure 3.7:

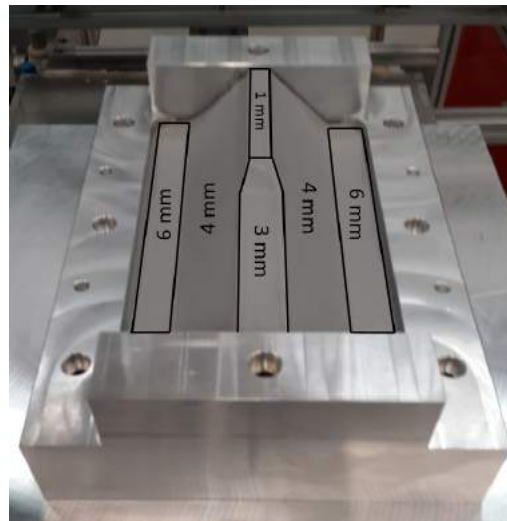


Figure 3.7: Rubber mould and the existing gaps with respect to the metal mould

As shown in the figure, the gap between moulds varies depending on the region. In the web flanks, a 4 mm gap is created in order to avoid the rubber mould from getting stuck due to barrelling effects. This phenomenon is critical because if the mould gets stuck during stamping, consolidation pressure does not build up and large micro-structural defects, such as voids and delaminations, may arise. In the flanges, a 6 mm gap is applied. In this case, it becomes even more critical to have a large gap. During forming and when the press is lowered, if the flanges are not the last regions to be formed, then all the other regions may not be formed. In such a situation, the pressure applied at the flanges would prevent the rest of the material to slide and completely conform into the metal mould's geometry. In other words, a laminate being formed would become clamped at the flanges and as pressure further builds up, the laminate instead of conforming into the mould's geometry, it may rupture, as shown in the following figure:

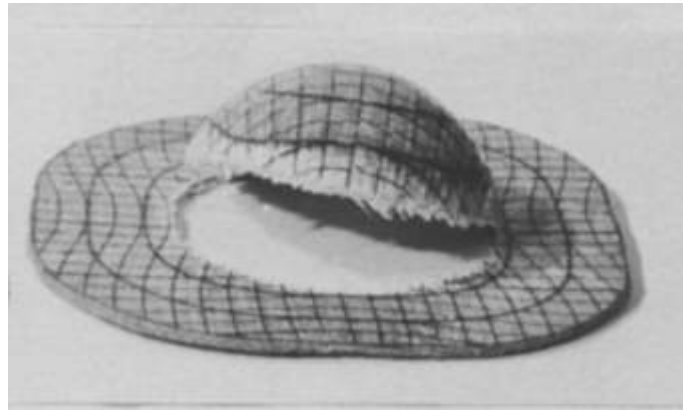


Figure 3.8: Material rupture upon forming with high clamping pressures [20]

With this in mind, consolidation pressure should start building up at the bottom of the product being formed. In this case, because there is a small joggle, it is wise to first fully close the mould at region 1 and then at region 2, as illustrated in the following figure:

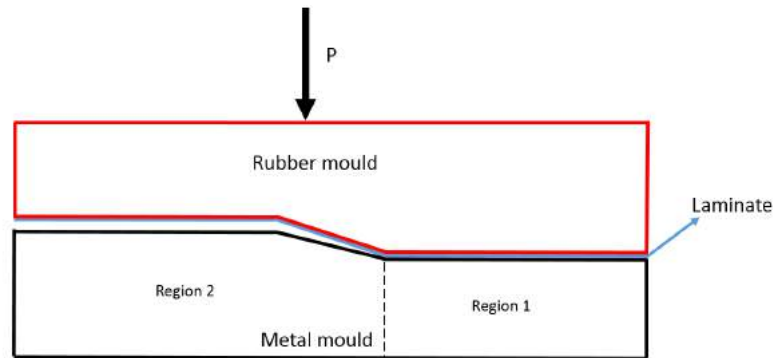


Figure 3.9: Schematic representation of mould closing sequence

Because intra-ply shear must be introduced in the laminate at the joggle region, shear wrinkling or shear buckling defects may arise. To avoid this, not only the blankholder should apply enough tension and the laminate temperature be high enough, but pressing this region after pressing region 1 can also be helpful. By forcing region 2 to be pressed after region 1, potential wrinkles that develop during mould closure can be eliminated, as demonstrated by Haanappel [32, 34]. A schematic representation of the possible scenarios after full mould closure is provided in the following figure:

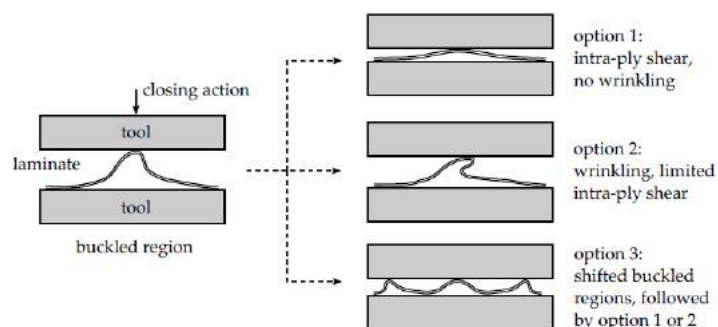


Figure 3.10: Laminate deformations [34]

Hereupon, gaps of 1 and 3 mm between the soft and hard moulds were applied in regions 1 and region 2, respectively. Note that the gaps were chosen through mere engineering judgement and a more

accurate approach would be to perform a FEM analysis with dedicated packages, such as ANIFORM or PAM-STAMP. However, several limitations such as lack of material data at processing temperatures and difficulties in modelling the behaviour of the rubber, make this approach much more involved.

### 3.2.4. Metal mould

In the previous section it was visible that the mould has an *Omega* shape with a small joggle. This resembles the shape of a hat stiffener, a structural element commonly used to reinforce aircraft fuselage and wing skins. This shape was chosen because on one hand it is not as complex as the double-dome benchmark geometry, a geometry commonly used by authors in forming experiments and forming simulations [31, 50] but highly susceptible to shear wrinkling defects. On the other hand, it is a shape where all the deformation mechanisms (inter, intra-ply shear and bending) can be introduced, thus making it possible to study the feasibility of the multiple step forming approach when forming three-dimensional shapes. Furthermore, because the joggle is located at the center of the mould (see Figure 3.11), one can opt for not introducing any intra-ply shear deformation and only use one of the mould halves instead .



Figure 3.11: Metal mould

### 3.2.5. Constraining blocks

Lateral and frontal constraining blocks are used to maintain the metal mould in position and prevent it from misaligning with respect to the rubber mould. The lateral and frontal constraining blocks are mechanically joined to the bottom mounting plate. The frontal constraining blocks also prevent the metal mould from being released from the mounting plate upon pressure removal after forming. When the press goes up after a forming and consolidation cycle there is a chance that, due to laminate sticking to the rubber and metal moulds, the press might take the metal mould with it. To prevent this, a small bolt coming from the frontal constraining block is inserted into the metal mould, as illustrated in Figure 3.12.



Figure 3.12: Constraining block preventing metal mould from being released from mounting plate

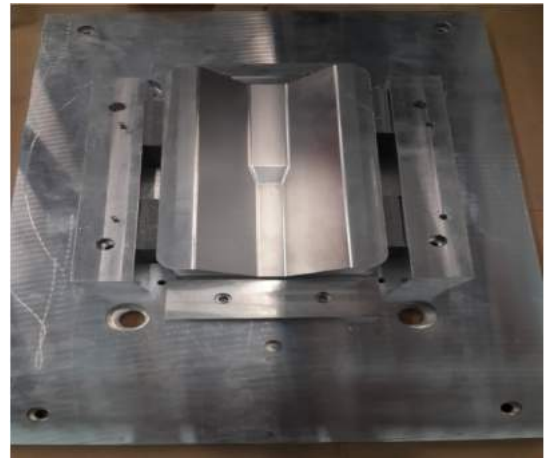
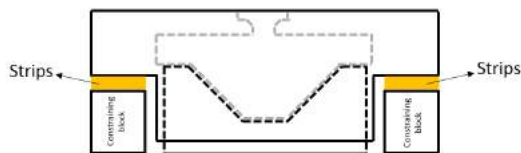


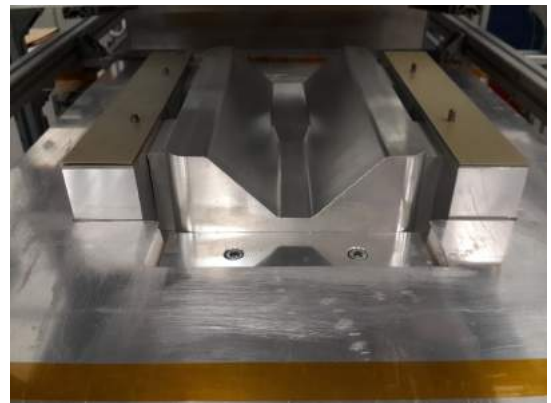
Figure 3.13: Metal mould constrained by blocks and rubber pads

Rubber pads are also placed in between the mould and the lateral constraining blocks, as shown in Figure 3.13. These rubber pads give some freedom of movement to the metal mould, which promotes more uniform consolidation pressures by allowing the mould to move slightly and better adapt its position with respect to the rubber mould.

Finally, the lateral constraining blocks are able to accommodate extra strips of aluminium that act as stoppers and ensure that the upper mould remains in a fully horizontal position when the press is completely lowered. This helps achieving uniform consolidation pressure over the entire surface of the formed laminate by allowing the rubber to expand uniformly. Another advantage of this mechanism is that the thickness of aluminium strips inserted on the constraining blocks can be changed, thereby allowing to adjust the extent at which the press is closed. This mechanism is depicted in Figure 3.14:



(a) Schematic representation of the metal strips acting as stoppers



(b) Lateral constraining blocks with metal strips acting as stoppers

Figure 3.14: (a) Schematic and (b) real representation of metal strips acting as stoppers

### 3.2.6. Bottom mounting plate

Similarly to the top mounting plate, one of the functions of the bottom mounting plate is to mount the metal mould and the elements that constrain it (i.e. constraining blocks and rubber pads). It also has two holes for the guiding pins, similarly to the top mounting plate (see Figure 3.6a). These guiding pins, shown in Figure 3.15, guarantee the alignment between the upper and lower moulds.

The mounting plate also establishes the joining and fixation of the bottom assembly to the press through the use of four M12 bolts. Two of the holes for these bolts are marked in red in Figure 3.15. These holes have a larger diameter than the bolts in order to facilitate the fixation of the bottom assembly to the press. This allows the bolts to move freely a few millimetres and more easily find the correct

location for fixation.

Before fixing the bottom assembly to the press, the upper and lower moulds are aligned. After alignment, the four fixation holes that are used to join and fix the bottom assembly to the press may not be perfectly aligned with the threaded holes in the press. Therefore, by making the fixation holes in the mounting plate with a larger diameter than the bolts, the assembly becomes much simpler. This way, when fixing the bottom assembly to the press, bolts can shift their position and more easily find their way into the threads. Finally, two M8 bolts are also used to join the mounting plate to the heating plate. The holes used for the insertion of these bolts are marked in orange in Figure 3.15.

The mounting plate is in direct contact with the heating plate, which provides the heat input to increase the mould temperature. However, the mould only takes up a small area of the mounting plate and as a result, a lot of the heat generated around the mould is not used and eventually dissipated. To make the heating system more efficient and to prevent a person from coming into contact with a hot plate, the area around the metal mould is covered with a Marinite I insulating block, as shown in Figure 3.16. Due to the high brittleness of this material, an additional aluminium protection plate was then applied to cover it.

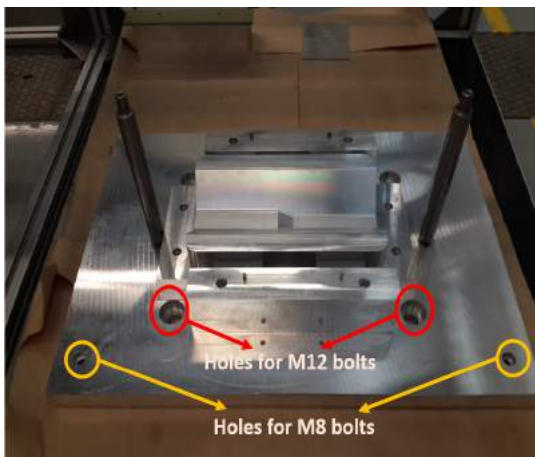


Figure 3.15: Guiding Pins

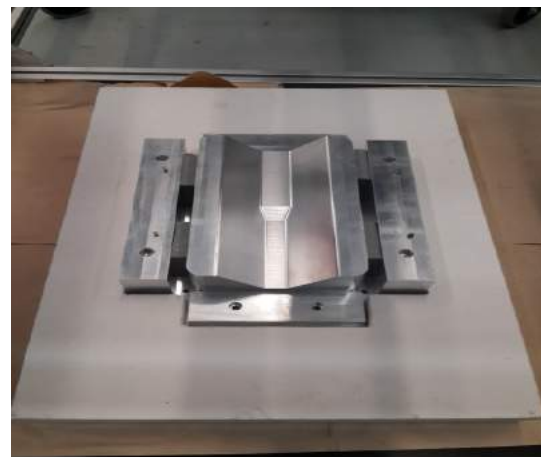


Figure 3.16: Insulating block around metal mould

### 3.2.7. Heating plate

The heating plate is responsible for heating the metal mould through conduction and it determines the metal mould temperature, one of the most important process parameters influencing:

1. Cooling rate of the material, thereby influencing matrix crystallinity (for semi-crystalline matrix systems). A high crystallinity level resulting from lower cooling rates typically results in higher levels of static strength and chemical resistance but lower fracture toughness [51, 52]. In this setup it is not possible to actively cool the metal mould, but with higher mould temperatures the material being formed does not cool down as fast as a material formed with a mould set to room temperature.
2. Material consolidation temperature, which subsequently influences the consolidation quality of the material. A higher consolidation temperature results in less voids [24–26, 48], better fibre compaction and better mechanical properties, such as inter-laminar shear strength [53], flexural and longitudinal modulus and tensile and flexural strength [54, 55]. Moreover, it has been reported by Dutta et al [56] that higher mould temperatures decrease the amount of surface wrinkles and delaminations compared to moulds set to room temperature.

Being able to increase the mould temperature is essential in producing good quality press formed shapes with better mechanical and physical properties and with less micro-structural or macroscopic defects. For the development of the multiple step forming approach, high mould temperatures are also important in order to achieve a high degree of autohesion, or inter-diffusion, at the interface between two laminates formed and co-consolidated in different steps.

When two thermoplastic composite laminates establish intimate contact at a temperature above  $T_g$ , a fusion bonding process takes place through the polymer-polymer interface. Upon the application of pressure and time, the interface gradually disappears through a diffusion process, where the molecular chains move across the interface and develop mechanical strength [57]. The concept of autohesion is then introduced to monitor the level of molecular diffusion. The degree of autohesion is a function of time, pressure and temperature. As higher temperatures promote higher molecular movement across the interface, better bonding can be achieved at shorter times.

The heating plate consists of two aluminium plates with embedded heating elements, as depicted in the following figure:



Figure 3.17: Heating plate with five heating elements

The figure depicts one of the plate halves with five heating elements and their correspondent electrical cables running through the insulating connector, depicted on the right side. These cables are then tight into a single bundle, which then goes through an aluminium "connector" and finally inserted into a metal hose.

Also embedded in the plate are four thermocouples, which are used to measure the temperature of the heating plate at different locations. The readings from one of the two thermocouples located at the center of the plate are sent to a PID controller, which is then used to control the power input to the heating elements. The temperature readings from these thermocouples are chosen as an input for the power controller because they are in the center of the plate, the same region as the metal mould. The other thermocouples, although not used for power control purposes, they are used to monitor the temperature at their corresponding locations if necessary. They also provide some redundancy in case the thermocouples at the centre fail.

On the other plate half, five thermal switches are integrated. Their function is to prevent electrical current from being fed to the heating elements in case temperature exceeds a certain threshold. Each thermal switch is programmed to change its mode (from normally closed to open) at a temperature of  $260 \pm 11 \text{ C}^\circ$ . This was the highest actuation temperature found in the market for such thermal switches. However, trial runs showed that the thermal switches actuate when temperatures of  $245^\circ\text{C}$  are reached. Therefore, to prevent the temperature from reaching this level, a maximum operational temperature of approximately  $240 \text{ }^\circ\text{C}$  was imposed. This ensures that temperature overshoots during heating are not high enough to reach the  $245^\circ\text{C}$  limit.

Thermal switches are placed in multiple cavities located at the center and along the width of the plate, as shown in Figure 3.18. By inserting multiple thermal switches, we make sure that the heating plate at any given location does not overheat.

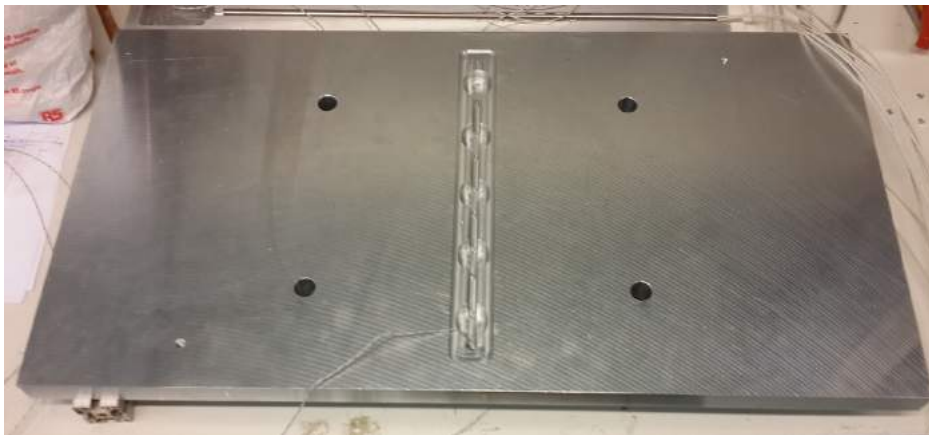


Figure 3.18: Heating plate cavities to insert thermal switches

Once the thermal switches were inserted and properly fixed, they were insulated by placing an UP-ILEX polyimide film around the side walls of the cavity. Then, the cavity was closed with an aluminium protection plate.

A schematic representation of the electrical circuits integrated in the heating plate is presented in Figures 3.19 and 3.20:

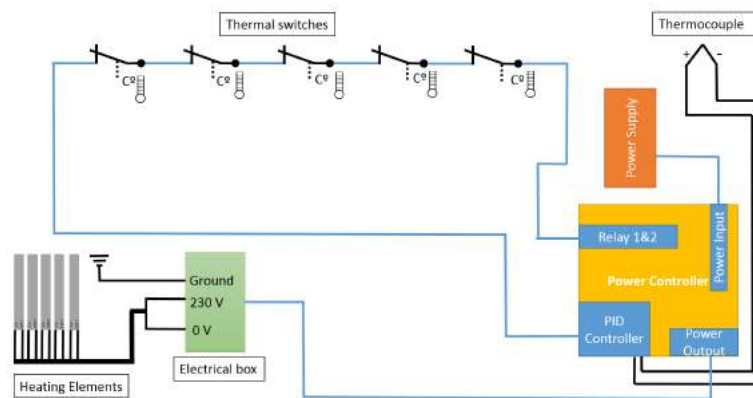


Figure 3.19: Schematic representation of electrical circuit integrated in the heating plate

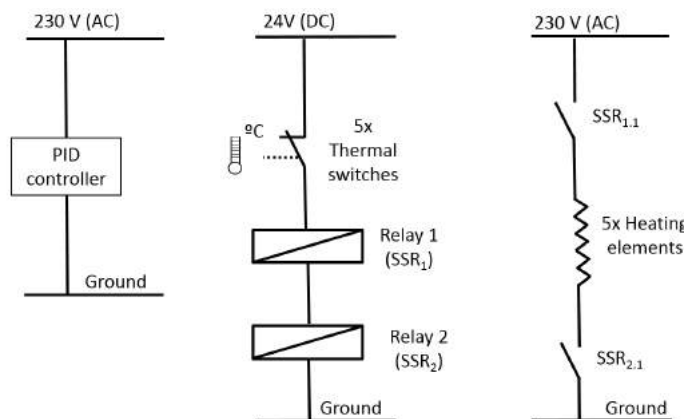


Figure 3.20: Technical representation of electrical circuit integrated in the heating plate

It's visible from the two figures that the five normally closed thermal switches are mounted in

series and connected to two solid state relays ( $SSR_1$  and  $SSR_2$ ) incorporated in the power controller board.

The two normally opened switches,  $SSR_{1,1}$  and  $SSR_{2,1}$  (see third circuit in Figure 3.20), close as soon as the solid state relays 1&2 are switched on. This allows electrical current to be fed to the heating elements. Therefore, when every thermal switch is closed, the relays are activated and current can be fed into the heating elements. However, if one or more thermal switches open, the relays switch off and the  $SSR_{1,1}$  and  $SSR_{2,1}$  switches open, thereby not allowing any current to go to the heating elements.

The thermocouple represented in Figure 3.19 is located at the center of the heating plate. The temperature measured with this thermocouple is read by the PID controller, which then controls the amount of power being fed into the heating elements through the cable connected to the power output. This cable is connected to an electrical box, which is responsible for transferring the power to the five heating elements. A grounding cable is also included in order to avoid electrocution.

Finally, the in-house built power controller is depicted in the following figure:



Figure 3.21: Power controller

### 3.3. Overview of the press assembly

The following figure depicts an overview of the press assembly and its components:

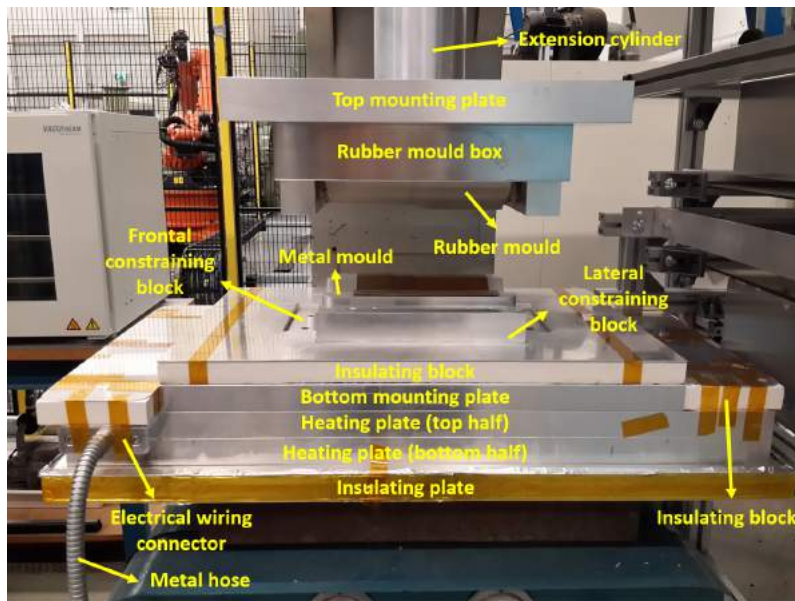


Figure 3.22: Overview of press assembly

Observing Figure 3.22 from the bottom-up, we can see that the first component is an insulating plate, protected all around with high temperature resistant kapton tape and also protected with aluminium sheets on the top and bottom surfaces. Above the insulating plate is the heating plate. Joined on the left side of the top half of the heating plate is the electrical wiring connector, where all the cables from the heating elements are tight into a single bundle. These cables then go through a metal hose, which is then connected to the power output source.

On top of the heating plate are the bottom mounting plate and two insulating blocks on the left and right sides. These two insulating blocks are used to prevent a person from coming into contact with the heating plate when heated to high temperatures. These insulating blocks are also protected on the bottom and top surfaces with aluminium sheets. The bottom mounting plate, where the mould and constraining blocks are fixed, is also protected with an insulating block around it. The metal mould is placed on the mounting plate and constrained by lateral and frontal constraining blocks.

As we move towards the top part of the press assembly we can identify the rubber mould encased in the metal box, which is then fixed to the top mounting plate. Finally, the extension cylinder, which is connected to the top mounting plate and fixed to the press, is also depicted.

As a final remark, the importance of the guiding pins, which are used to align the moulds, must be stressed. In the aligning process, the guiding pins are fixed to the top mounting plate and then the press is lowered. The alignment between the guiding pins and the holes in the bottom mounting plate, marked red in Figure 3.23, is then checked. If there's no perfect alignment, slight adjustments are made to the bottom assembly and the press is lowered again to check if alignment is proper. This procedure is repeated until both guiding pins are able to go through the holes on the mounting plate. Once alignment is achieved, the bottom assembly is fixed to the press through four M12 bolts.

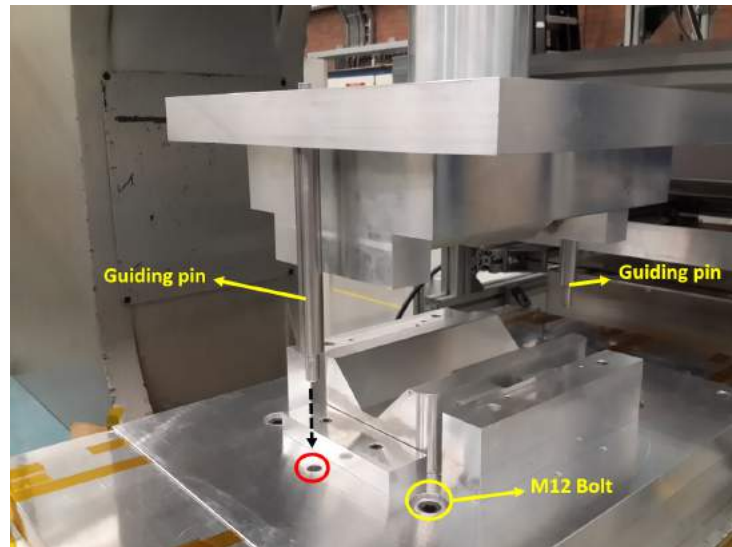


Figure 3.23: Guiding pins fixed to the top mounting plate and M12 bolts used to fix the bottom press assembly to the press

# 4

## Multiple Step Forming of GF/PEI Woven Composite Laminates

Press forming of thermoplastic composites into two and three-dimensional shapes is a commonly applied manufacturing process to produce aircraft structures. One of the materials used for aerospace applications, such as aircraft interiors and secondary structures, is glass fibre reinforced PEI. The high toughness and excellent fire resistance, together with the low moisture absorption and good solvent resistance of this matrix system make this composite material attractive for aerospace applications.

The amorphous PEI polymer has a glass transition temperature of 210°C, 30°C below the maximum temperature that can be achieved in the metal mould. Given the limited temperatures above  $T_g$  that can be achieved, the main objective of this experimental study was to investigate the feasibility of the multiple step forming approach from a formability standpoint. The main research questions that are set out to be answered at the end of this chapter are provided as follows:

1. Is the multiple step forming approach feasible from a formability standpoint?
2. How does the temperature at the interface, rubber and metal moulds develop during the process?
3. Is a tool temperature of 240 °C high enough to produce a strong bond between two formed and co-consolidated blanks?

To answer these questions, four forming experiments with different tool temperatures and consolidation times are performed. Temperature curves of each experimental run are analysed and correlated with experimental observations. The feasibility is then further investigated by producing a demonstrator part manufactured via three forming steps.

## 4.1. Experimental Procedure

### 4.1.1. Materials and blank preparation

The material used in the forming experiments and in the manufacturing of the demonstrator part was a glass fibre reinforced polyetherimide woven composite (GF/PEI 8HS), supplied by Ten Cate Advanced Composites, with a fabric style referenced as US 7781 and a ply thickness of  $0.23 \pm 0.03$  mm.

For the forming experiments, laminates with a [(0/90) (0/90)] stacking sequence were produced by cutting, laying up and subsequently consolidating 580x580 mm stacks of pre-preg in a hot press. The layup process of [(0/90) (0/90)] laminates was carried out by placing the two (0/90) layers in a way that induced warpage after consolidation could be avoided. This is achieved by placing each layer with an opposite curvature direction with respect to each other, as shown in Figure 4.1. For the sake of consistency, pre-preg surfaces corresponding to the inner side of the roll were coincident with the laminates' midplane, while pre-preg surfaces corresponding to the outer side of the roll coincided with the laminates' top and bottom surfaces.



Figure 4.1: Layup schematic representation

After the lay-up, the 580x580 stacks of pre-preg were placed in between two 600 x 600 mm stainless steel plates coated with release agent, and brought to a hot press to perform a consolidation cycle. The consolidation cycle consisted of increasing the temperature to 320 °C, holding it for 10 minutes before applying a 20 bar pressure, maintaining 320 °C and 20 bar for 15 minutes and then cool down under pressure until temperatures reaches 40 °C. This cycle is schematically represented in Figure 4.2:

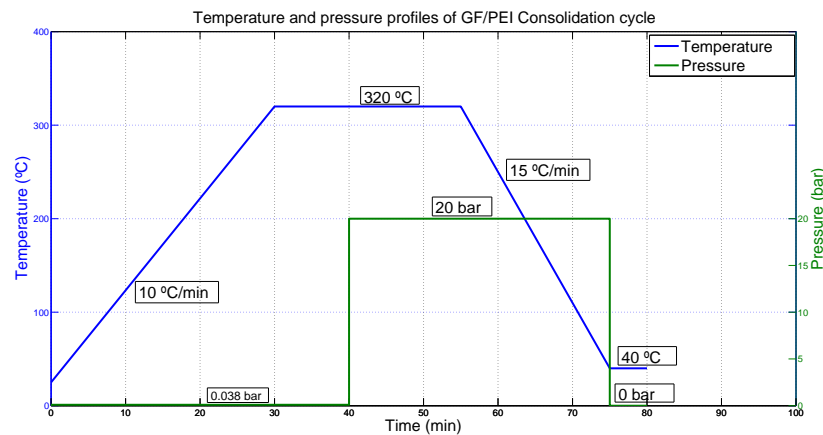


Figure 4.2: Consolidation temperature and pressure profiles of GF/PEI laminate

Once 580x580 laminates were consolidated, 335x210 mm and 335x110 mm blanks were cut using a Darley guillotine. The warp and weft directions coincided with the width and length directions of the blanks respectively, as illustrated in the following figure:

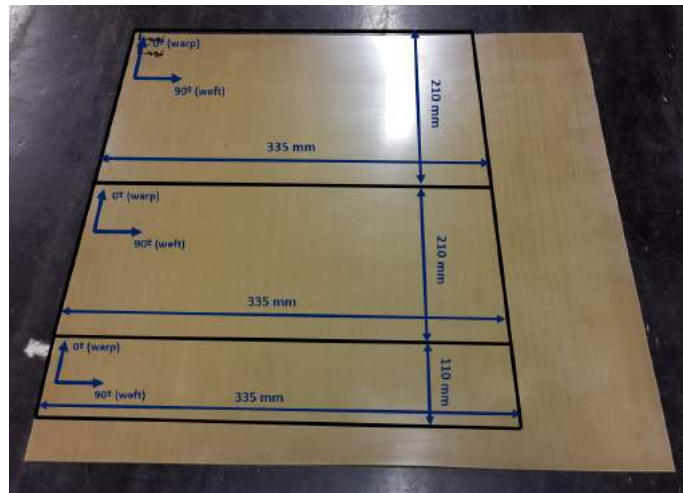


Figure 4.3: Blank cutting layout

For the manufacturing of the demonstrator part, 335x195 mm, 335x105 and 335x55 mm blanks were cut. The 335x195 mm and 335x55 mm blanks were cut from a 580x580 mm [(0/90) (0/90)]<sub>s</sub> laminate, consolidated with the same temperature and pressure profiles as shown in Figure 4.2. The 335x105 mm blank was cut from a 580x580 mm [(±45) (±45)]<sub>s</sub> laminate, also consolidated under the same conditions as shown in Figure 4.2.

Blanks used for the forming experiments and the manufacturing of the demonstrator were sanded using P800 grinding paper and water in order to remove release agent residue on the surfaces which could affect the co-consolidation bond quality. Then, blanks were dried for at least 12 hours at 130 °C in order to remove absorbed moisture and prevent air pockets from arising when blanks are heated in the IR oven prior to being press formed. Note that these time and temperature levels were chosen based on results from a preliminary trial, where no air pockets were observed during the heating process in the IR oven.

#### 4.1.2. Press Forming

Four forming experiments were performed, where the values for tool temperature and consolidation time were varied, while maintaining a constant pressure. The rubber mould temperature was kept at approximately room temperature. The parameters used in each forming experiment are summarized in the following table:

Table 4.1: Parameters used in forming experiments

Run	Mould Temperature (°C)		Pressure (bar)		(Co) Consolidation time (min)		Blank dimensions (mm)	
	Step 1	Step 2	Step 1	Step 2	Step 1	Step 2	Step 1	Step 2
1	220	N/A*	40	N/A*	5	N/A*	335x210	N/A*
2	220	N/A*	40	N/A*	15	N/A*	335x210	N/A*
3	240	240	40	40	5	15	335x210	335x110
4	240	240	40	40	5	45	335x210	335x110

\*Unable to perform forming step n°2, as will be explained in section 4.2

Each forming step consisted of five stages, where (1) the blank clamped in the blankholder was manually transported from the forming station to the IR oven, (2) heated up to approximately 320 °C, (3) manually transported to the forming station, (4) formed and (5) (co-)consolidated under pressure.

A schematic representation of processing stages 2-5 together with laminate and moulds' temperatures is given in the following figure:

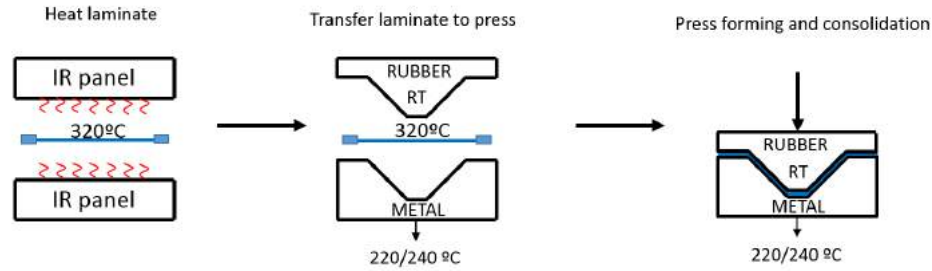


Figure 4.4: Press forming stages and indication of laminate and moulds' temperatures

After forming and while blanks were being (co-)consolidated under pressure, springs from the blankholder were removed. This procedure must be done since the tension exerted by the springs causes laminate springback and release from the mould once consolidation pressure is removed.

Two forming steps were performed in experimental runs n°3 and n°4, whereas only one forming step was performed in experimental runs n°1 and n°2. The second forming step could not be performed in these runs because of springback effects in the laminate, which led to its release and misalignment with respect to the metal mould. This phenomenon will be further explained in section 4.2.2.

Blank dimensions were varied between the 1<sup>st</sup> and 2<sup>nd</sup> forming steps in order to produce a variable thickness shape. Mould temperature values of 220°C and 240°C were chosen because these are above the glass transition temperature of the PEI matrix (210 °C), the threshold at which it becomes possible to co-consolidate and bond two laminates. Due to maximum temperature limitations imposed by the thermal switches integrated in the heating plate (see section 3.2.7), the temperature of the metal mould could not be further increased.

A constant pressure level of 40 bar was chosen for all experimental runs. This high value ensures that any potential weak bond between co-consolidated and formed laminates can be attributed either to a not sufficiently high temperature or to a short co-consolidation time.

A consolidation time of 5 minutes was applied in experimental run n°1 because it is a rather short time and it was one of the objectives to determine if such a short time, combined with a tool temperature of 220°C, was sufficient to enable the execution of a second forming step. In run n°2 the consolidation time was increased to 15 minutes in order to determine if higher laminate temperatures could be reached during the consolidation stage compared to the temperatures obtained in run n°1. Ultimately, the goal was to see if a slight increase in temperature was efficient in enabling a second forming step.

In runs n°3 and n°4 long co-consolidation times of 15 and 45 minutes were applied to make sure that poor co-consolidated bonds would not be negatively affected by short co-consolidation times and (2) to qualitatively assess if a 45 minute co-consolidation time yields in a significant improvement of bond quality.

In experimental runs n°3 and n°4, cooling of the material under pressure started after the co-consolidation time in the second forming step was reached. Cooling was achieved by switching off the power output to the heating elements. Pressure was removed when the metal mould temperature reached 170 °C, 40 °C below  $T_g$  of the PEI matrix. After pressure removal, formed shapes were removed from the mould and further cooled down through free surface convection.

A demonstrator part consisting of three regions with different thicknesses and stacking sequences was also manufactured by press forming three blanks in three different steps. The three blanks that were used to manufacture the demonstrator comprised of four plies. The fibre orientation of the blank formed in step 2 was different from blanks formed in steps 1 and 3. This was to prove that shapes with variable fibre orientation can also be obtained through a multiple step forming process.

The parameter configuration used in the manufacturing of the demonstrator is summarized in the following table:

The base layup of the part was the same as the layup of the laminate formed in the 1<sup>st</sup> forming step, thus [(0/90) (0/90)]<sub>s</sub>. Then, the first reinforcement region had a [(0/90) (0/90) (0/90) (0/90) (±45) (±45) (±45)] layup, which was obtained by forming and co-consolidating the blank formed in

Table 4.2: Demonstrator manufacturing parameters

Step n°	Mould Temperature (°C)	Pressure (bar)	(Co) Consolidation time (min)	Blank dimensions (mm)	Blank layup
Step 1	240	40	5	335x195	[(0/90) (0/90)] <sub>s</sub>
Step 2	240	40	5	335x105	[(±45) (±45)] <sub>s</sub>
Step 3	240	40	45	335x55	[(0/90) (0/90)] <sub>s</sub>

the 2<sup>nd</sup> step to the base laminate. Finally, the second reinforcement region had a 12-ply [(0/90) (0/90) (0/90) (0/90) (±45) (±45)]<sub>s</sub> layup, which was obtained by forming and co-consolidating a [(0/90) (0/90)]<sub>s</sub> blank over the first reinforcement region.

Similarly to experimental runs 3 and 4, cooling under pressure began after the 45 minute co-consolidation time in step 3 was reached. When the mould reached 170°C, the shape was removed from the mould and further cooled down through free surface convection.

#### 4.1.3. Temperature measurements

In the four forming experiments, temperatures were measured and recorded from the moment the blank was transported to the IR oven until the moment consolidation pressure was removed. Rubber and metal mould temperatures were measured in both the first and second forming steps. Blanks' top and bottom surfaces temperatures were also measured in the first forming step. In the second forming step, the interface temperature between blanks formed in the first and second steps was measured with two thermocouples: one instrumented at the top surface of the blank formed in the 1<sup>st</sup> step and another one instrumented at the bottom surface of the blank formed in the 2<sup>nd</sup> step.

Temperatures were recorded every 2 seconds with a Keithley data acquisition system. The following figures illustrate the location at which thermocouples were instrumented and how the thermocouples were connected to the data acquisition system:

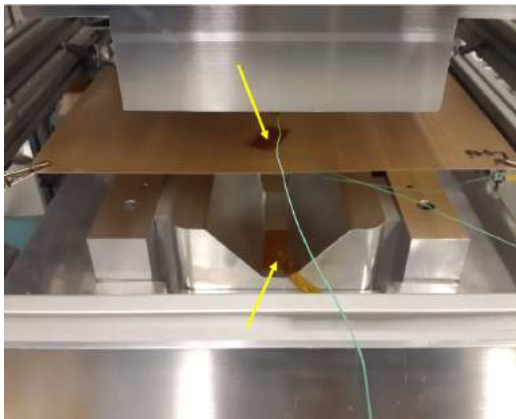


Figure 4.5: Thermocouples instrumented at the bottom surface of the metal mould and at the center of the laminate to be formed in the first step

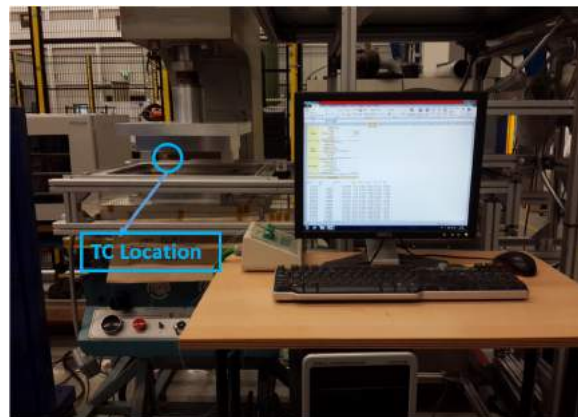


Figure 4.6: Data acquisition system and thermocouple instrumented on the side wall of the rubber mould

#### 4.1.4. Microscopy

Samples from multiple step formed shapes in experimental runs n°3 and n°4 were cut from the flanges with a diamond blade and then dried in the oven for 3h at 130° to remove absorbed moisture during the water cooled cutting process. The temperature level of 130°C was applied based on successful preliminary trials in removing moisture in GF/PEI laminates at this temperature level.

After drying, samples were embedded in fast-curing Technovit 4071 resin for cross-section microscopy analysis. After curing, samples were sanded with 180, 320, 1000 and 2400 grinding paper

and then polished with 6, 3 and 1  $\mu\text{m}$  cloth and 6, 3 and 1  $\mu\text{m}$  diamond paste. Cross-sectional observations were then performed with a Leica optical microscope with 10x magnification.

## 4.2. Results and Discussion

### 4.2.1. Temperature curves

Temperature curves from the first experimental run (see Figure 4.7) show that, at the moment the blank is formed, both the metal and rubber mould temperatures increase rapidly. In the metal mould, where the initial temperature before pressing was around 185 °C, temperature quickly raised to 210 °C followed by a steady increase to 214°C. The initial temperature before forming is well below the setpoint temperature of 220°C due to the fact that the thermocouple does not have perfect contact with the mould. Temperature after pressing then increases because perfect contact of the thermocouple with the mould is established. However, the 220°C setpoint temperature is never achieved during the process because the rubber mould temperature, despite increasing significantly after pressing as well, still remains at a much lower level due to its low ability to absorb heat. As a result, the colder rubber mould cools down not only the metal mould but also the laminate, thus disabling the whole system from achieving 220°C during the 5 minute consolidation stage.

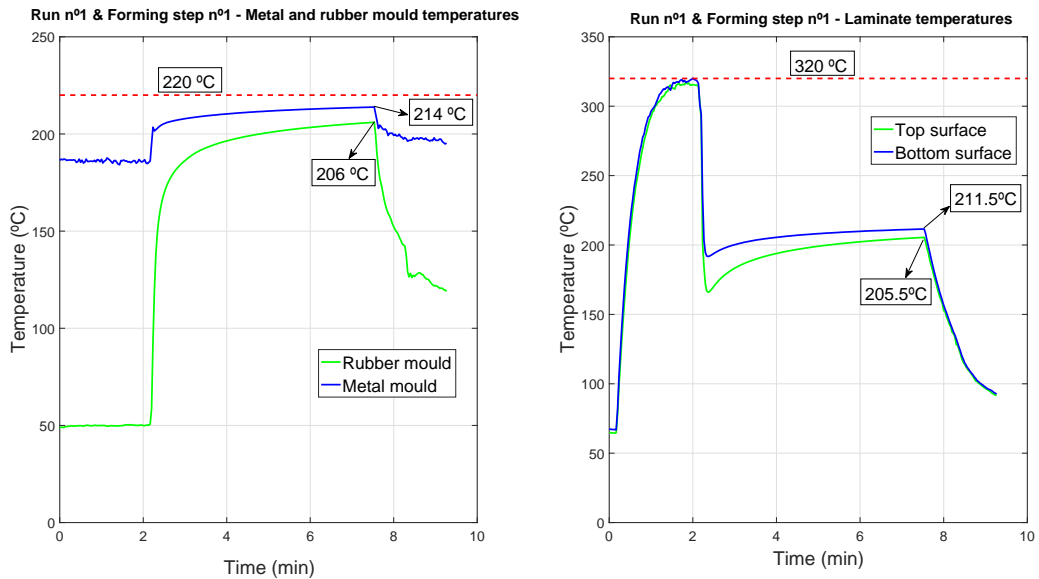


Figure 4.7: Experimental run n°1 & Forming step n°1 - Laminates and moulds' temperature curves

In the following figure, a representation of the different heat sources is depicted:

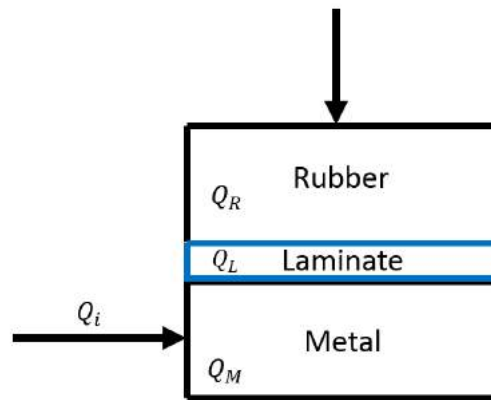


Figure 4.8: Heat sources during the consolidation stage of a press forming process

The metal mould is actively heated through the heat source  $Q_i$  and stores a certain amount of energy,  $Q_M$ . The energy stored in the laminate,  $Q_L$ , is very small in comparison to  $Q_M$  due to the very small mass of the laminate. Before forming, if we assume the rubber mould to be at room temperature, then its energy,  $Q_R$ , is zero (considering reference temperature to be room temperature). When the three components (metal mould, rubber mould and laminate) make contact, the system will tend to an equilibrium temperature. Due to the greater mass of the metal mould, its high thermal conductivity and ability to absorb heat (compared to the laminate and rubber mould), the equilibrium temperature will tend to be slightly below the metal mould temperature.

It is visible from Figure 4.7 that laminate temperatures are affected by temperature differences between the rubber and metal moulds. The laminate's bottom surface temperature is higher than the top surface's during the consolidation stage of the process. Moreover, a temperature difference of 30°C is observed at the moment of stamping. This difference should be minimized because it may induce large differences in the forming behaviour between the top and bottom plies of the laminate, residual stresses or the occurrence of defects such as fibre buckling due to hindrance of the inter-ply shear deformation mechanism.

The drop in temperature at the moment of stamping was sufficient to bring the laminate below the  $T_g$  of the PEI matrix. This is not convenient given that the material formability decreases significantly when its temperature drops below  $T_g$  and performing a co-consolidation in a subsequent forming step would not be possible since temperature takes too much time to go beyond  $T_g$ . Ideally, laminate temperatures should always be kept at a level equal or higher than tooling temperature. This may be achieved by decreasing the transferring time of the laminate from oven to the press or by using a different tooling material, with lower ability to absorb heat.

Temperature curves measured in the second experimental run are depicted in Figure 4.9:

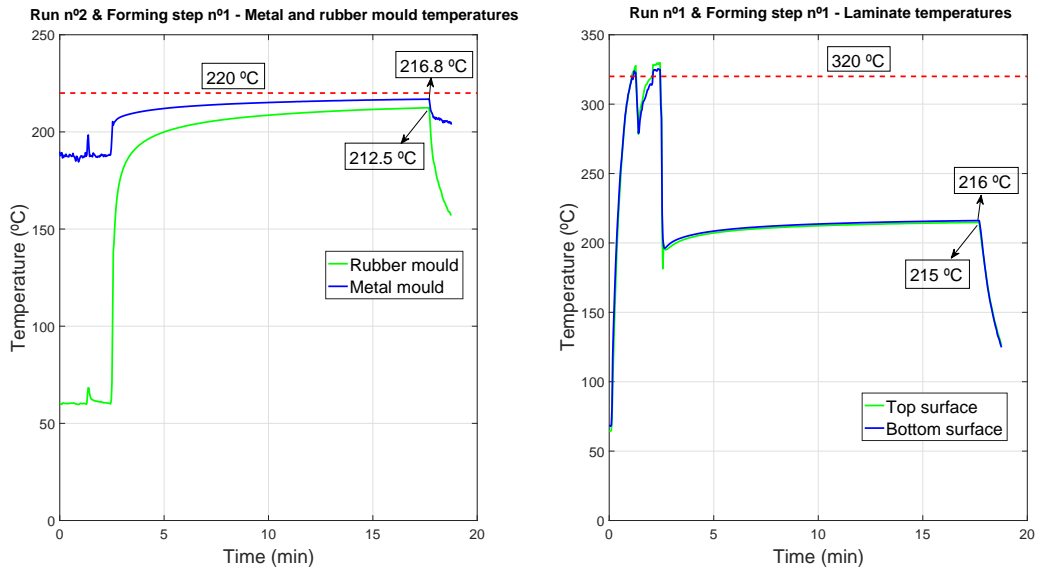


Figure 4.9: Experimental run n°2 & Forming step n°1 - Laminates' and moulds' temperature curves

A drop in laminate temperature is observed at the same time there is an increase of rubber and metal mould temperatures during the heating process of the blank. This temperature discontinuity occurred when the blank was transported to the press but unsuccessfully formed due to a small malfunction in the press. As a result, the blank had to be transported back to the oven before the malfunction was repaired and then brought back to the press to be formed again.

Except from this behaviour, the overall trends of these curves are the same as the curves from the first experimental run. Metal and rubber mould temperatures increased quickly upon forming, followed by a steady increase to 216.8°C and 212.5°C, respectively, thus slightly higher than the maximum temperatures achieved in the first experimental run. This increase in maximum temperature is attributed to the increased consolidation time.

According to laminate temperature curves, maximum temperatures of bottom and top surfaces were 215°C and 216°C, respectively, at the end of the consolidation stage, thus higher than the temperatures obtained in the first run (205.5°C and 211.5°C). These temperatures, however, were still not sufficient to enable a second forming step, as will be explained in section 4.2.2.

Temperature curves measured in the third experimental run are depicted in Figure 4.10 and Figure 4.11:

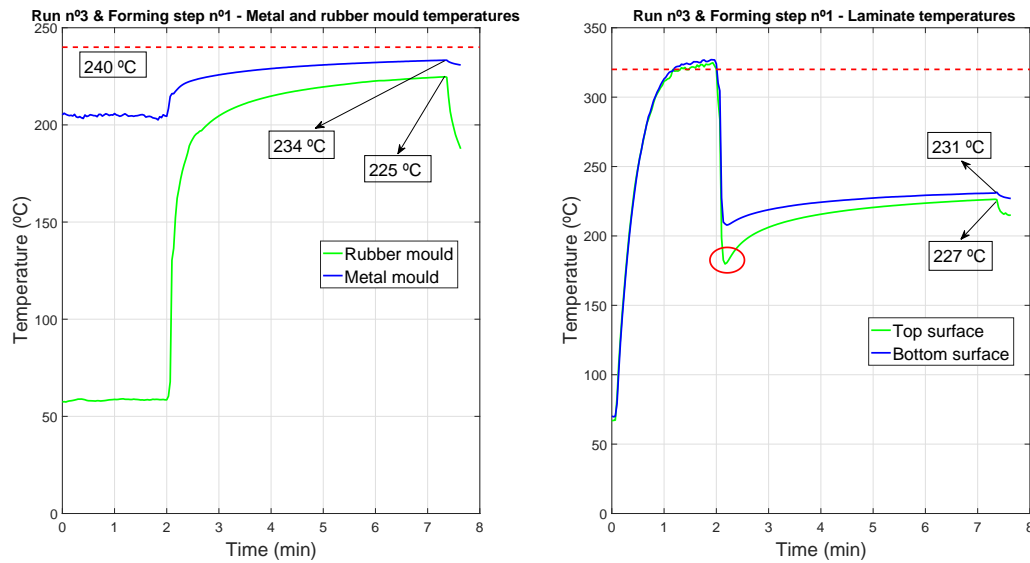


Figure 4.10: Experimental run n°3 & Forming step n°1 - Laminate and moulds' temperature curves

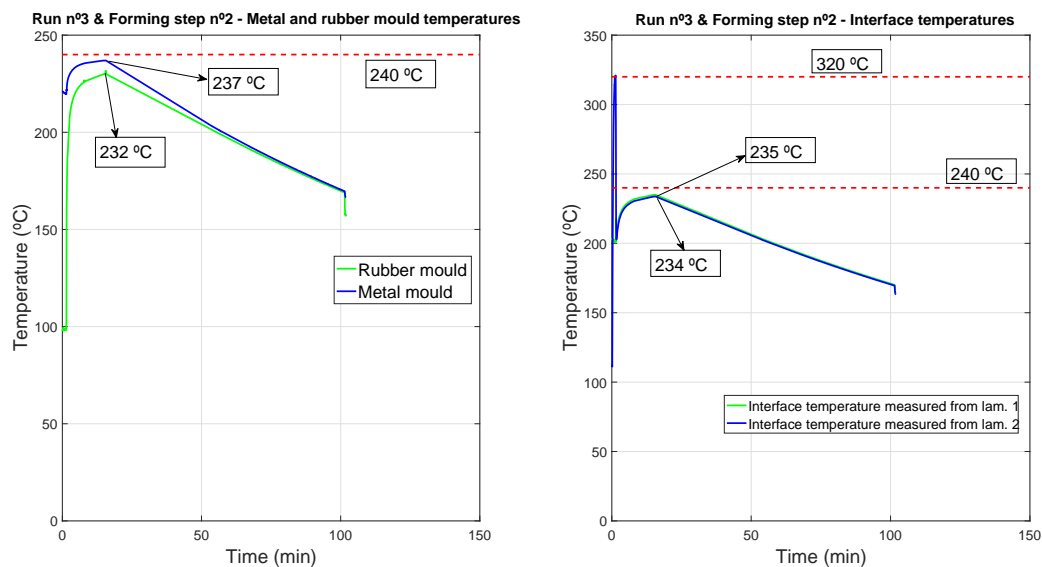


Figure 4.11: Experimental run n°3 & Forming step n°2 - Interface and moulds' temperature curves

Maximum temperatures achieved in the 1<sup>st</sup> forming step were 234°C and 225°C at the metal and rubber moulds, respectively. Temperatures of 231°C and 227°C were achieved at the bottom and top surfaces of the laminate, respectively. Despite the temperature differences, levels were now well above  $T_g$  after 5 minutes consolidation time, which allowed the formed laminate to accurately follow the metal mould's shape after pressure removal. The laminate was kept in position and aligned with respect to the mould, which subsequently enabled a second forming step. This will be further discussed and presented in section 4.2.2. The laminate's top surface, however, dropped below  $T_g$  (see Figure 4.10) at the moment of stamping, while the bottom surface was always kept above  $T_g$ . This indicates a large temperature difference, even larger than the one shown in Figure 4.7, and therefore undesirable for the process.

Due to a longer consolidation time, the maximum temperatures of the rubber and metal moulds were higher in the second forming step (see Figure 4.11). Here, metal and rubber moulds maximum temperatures were 237°C and 232°C, respectively.

Before stamping, the interface temperature measured from laminate n°1 was around 200°C, which is lower than the metal mould temperature. This is due to lack of perfect contact between the thermocouple and the laminate and also between the laminate and the mould. At the end of the consolidation stage, however, interface temperatures of 235°C and 234°C were recorded. This indicates that co-consolidation occurred at least 5°C below the setpoint temperature of 240°C. Therefore, with the current setup, it is wise to take this offset into account in future experiments.

Through these curves, it is also possible to notice that the cooling rate was very low (around 0.85°C/min) due to the inability to actively cool the metal mould. Naturally, this causes a substantial increase in processing time. As a result, active cooling mechanisms should be further investigated so that cycle times can be significantly reduced.

Temperature curves of experimental run n°4 are depicted in Figures 4.12 and 4.13:

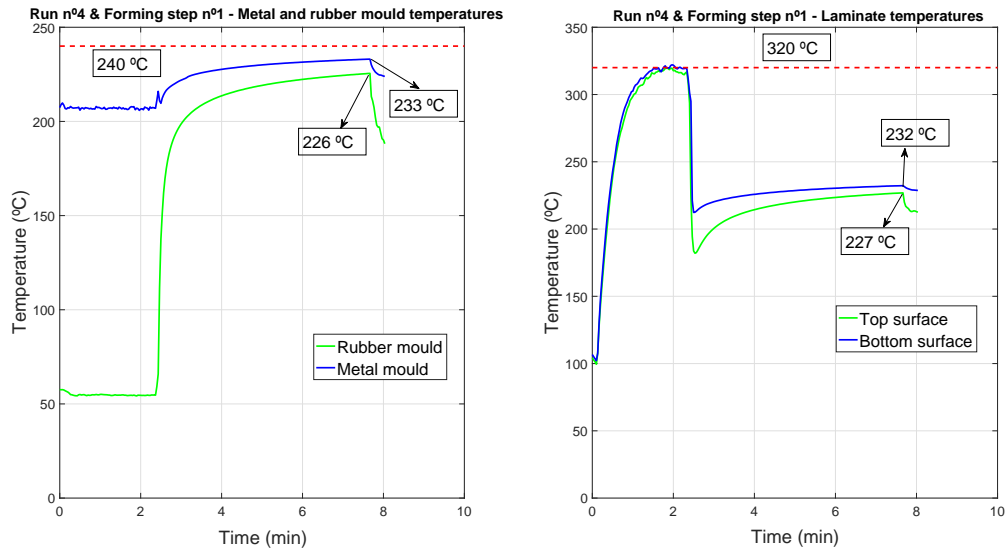


Figure 4.12: Experimental run n°4 & Forming step n°1 - Laminates and moulds' temperature curves

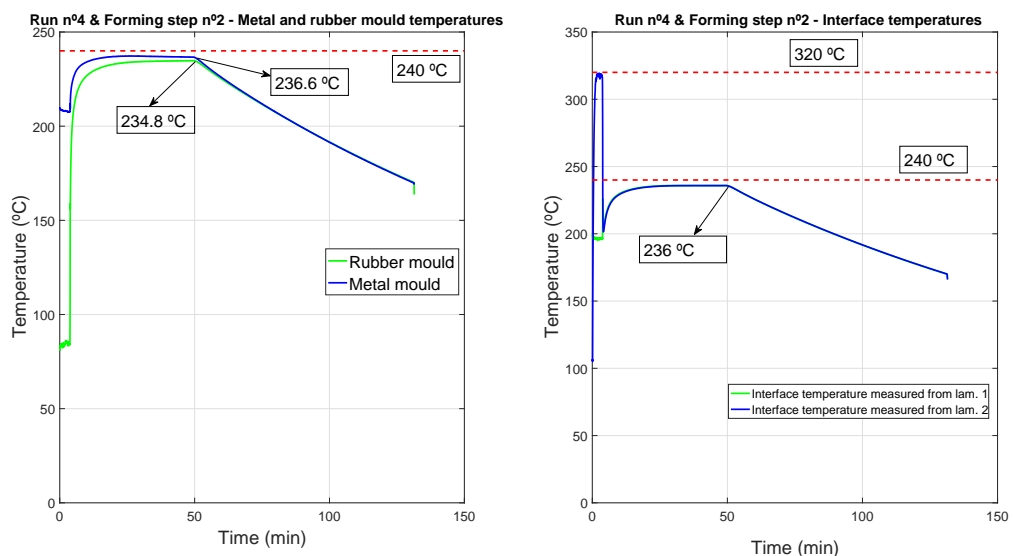


Figure 4.13: Experimental run n°4 & Forming step n°2 - Interface and moulds' temperature curves

Temperature measurements of the first forming step (see Figure 4.12) correlate well with temperature measurements of the first forming step in run n°3. Maximum temperatures achieved in metal and

rubber moulds were 233°C and 226°C respectively, thus comparable to the 234°C and 225°C measured in run n°3. Laminate's maximum temperatures were 232°C and 227°C in the bottom and top surface respectively, thus also very similar to the 231°C and 227°C achieved in run 3. This indicates a good level of reproducibility of the experimental setup.

In the second forming step (see Figure 4.13), metal and rubber mould temperatures stabilize at 236.6°C and 234.8°C respectively. The interface temperature measured from both laminates was the same and had a maximum level of 236°C, thus slightly higher than the 235°C temperature achieved in run n°3.

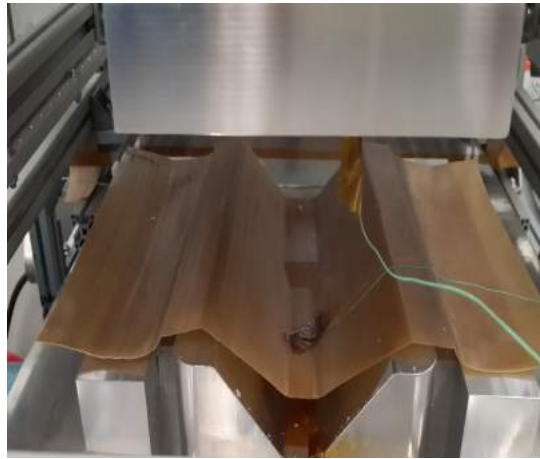
On the basis of the temperature curves presented in this section, the following conclusions are outlined:

1. The laminate surface in contact with the rubber mould has a lower temperature than the surface in contact with the metal mould, thus leading to temperature gradients through the thickness
2. Laminates tend to drop their temperature to levels below  $T_g$  at the moment of stamping. Faster laminate transferring times and different tooling materials (e.g. steel) may help reducing temperature drops
3. Maximum consolidation temperatures increase with longer consolidation times
4. Maximum consolidation temperatures are slightly lower than tooling setpoint temperatures
5. Metal mould active cooling mechanisms should be further investigated, as only a 0.85°C/min cooling rate can be achieved

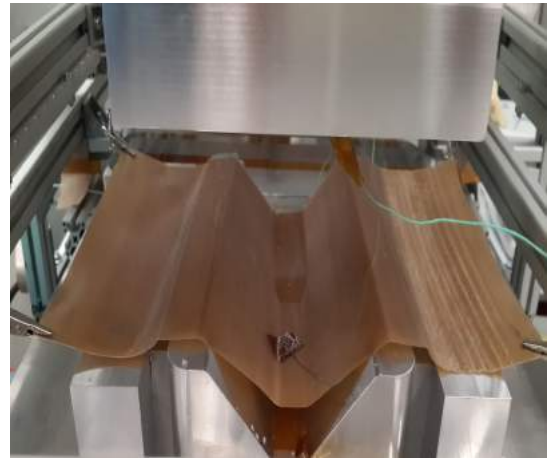
#### 4.2.2. Forming behaviour

As mentioned in the previous section, it was only possible to perform one forming step in runs n°1 and n°2. The second forming step could not be performed because when pressure was removed after the first forming step, formed laminates were released from the mould and sprung back, as shown in Figure 4.14. This led to blank misalignment with respect to the tooling, an essential requirement in performing a second forming step.

The springback behaviour in the formed blank was not anticipated and not common in composites press forming processes. As a matter of fact, spring-in behaviour is usually observed in composites forming processes [36–43] due to thermal shrinkage of the polymer matrix. In this case, however, the laminate built up significant elastic stresses during the forming process. Elastic stresses are generated because the material temperature dropped below  $T_g$  in the first seconds after stamping (see Figures 4.7 and 4.9). The temperature then increased during the consolidation stage, but only just a few degrees above  $T_g$ , and therefore insufficient to release elastic stresses. As a result, when pressure was removed, significant elastic stresses were still stored in the material, which then led to springback behaviour. On the basis of this behaviour, we can conclude that a tool temperature of 220°C is not feasible for the multiple step forming process in PEI based composites.



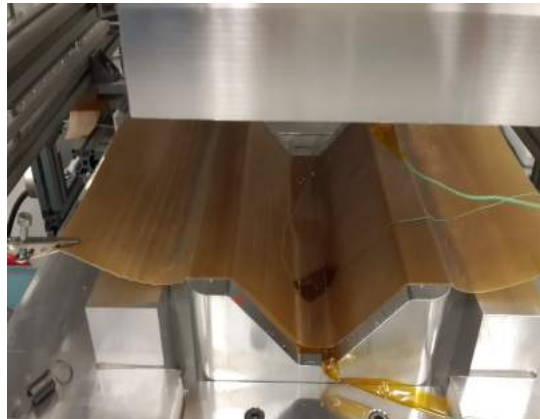
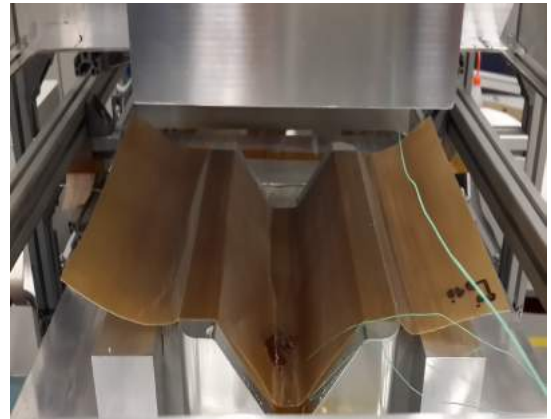
(a) Blank formed in run 1



(b) Blank formed in run 2

Figure 4.14: Blank springback and release from the mould in experimental runs 1 and 2

In experimental runs n°3 and n°4, due to the higher tool temperature, and therefore higher consolidation temperatures, formed blanks were kept aligned and formed accurately according to the metal mould's shape after the first forming step, as shown in Figure 4.15:

(a) Run 3 - Blank formed in 1<sup>st</sup> forming step(b) Run 4 - Blank formed in 1<sup>st</sup> forming stepFigure 4.15: Blanks formed in 1<sup>st</sup> forming step on runs 3 and 4

Formed blanks followed the contour of the metal mould's surfaces quite accurately after pressure removal, but not perfectly. Towards the edges of the formed shape (in longitudinal direction, coincident with the length direction of the mould), the formed corners in the cap region of the formed shapes did not make contact with the metal mould's surfaces after pressure removal. This, however, did not occur at the center region of the mould. At the center, pressure was always present and maximum, but towards the edges, where the rubber mould is not fully constrained and can expand sideways for about 3 mm, pressure was much lower. This non-uniform pressure distribution along the length of the mould was the main driver for the absence of contact between the laminate and the mould's surfaces towards the edges. The lack of consolidation pressure in these regions led to the generation of a larger corner radii towards both edges of the formed shape, as shown in the following figure:

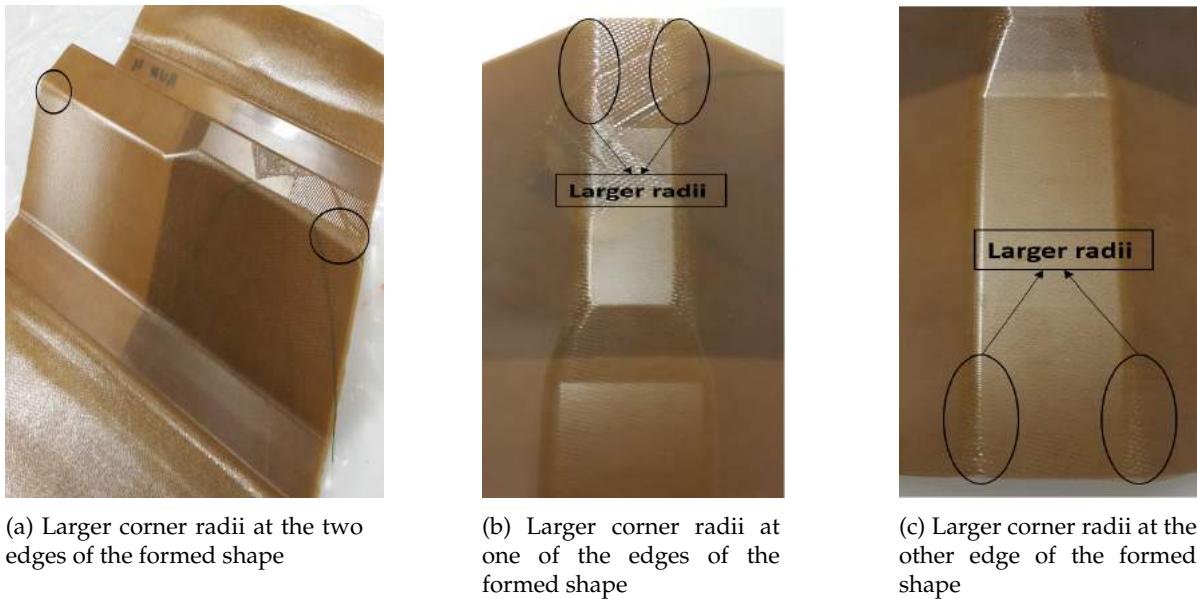


Figure 4.16: Larger corner radii at the two edges of the formed shape

Therefore, pressure distribution is a parameter that must be optimized in the current setup. A possible solution can be to further constrain the rubber mould on both sides, as shown in Figure 4.17, so that sideways expansion can be better prevented.

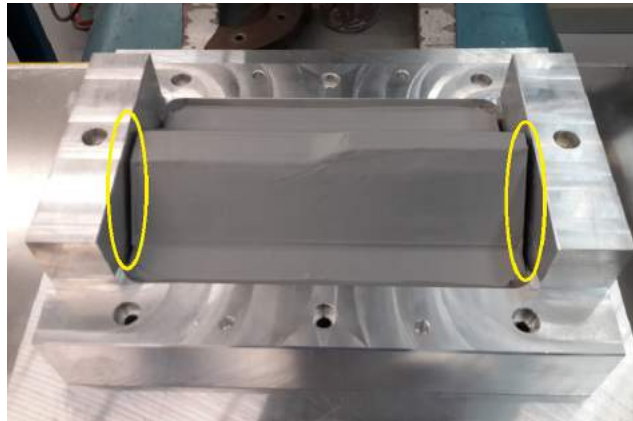
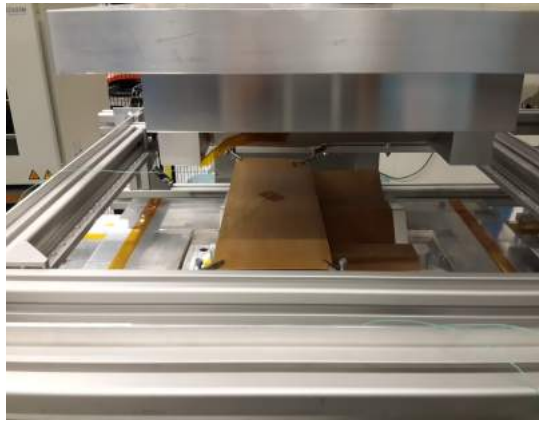


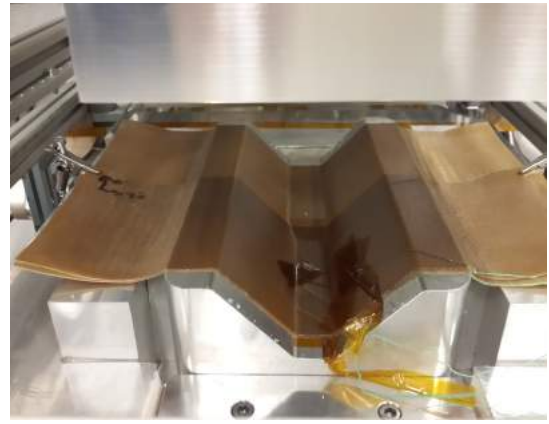
Figure 4.17: Constraint of rubber mould's sides in order to reduce non-uniform pressure distributions

Once sideways expansion becomes restricted, the whole rubber mould becomes constrained, thus forcing it to expand to other locations. This, however, may not be sufficient to fully prevent non-uniform pressure distributions because the rubber compound is quite soft and it might have some difficulty in reproducing sharp corners. As a result, a slightly more rigid rubber can be useful in fully reproducing details, while maintaining the required expansion capabilities which promote more uniform pressure distributions.

Despite the non-uniform pressure distribution along the length of the formed shape, the high pressure at the center region, combined with sufficiently high laminate temperatures above  $T_g$  during the consolidation stage of the 1<sup>st</sup> forming step (see Figures 4.10 and 4.12), were enough to allow the formed laminate to be kept in position and aligned to the metal mould's shape after pressure removal. This, in turn, enabled a 2<sup>nd</sup> forming step, where another blank was appropriately clamped in the blankholder with respect to the first laminate, heated in the IR oven and subsequently formed and co-consolidated to the laminate formed in the first step, as shown in Figure 4.18:



(a) Run 4 - Second blank placed in position for 2<sup>nd</sup> forming step



(b) Run 4 - Multiple step formed shape after pressure removal

Figure 4.18: Multiple step formed shape with 2<sup>nd</sup> blank co-consolidated to 1<sup>st</sup> blank

The second laminate was successfully formed over the first laminate, and potential sticking issues (laminates sticking to each other during the forming stage) were prevented by employing a spring - clamp blankholder mechanism (see Chapter 3 - Figure 3.3). This blankholder system allows the laminate to be draped into the mould without making too much contact with the laminate formed in the first step.

Let's consider two extreme forming scenarios:

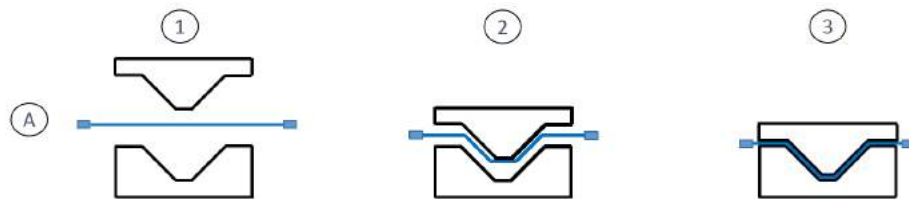


Figure 4.19: Forming scenario A, where blank doesn't make contact with metal mould's surface during forming

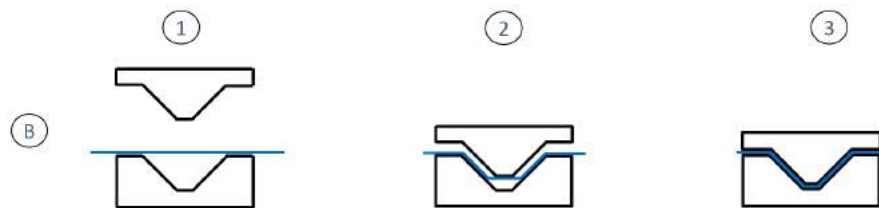


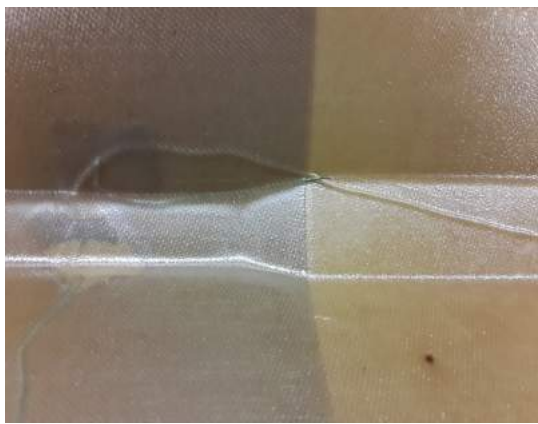
Figure 4.20: Forming scenario B, where blank makes contact with metal mould's surface during the entire forming process

In scenario B, the laminate slides into the metal mould while touching its surfaces, while in scenario A a spring is exerting tension in the clamped laminate, thus forcing it to make contact with the metal mould only when the press is fully closed. The forming behaviour achieved in the performed experimental runs resembles the one from scenario A. As a result, when the second laminate is formed, little or no contact with the first laminate is established, thus preventing them from sticking to each other.

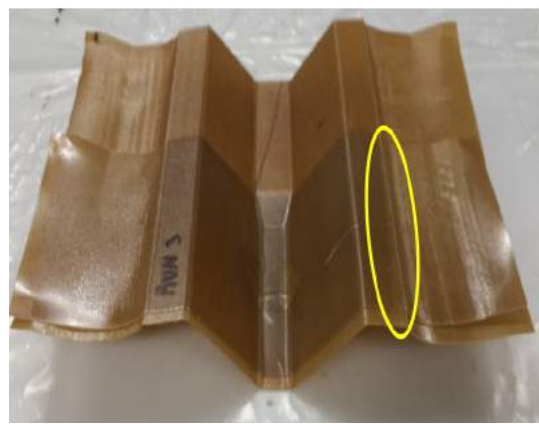
After the multiple step formed shapes in runs 3 and 4 were removed from the mould, a visual inspection was made. No visible defects, such as wrinkling, fibre buckling or ply folding were detected in shapes formed in both runs. A relevant feature worth mentioning is the fact that the joggle region was well reproduced with no sign of wrinkles (see Figure 4.21a), thus indicating the feasibility for forming three-dimensional shapes through the multiple step forming approach.

The defect-free multiple step formed shapes indicate that the blankholder system is efficient in multiple aspects. Springs and crocodile clamps are very efficient in applying tension to the blanks during the forming process such that no defects, like shear wrinkling, are observed. Moreover, forming one laminate over the other is performed with no issues due to the fact that the blankholder prevents the laminate formed in the second step from shearing with respect to the laminate formed in the first step. The blankholder is also capable of accurately positioning the blanks with respect to the tooling. As intended, the thickness transition region began exactly at the beginning of the joggled region. Hereupon, we can conclude that such a blankholder system is suitable for the multiple step forming approach.

In addition to the visual inspection to check for forming defects, the bond between the two formed and co-consolidated laminates was qualitatively assessed. The bond achieved in both runs n°3 and n°4 was very weak and easily peeled off by hand (see discoloration at the peeled off flange in Figure 4.21b). Weak bonds were achieved when applying both a 15 minute and 45 minute co-consolidation time. Therefore, we can conclude that a 240°C co-consolidation temperature is not high enough to generate a strong bond between GF/PEI laminates and that higher temperatures must be applied. With higher temperatures, molecular movement and inter-diffusion across the interface increases, thereby increasing the degree of autohesion and generating a higher bond strength [57–59].



(a) Run 3 - Defect free joggle region



(b) Run 3 - Discoloration at the flange caused by peeling of the co-consolidated bond

Figure 4.21: Run 3 - Multiple step formed shape with (a) no visual forming defects, but (b) with very weak bond

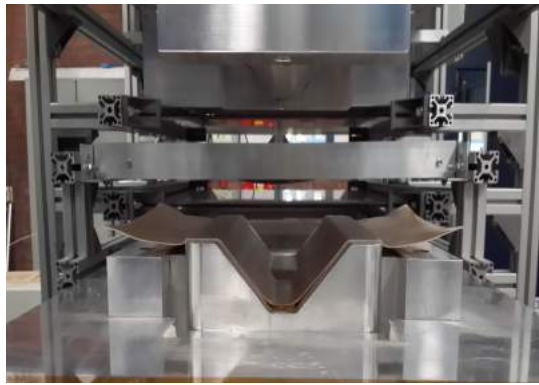
The experimental setup is not able to provide higher tooling temperatures due to the 240°C limit imposed by the thermal switches. As a result, while the multiple step forming concept has been proven from a material formability standpoint, a new strategy is needed to prove that it is possible to achieve a strong co-consolidated bond between formed laminates in different steps. This new strategy, which will form the basis of the work developed in the next chapters, will be discussed later in section 4.3.

### 4.2.3. Demonstrator

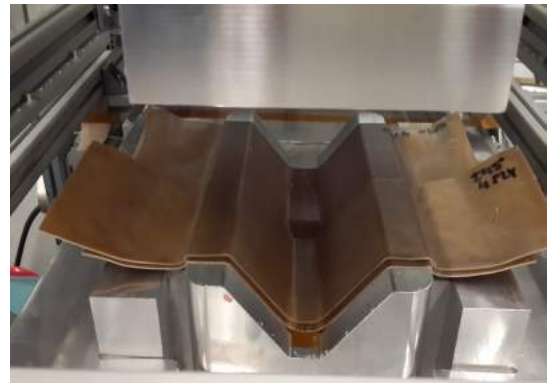
The demonstrator part was successfully manufactured in three forming steps. In each forming step, formed blanks were kept in position and aligned with respect to the tooling, as shown in Figure 4.22. A relevant feature in the manufacturing of this part is the fact that the blank formed in the 2<sup>nd</sup> step was bonded to the first formed blank by applying 5 minutes consolidation time and no cooling under pressure. This means that time-consuming cooling under pressure stages are not required in intermediate forming steps. Thus, rather than waiting for the mould to cool down and heat up again, the 3<sup>rd</sup> forming and final co-consolidation step can be performed just 5 minutes after the second forming step.

This is a relevant feature for the development and implementation of the multiple step forming approach concept. Production cycle times for parts formed in three or more steps can be reduced significantly given that there's no need to perform cooling under pressure after every forming step. Instead, cooling under pressure can be performed only at the last forming and (co-)consolidation step of the process.

Finally, the manufacturing of the demonstrator further proved the feasibility of the multiple step forming approach from a formability standpoint. A  $[(\pm 45^\circ)]_4$  blank was successfully formed with no visual forming defects, thereby introducing a region with variable fibre orientation in the formed shape. Herewith, a part with three different thicknesses and with variable fibre orientation was produced, as depicted in Figure 4.23.



(a) Demonstrator after 1<sup>st</sup> forming step



(b) Demonstrator after 2<sup>nd</sup> forming step

Figure 4.22: Demonstrator part after (a) 1<sup>st</sup> and (b) 2<sup>nd</sup> forming steps, showing accurate dimensional control and alignment with respect to the mould

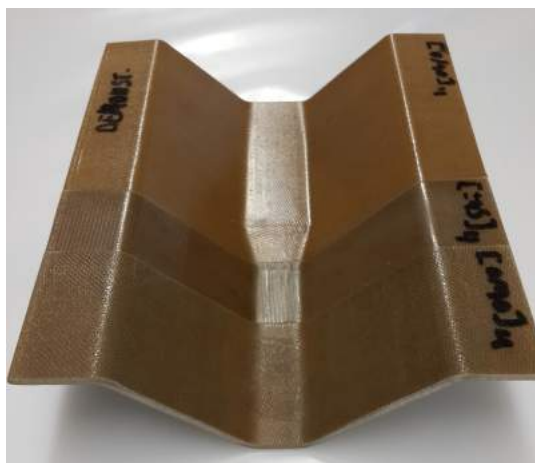


Figure 4.23: Demonstrator part manufactured via three forming steps

#### 4.2.4. Microscopy

Cross-sections of samples taken from the flanges of formed shapes in runs n°3 and n°4 are depicted in Figure 4.24.

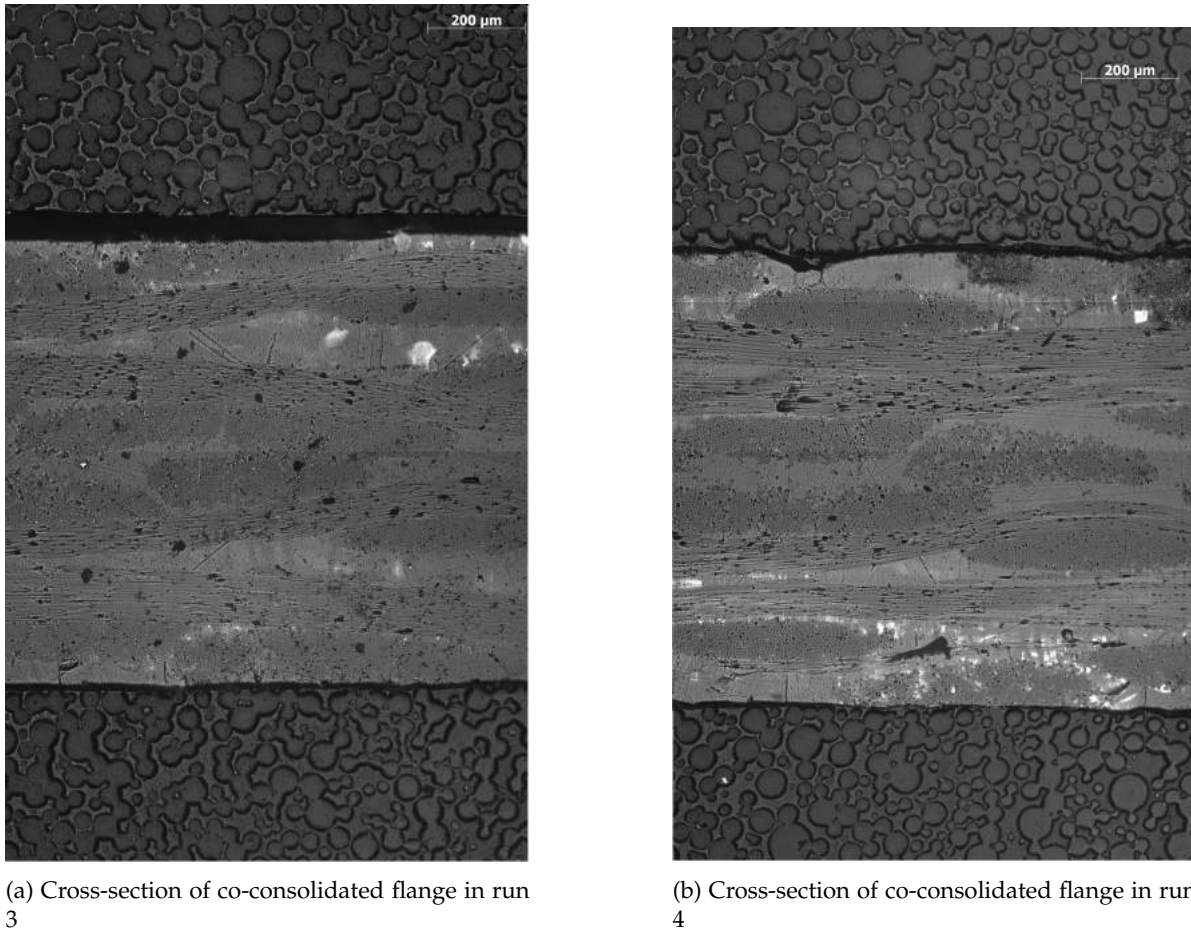


Figure 4.24: Cross-sections of co-consolidated flanges in runs (a) 3 and (b) 4 (10x magnification), showing no evidence of an interface between co-consolidated laminates

Despite the poor co-consolidation quality and weak bond strength, there is no clear evidence of voids or delaminations at the midplane, neither there is a visible distinction of an interface. This makes the qualitative microscopical analysis of this kind of co-consolidated bonds inconclusive when it comes to identifying potential microscopical differences that can justify the weak bond. As a result, in order to provide more conclusive and detailed analysis on the bond quality of co-consolidated laminates, it is necessary to perform mechanical tests. Mode I interlaminar fracture toughness testing was, as will be discussed in the next chapter, the preferred method of quantitatively determining the influence of processing parameters, such as temperature, pressure and time, on the quality of co-consolidated bonds.

### 4.3. Summary

From this experimental study, it is possible to conclude that the multiple step forming concept is feasible from a material formability standpoint, but achieving a high bond strength between co-consolidated formed laminates still remains to be proven. With a tool temperature of 240 °C, GF/PEI composite laminates can be formed in multiple steps without visual defects. However, at this temperature level, a poor quality bond is achieved between formed and co-consolidated laminates.

The inability to co-consolidate and obtain a strong bond between formed laminates in different steps with the current capabilities of the experimental setup leads to the development of a strategy which ultimately can prove the feasibility of the multiple step forming approach for thermoplastic composites. The strategy which forms the basis of the work developed in the next chapter is outlined as follows:

1. Co-consolidate flat laminates using a hot press with different time, pressure and temperature combinations
2. Mechanically test these laminates to determine the mode I interlaminar fracture toughness ( $G_{IC}$ )
3. Compare the  $G_{IC}$  of co-consolidated laminates with the  $G_{IC}$  of preconsolidated laminates and determine the feasible process window
4. Multiple step form GF/PEI laminates and perform a post-consolidation step in a hot press with parameters (pressure, time and temperature) which are within the feasible process window
5. Determine the  $G_{IC}$  of specimens retrieved from the post-consolidated shape and compare it with the  $G_{IC}$  of preconsolidated laminates
6. If the two are comparable, then a strong bond between formed blanks in different steps is achieved and the multiple step forming concept can be proven

## Mode I Interlaminar Fracture Toughness of Co-Consolidated GF/PEI Composites

In Chapter 4 it was determined that a tool temperature of 240°C is not high enough to produce a strong bond between formed and co-consolidated GF/PEI laminates. This means that the multiple step forming approach could not be proven from a structural integrity standpoint, given that very weak co-consolidated bonds would easily lead to the occurrence of delaminations in a structural part when submitted to mode I opening loads, as shown in Figure 5.1 a):

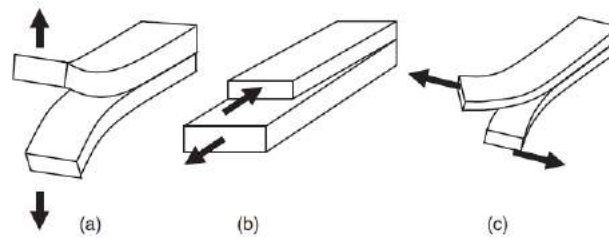


Figure 5.1: Three modes of loading a delamination: (a) opening, (b) shearing and (c) tearing [60]

Naturally, weak co-consolidated bonds would also lead to disbondings when submitted to shearing and tearing loads, as depicted in Figure 5.1 b) and c). This means that mechanical tests able to reproduce either one of these load cases could be suitable for evaluating the interlaminar properties of co-consolidated laminates and to determine how these are influenced by processing temperature, pressure and time.

A test that would potentially be able to characterize interlaminar properties is the Short Beam Shear (SBS) test. In this test, an interlaminar shear load, similar to the one depicted in Figure 5.1 b), is introduced in a specimen by loading it in three-point-bending. The specimen in this test is purposely made very short so that the applied moment is reduced and a longitudinal compressive or tensile failure is prevented. However, preliminary Short Beam Shear tests performed in GF/PEI woven composite specimens according to both ASTM D2344/D2344M [61] and EN ISO 14130 [62] test standards showed that, due to the high interlaminar shear strength of this material relative to its tensile and compressive strength, the interlaminar shear failure could not be produced. Specimens tended to fail predominantly in longitudinal tension, as shown in Figure 5.2, and some cases in longitudinal compression.



Figure 5.2: Longitudinal tensile failure in SBS test specimen

Hereupon, despite the ease of the SBS test and its fast specimen preparation, the mechanical test chosen to evaluate and determine the interlaminar properties of both preconsolidated and co-consolidated GF/PEI woven composites was the Double Cantilever Beam test (DCB), in which the mode I interlaminar fracture toughness ( $G_{IC}$ ) can be determined. This test reproduces the opening load case depicted in Figure 5.1 a) and is able to determine the amount of energy needed to initiate and propagate a crack under mode I opening loads. As a result, one would expect that a stronger bond would result in a higher  $G_{IC}$  value compared to weaker bonds. This test was chosen because the mode I fracture toughness of composite materials is typically lower than the mode II fracture toughness [67], so it is easier to grow and propagate a crack or delamination under mode I loading. As a result, this load case may be considered as the most critical.

In this chapter,  $G_{IC}$  is characterised in both preconsolidated and co-consolidated laminates. In the latter, specimens are produced using different combinations of temperature, pressure and time values to determine the influence of each of these parameters on  $G_{IC}$ . The  $G_{IC}$  of co-consolidated laminates is also compared to the  $G_{IC}$  of reference preconsolidated laminates. Ultimately, this experimental study aims to answer the following research questions:

1. Within the values studied, what is the influence of temperature, pressure and time on the  $G_{IC}$  of co-consolidated laminates?
2. How does the  $G_{IC}$  of co-consolidated laminates compare to the  $G_{IC}$  of preconsolidated laminates?
3. What is the feasible process window that enables the production of co-consolidated laminates with high  $G_{IC}$ ?

## 5.1. Experimental Procedure

### 5.1.1. Preconsolidated laminates

The material used in the mode I interlaminar fracture toughness tests was the same GF/PEI woven composite specified in section 4.1.1. Preconsolidated laminates were produced by cutting, laying up and consolidating a 250x250 mm 14-ply laminate with a  $[(0/90)]_7$ s stacking sequence in a hot press. The layup process was similar to the one described in Figure 4.1 (Chapter 4), where seven (0/90) layers with the same curvature were first laid, followed by other seven (0/90) layers with an opposite curvature. In order to create an initial crack in the laminate, a 250x135 mm and 50  $\mu\text{m}$  thick Kapton film coated with release agent was placed at the midplane of the laminate during the layup process, as depicted in Figure 5.3:

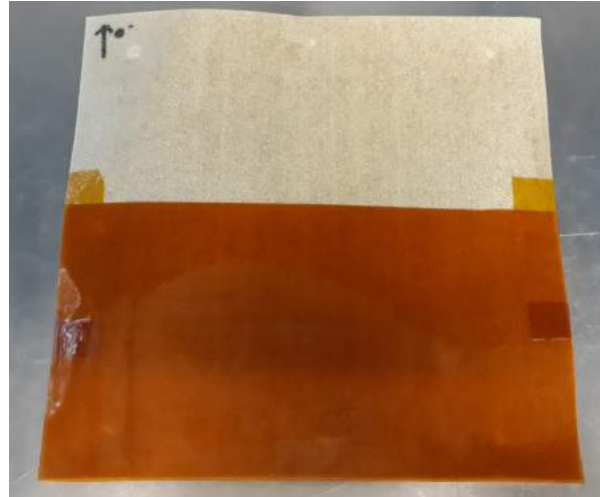


Figure 5.3: Layup of 14-ply laminate with Kapton film inserted at the midplane

The 250x250 mm stack of pre-preg was then placed in between two 275x275 mm stainless steel plates coated with release agent and brought to a hot press to perform the consolidation cycle according to the following pressure and temperature cycle:

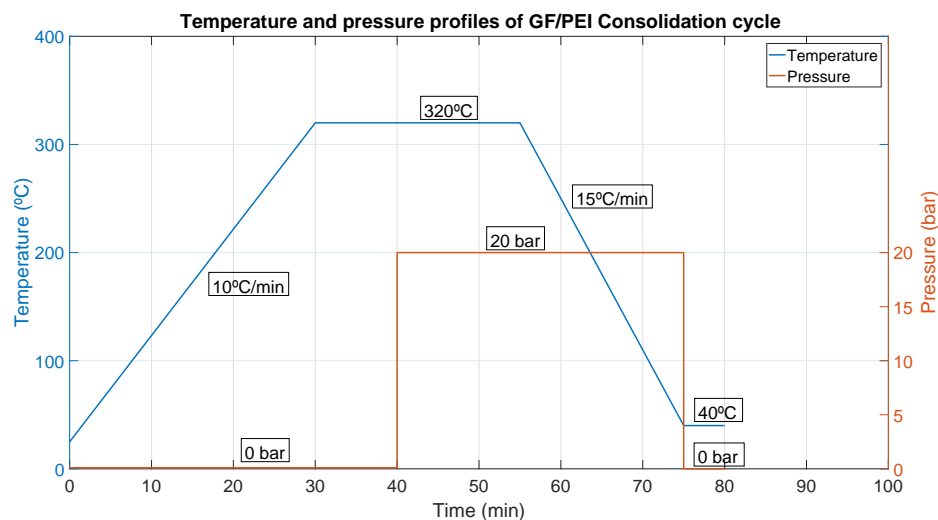


Figure 5.4: Temperature and pressure profiles of GF/PEI preconsolidated specimens

### 5.1.2. Co-consolidated laminates

Co-consolidated laminates were produced by first consolidating 580x580 mm 7-ply [(0/90)]<sub>7</sub> laminates in a hot press according to the temperature and pressure cycle depicted in Figure 4.2 (Chapter 4). The layup process of these laminates was carried slightly differently from the layup process of preconsolidated 14-ply laminates in the sense that all layers were stacked with the same curvature, as shown in Figure 5.5a.

When the 580x580 mm [(0/90)]<sub>7</sub> laminates were consolidated in the hot press, 250x250 mm plates were cut using a Darley guillotine. The surfaces of these 250x250 mm laminates were then ground using P800 sand paper and water in order to remove release agent residue, degreased with isopropanol and then dried for 3h at 130°C to remove absorbed moisture. After drying, pairs of 250x250 mm preconsolidated laminates were assembled according to the scheme depicted in Figure 5.5b, with a 50 μm thick Kapton film inserted at the interface, as shown in Figure 5.5c.

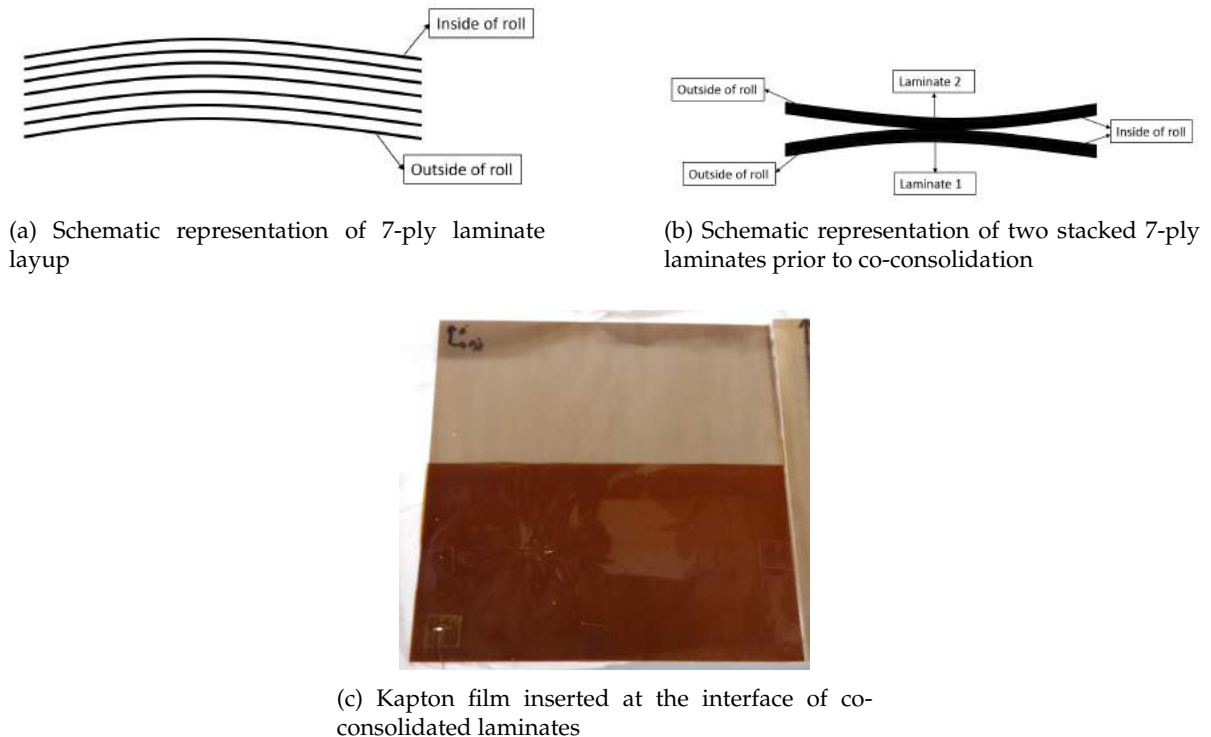


Figure 5.5: Production sequence of 14-ply co-consolidated plates with (a) lay up and consolidation of 7-ply laminate, (b) stacking of two 7-ply preconsolidated laminates with (c) a Kapton insert at the interface

Nine 250x250 mm samples were then submitted to co-consolidation cycles with different combinations of temperature, pressure and time values (see Table 5.1). In order to validate and verify if the setpoint temperature values were achieved during the co-consolidation cycles, the laminates co-consolidated with parameter configuration n°3 (see Table 5.1) were instrumented with a type K thermocouple at the interface and temperatures were recorded by using a Keithley data acquisition system. Temperature measurements were performed in this cycle because it was one of the cycles with the highest co-consolidation temperature, thus more likely to have larger temperature deviations.

Note that in every co-consolidation run, pressure was not applied right after the setpoint temperature was reached but rather 10 minutes later so that the temperature level could stabilize before applying pressure. With this in consideration, both the programmed and the measured co-consolidation cycles with parameter configuration n°3 are given in Figures 5.6 and 5.7:

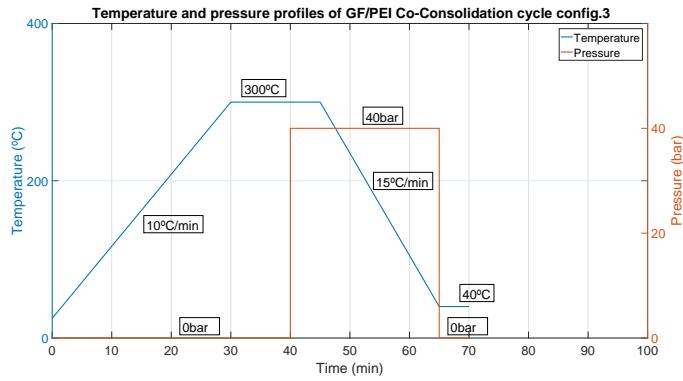


Figure 5.6: Co-consolidation run 3 - Programmed temperature and pressure profiles

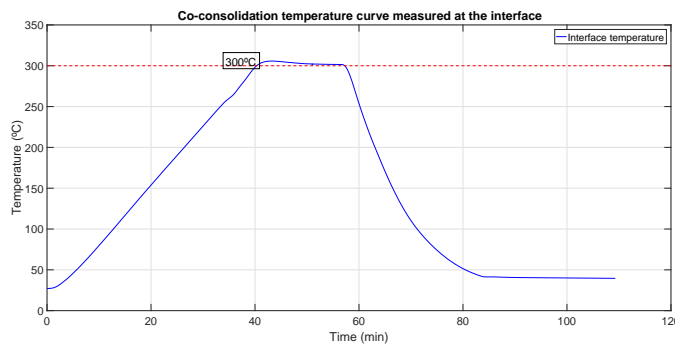


Figure 5.7: Co-consolidation run 3 - Measured temperature

Comparing the two temperature curves, it's possible to conclude that the co-consolidation temperature of 300°C was accurately achieved during the co-consolidation cycle. Therefore, based on the accurate temperature control of the hot press suggested by Figure 5.7, we can assume that all the co-consolidation cycles were carried with a similar accuracy. The time mismatch between the programmed and measured cycles is due to the inability for the hot press to follow precisely the programmed heating and cooling rates.

### 5.1.3. Specimen preparation

Following the production of 250x250 mm preconsolidated and co-consolidated laminates with a stop-off layer at the midplane interface, 132x25 mm specimens for mode I interlaminar fracture toughness testing were cut by using an automated and high precision diamond blade cutting machine according to the layout depicted in Figure 5.8:

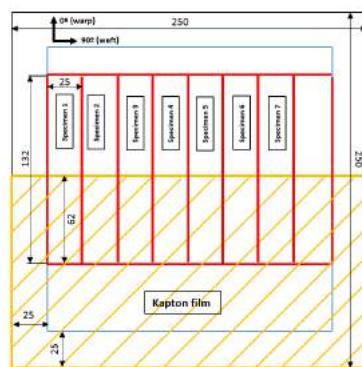


Figure 5.8: Specimen cutting layout

Specimens were then dried in the oven for 12h at 130°C to remove moisture absorbed during the water cooled cutting process. After drying, the specimens' surfaces were ground with P600 sand paper to increase surface wettability and promote a good quality bond with the aluminium loading blocks, which are used to introduce the opening load in the specimens. Aluminium loading blocks, on the other hand, were grit blasted.

Once the loading blocks and the specimens were submitted to their corresponding surface treatments, a bi-component structural adhesive, supplied by 3M and referenced by the supplier as EC-9323 B/A, was mixed with 10% wt 200/300  $\mu\text{m}$  glass beads and then applied on the specimens' surfaces. The aluminium blocks were then bonded to the specimens by placing them on top of the bondlines without the aid of additional pressure. The adhesive was then cured at room temperature for at least 12h before being post-cured for 2h at 65°C. After the post-cure process, the excess adhesive, which squeezed out as shown in Figure 5.9, was sanded away by using a Dremel tool so that the crack could be opened during testing.

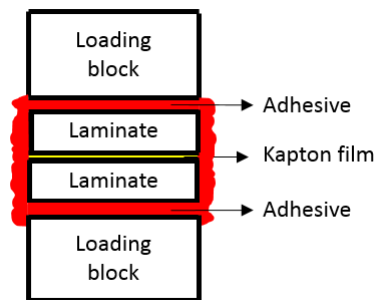


Figure 5.9: Excess adhesive after post-curing

After removing the excess adhesive, the specimens were prepared and ready for testing. A schematic representation of a DCB test specimen is depicted in the following figure:

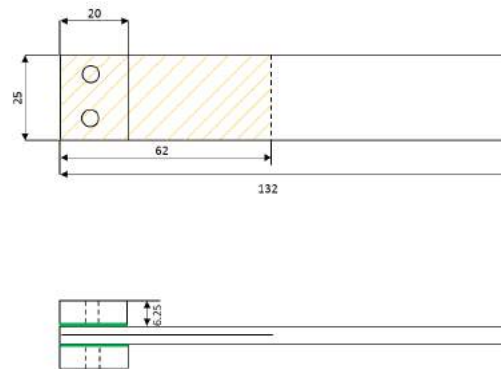


Figure 5.10: DCB specimen configuration

#### 5.1.4. Microscopy

Samples from co-consolidated and preconsolidated laminates were cut with a diamond blade, dried in the oven for 3h at 130°C and then embedded in Technovit 4071 resin for cross-section microscopy analysis. After curing, samples were ground with 180, 320, 1000 and 2400 grinding paper and then polished with 6, 3 and 1  $\mu\text{m}$  cloth and diamond paste, respectively. Cross-sectional observations were then performed with a Leica optical microscope with a 2.5x magnification.

## 5.2. Methodology

### 5.2.1. Orthogonal array experiment

In order to determine the effect of certain parameters on the quality of a certain process, it is common to perform a set of experimental runs where these parameters are set at various values. The approach used in this study consists of an orthogonal array experiment, whose design methodology is described in Appendix A. This approach only requires a fraction of the full factorial parameter combinations to determine the effect of each control factor. Therefore, instead of performing 27 experimental runs, only 9 are required, as suggested by Table 5.1:

Table 5.1: Co-consolidation L9 orthogonal array experiment

Run	Time (min)	Temperature (°C)	Pressure (bar)
1	5	240	20
2	5	270	30
3	5	300	40
4	15	240	30
5	15	270	40
6	15	300	20
7	30	240	40
8	30	270	20
9	30	300	30

The levels' choice of each control factor, although not associated with any statistical method, was not random. For co-consolidation time, a minimum time of 5 minutes was chosen for two reasons. First, because it was known from Chapter 4 that 5 minutes is enough to bond two GF/PEI laminates at a temperature of 240°C. Therefore, since there was no knowledge that shorter times would potentially create a bond as well, this threshold was chosen. The second reason is because 5 minutes can be considered as relatively short time and therefore it would be interesting to know if short co-consolidation times combined with high temperatures would be able to achieve high fracture toughness values. A maximum time level of 30 minutes was chosen to see if very long times can actually increase the fracture toughness significantly or play a counter-productive effect instead. Finally, an intermediate time of 15 minutes was chosen because it is well spaced between the two boundary values and therefore more likely to capture the effects of time on the fracture toughness.

For the temperature parameter, a minimum level of 240°C was chosen in order to make a link to the current capabilities of the experimental setup and be able to quantitatively identify how far from a feasible process window it is at the moment. A maximum temperature of 300°C was chosen because it is 20°C below the temperature at which preconsolidated laminates were processed and therefore it can tell us if such high temperatures are really necessary to achieve a high fracture toughness or if 20°C below preconsolidation temperature still generates significantly lower fracture toughness results compared to preconsolidated laminates. An intermediate temperature of 270°C was chosen because, once again, it is adequately spaced from the two boundary values, thus better capturing the effects of temperature on fracture toughness. It can also tell if lower temperatures are sufficient to achieve a high fracture toughness.

Pressure values were varied between 20 and 40 bar. The minimum value of 20 bar was chosen because it is a commonly applied pressure in press forming processes due to its ability to provide good consolidation quality with reduced void content. A maximum level of 40 bar was applied due to the limited capabilities of the rubber mould. Following the experimental runs described in the previous chapter, where 40 bar consolidation pressures were applied, some damage in the rubber mould was visible. Therefore, a 40 bar consolidation pressure can be regarded as a recommended limit. As a result, and given that a link will have to be made between the fracture toughness test results obtained

here and the ones obtained in the last experimental study (where pre-formed laminates are submitted to a post-consolidation step), this limit was imposed. Given the 20 and 40 bar boundary values, a 30 bar intermediate level was then logically chosen.

### 5.2.2. Double Cantilever Beam tests

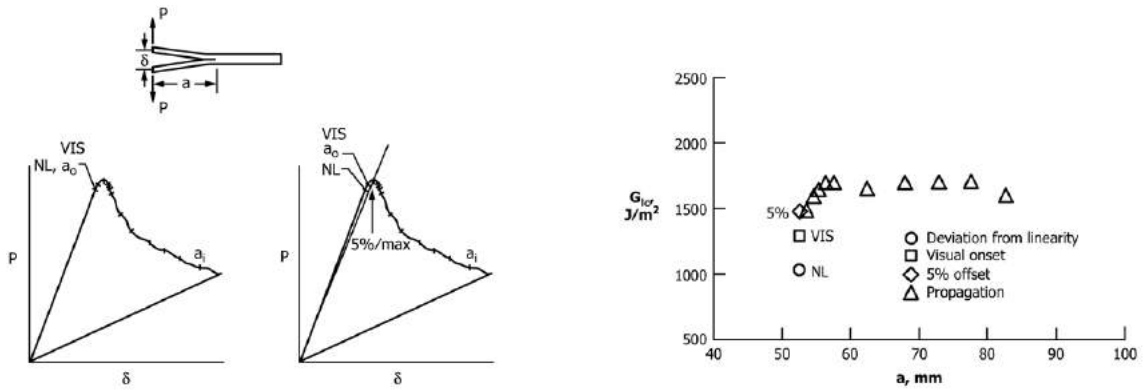
The mode I interlaminar fracture toughness ( $G_{IC}$ ) of co-consolidated and preconsolidated GF/PEI composite laminates was determined by performing Double Cantilever Beam (DCB) tests according to the ASTM D5528-13 standard [63]. In this test method, the  $G_{IC}$  value is calculated based on the strain energy release rate ( $G$ ).  $G$  is the rate at which strain energy ( $U$ ) is stored in a cracked body as a function of crack area:

$$G = -\frac{dU}{dA} = -\frac{1}{b} \frac{dU}{da} \quad (5.1)$$

Where  $A$  is the crack area,  $b$  is the crack width and  $a$  the crack length. As the energy stored in the body reduces when the crack propagates, a minus sign is introduced on the left side of the equation. The mode I interlaminar fracture toughness,  $G_{IC}$ , is then defined as the critical value of  $G$  that causes mode I crack growth. Under the mode I opening load case introduced in the DCB test method (see Figure 5.11), the strain energy release rate expression calculated through the Modified Beam Theory (MBT) is written as follows:

$$G_I = \frac{3P\delta}{2ba} \quad (5.2)$$

Where  $P$  is the applied load and  $\delta$  is the load point displacement. This equation can be applied to calculate  $G_{IC}$  initiation values, which represent the energy needed to initiate a crack, and also propagation values, which represent the energy needed to propagate a crack once it has initiated. These values are typically different from each other, with the initiation values usually being lower than propagation values. A schematic representation of the load-displacement curve and a delamination resistance curve, depicting higher  $G_{IC}$  propagation values compared to initiation values, is provided in Figure 5.11:



(a) Schematic representation of the DCB load-displacement curve [63]

(b) Delamination resistance curve from DCB test [63]

Figure 5.11: (a) DCB test load-displacement curve and (b) delamination resistance curve showing higher  $G_{IC}$  propagation values than initiation values

In this study, more focus was given to  $G_{IC}$  initiation values calculated at the load and displacement values at which crack initiation was visually (VIS) observed. This is because  $G_{IC}$  VIS values could be determined more accurately and consistently. Other initiation values, such as the point of deviation from linearity in the load-displacement curve (NL) and the point at which the compliance ( $\delta/a$ ) had increased by 5% (5% max), could not be consistently calculated because load-displacement curves not always followed the same trends. Furthermore, software crashing after completion of DCB tests led to loss of some of the load-displacement curve data. Propagation values were also difficult to be accurately determined through equation 5.2 because there was no reliable method to identify where the tip

of the crack was as it propagated. As a result, it became difficult to record the load and displacement values correspondent to certain crack lengths.

Instead of producing resistance curves, an average propagation value,  $G_{IC} AVG$ , was calculated using the area method. This method of calculating a  $G_{IC}$  propagation value has been used by Gillespie et al [65] to characterise the strain energy release rate during crack propagation of Graphite/Epoxy and Graphite/PEEK composites. This method consists of dividing the area under the load-displacement curve by the crack area generated during the test. Thus, the following equation is used:

$$G_{IC} AVG = \frac{Area}{b\Delta a} \quad (5.3)$$

And the area under the load-displacement curve is represented as follows:

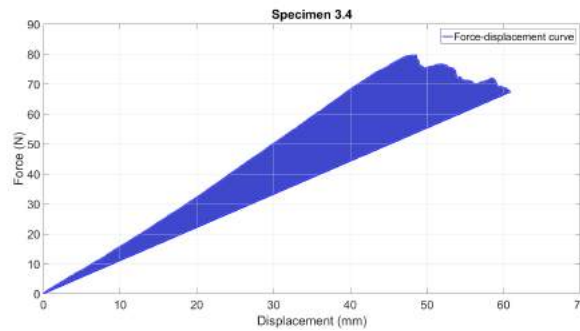


Figure 5.12: Area under load-displacement curve of DCB tested specimen

Note that the unloading curve depicted in the figure is linear and it returns to the zero displacement and force values. During testing, however, the measured force-displacement curves were not linear, as shown in Appendix C. This non-linear behaviour yielded in very large and unrealistic values of  $G_{IC} AVG$ , in most cases significantly higher than the  $G_{IC}$  of the pure PEI matrix, which was found to be  $3.9 \text{ KJ/m}^2$  by Akkerman et al [64]. Therefore, to correct for this incongruence, the  $G_{IC} AVG$  was calculated by assuming the unloading curve to be linear. This correction yielded in more realistic  $G_{IC}$  propagation values, but there was still no accurate method to determine the extent to which a crack had grown after testing. Furthermore, some of the load-displacement curve data was lost. As a result,  $G_{IC} AVG$  values were likely less accurate than  $G_{IC} VIS$  values.

$G_{IC} VIS$  values were calculated through Equation 5.2, where  $P$ ,  $\delta$  and  $a$  were replaced by the load and displacement values at which crack initiation was visually observed and by the initial crack length of the specimen. For the cases where  $\delta/a$  exceeded 0.4 at the moment of crack initiation, the expression in Equation 5.2 was multiplied by a large displacement correction factor,  $F$ , described in the test standard [63] as:

$$F = 1 - \frac{3}{10} \left( \frac{\delta}{a} \right)^3 - \frac{3}{2} \left( \frac{\delta t}{a^2} \right) \quad (5.4)$$

Where  $t$  is the quantity depicted in the following figure:

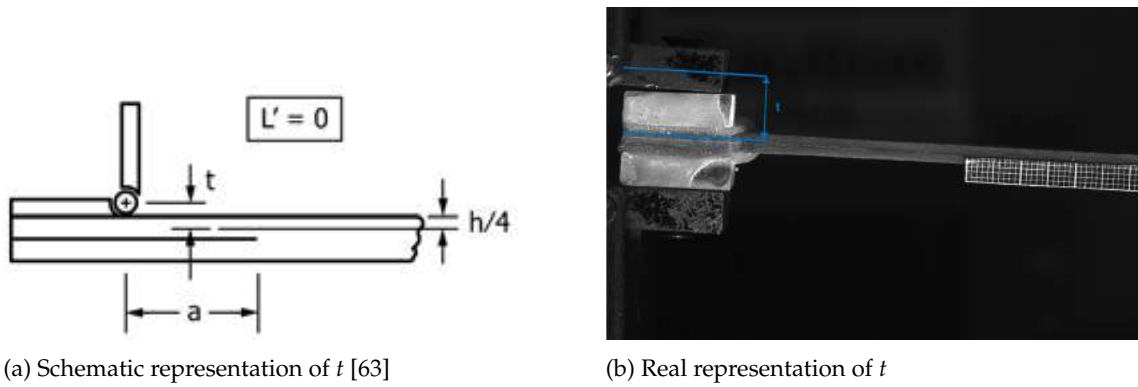


Figure 5.13: (a) Schematic and real (b) representations of the variable  $t$

Tests were performed at a displacement rate of 5 mm/min and cracks were allowed to grow 10-15 mm before the load was removed at a displacement rate of 25 mm/min. In some cases, where crack growth was unstable, cracks became a bit larger than 15 mm. The load and displacement values at which crack initiation was visually observed were recorded and then plugged into Equation 5.2 to calculate  $G_{IC}$  VIS. For the  $G_{IC}$  AVG calculation, the area under the load-displacement curves (see Figure 5.12) was calculated in MATLAB.

### 5.2.3. Statistical analysis

In this section, the results obtained from the statistical methods and equations provided in Appendix B will be presented. These results are related to the  $G_{IC}$  VIS results obtained from DCB tests and presented in the following table:

Table 5.2:  $G_{IC}$  VIS results

Run	Time (min)	Temperature (°C)	Pressure (bar)	$G_{IC}$ VIS (KJ/m <sup>2</sup> )
1	5	240	20	0.287
2	5	270	30	1.761
3	5	300	40	1.824
4	15	240	30	0.415
5	15	270	40	1.713
6	15	300	20	1.706
7	30	240	40	0.525
8	30	270	20	1.651
9	30	300	30	1.628

### Analysis of means (ANOM)

The equations applied in the ANOM are described in Appendix B.1. Results obtained from these equations are summarized as follows:

$$\overline{G_{IC}(5min)} = 1.291 \quad [KJ/m^2]$$

$$\overline{G_{IC}(15min)} = 1.278 \quad [KJ/m^2]$$

$$\overline{G_{IC}(30min)} = 1.268 \quad [KJ/m^2]$$

$$\overline{G_{IC}(240^\circ C)} = 0.409 \quad [KJ/m^2]$$

$$\overline{G_{IC(270^{\circ}\text{C})}} = 1.708 \quad [\text{KJ}/\text{m}^2]$$

$$\overline{G_{IC(300^{\circ}\text{C})}} = 1.719 \quad [\text{KJ}/\text{m}^2]$$

$$\overline{G_{IC(20\text{bar})}} = 1.215 \quad [\text{KJ}/\text{m}^2]$$

$$\overline{G_{IC(30\text{bar})}} = 1.268 \quad [\text{KJ}/\text{m}^2]$$

$$\overline{G_{IC(40\text{bar})}} = 1.354 \quad [\text{KJ}/\text{m}^2]$$

Main effects plots are then obtained for each factor (i.e. main effects plot of time, temperature and pressure) by associating each factor's level to its correspondent  $\overline{G_{IC}}$  value. So, for instance, in the time main effects plot, the first data point will be (5 min, 1.291 KJ/m<sup>2</sup>), the second (15 min, 1.278 KJ/m<sup>2</sup>) and the third (30 min, 1.268 KJ/m<sup>2</sup>). The three main effects plots are presented in Figure 5.20.

### *Analysis of variance (ANOVA)*

Followed by the ANOM, an analysis of variance (ANOVA) is performed. The methodology used in this analysis is described in Appendix B.2. Results are summarized as follows:

$$\overline{G_{IC}} = 1.279$$

$$GTSS = 18.18$$

$$SS \text{ due to mean} = 14.72$$

$$Total \ SS = 3.459$$

The sum of squares of each control factor is:

$$SS_{time} = 0.0007742$$

$$SS_{temperature} = 3.405$$

$$SS_{pressure} = 0.02965$$

$$SS_{error} = 0.02351$$

$$SS_{total} = 3.459$$

The percentage contribution of each control factor is:

$$Time : 0.02238\%$$

$$Temperature : 98.44\%$$

$$Pressure : 0.8572\%$$

$$Error : 0.6795\%$$

Finally, the F-ratio of each control factor is:

$$F_{prac(time)} = 0.03294$$

$$F_{prac(temperature)} = 144.9$$

$$F_{prac(pressure)} = 1.262$$

These results are summarized and interpreted further in section 5.3.3.

## 5.3. Results and Discussion

### 5.3.1. DCB test results

Results for  $G_{IC}$  VIS, the energy required to initiate a crack, and  $G_{IC}$  AVG, the average energy required to propagate and grow a crack, of preconsolidated and co-consolidated laminates are presented in the following bar chart:

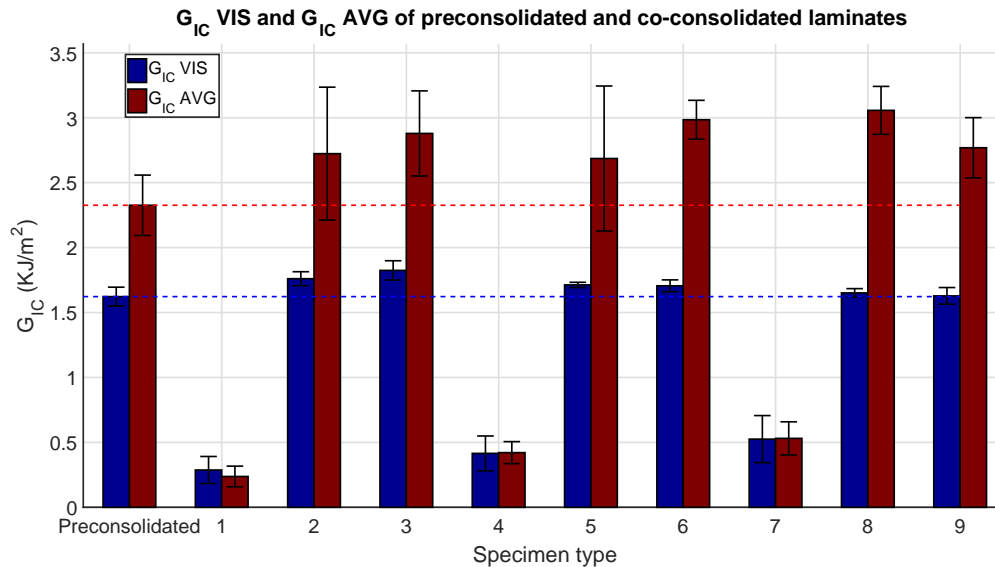


Figure 5.14: DCB test results of preconsolidated and co-consolidated laminates

According to the bar chart, specimens from runs n°1, 4 and 7 have a much lower fracture toughness than all the other specimens. This is due to the low co-consolidation temperature of 240°C, which is not high enough to allow high molecular diffusion across the interface and promote a high degree of autohesion. This result is in agreement with observations presented in Chapter 4, where co-consolidated bonds between formed laminates were easily peeled off. Crack propagation during mechanical testing of these specimens was also very unstable, as suggested by the sudden load drops in the force - displacement curves (see Appendix C.2, C.5, C.8). Herewith, a co-consolidation temperature of 240°C is not feasible for the multiple step forming process of GF/PEI composite laminates.

$G_{IC}$  VIS values for laminates co-consolidated at temperatures of 270°C and 300°C are very similar to the ones of preconsolidated laminates. Values ranging between 1.6 - 1.8 KJ/m<sup>2</sup> were obtained, which are in good agreement with those reported by Kim et al [66] for the same GF/PEI woven composite material with a 5-harness weave structure. Values are also comparable to those reported in high-toughness AS4/PEEK (carbon fibre reinforced PEEK) composites, which range from 1.3 to 1.8 KJ/m<sup>2</sup> [65, 67–70]. The mode I interlaminar fracture toughness of these thermoplastic composites are an order of magnitude higher than typical carbon/epoxy composites, which typically range between 0.1 and 0.225 KJ/m<sup>2</sup> [67]. This goes to show the feasibility for having thickness drops on the outer surfaces of thermoplastic composite parts rather than using ply-drop techniques commonly applied in thermoset composites. The much higher toughness of thermoplastic composites offers much more resistance to free-edge delaminations.

Laminates co-consolidated in runs n°2, 3, 5 and 6 have slightly higher  $G_{IC}$  VIS than preconsolidated laminates and all co-consolidated laminates at temperatures of 270°C and 300°C have higher  $G_{IC}$  AVG compared to preconsolidated laminates. The high  $G_{IC}$  AVG standard deviation in specimens from run n°2 was due to unstable crack growth in some tests, as shown by the sudden load drops in the force-displacement curves (see Appendix C.3). Specimens from run n°5 also have a high  $G_{IC}$  AVG standard deviation, but this is because only two load-displacement curves were used to calculate this value. All the other curves were lost due to software crashing after the test.

Higher fracture toughness values in co-consolidated laminates can be attributed to the combination of multiple phenomena. The first parameter possibly contributing to the increase of  $G_{IC}$  is the higher

applied pressure in co-consolidation cycles compared to the preconsolidation cycle (see Figure 5.4). Some of the co-consolidation runs, namely runs n°2, 3, 5 and 9, were performed at either 30 or 40 bar, thus higher than the 20 bar pressure applied in the preconsolidation cycle. With higher pressures, the required time to achieve complete degree of intimate contact is lower [58], thereby promoting a higher degree of autohesion.

Another phenomenon possibly playing a role in the increase of  $G_{IC}$  is the re-consolidation process of co-consolidated laminates. According to Vieille [71], the re-consolidation process of composite laminates promotes (1) the re-compaction of the fibre network and (2) the migration of melted matrix. These two phenomena result in better interlaminar adhesion and in the improvement of the interlaminar shear strength, which according to experimental tests increased by 10% with respect to preconsolidated laminates.

Co-consolidated laminates also show a substantial increase in thickness with respect to preconsolidated laminates, as shown in the following bar chart:

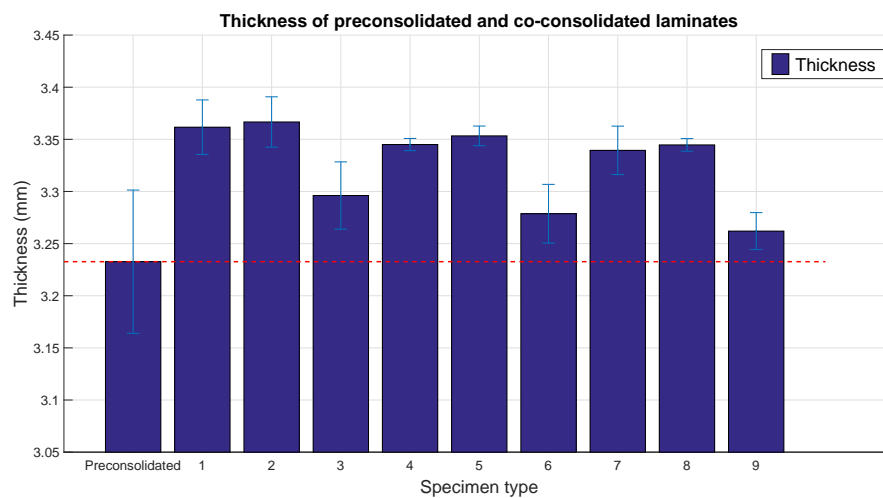
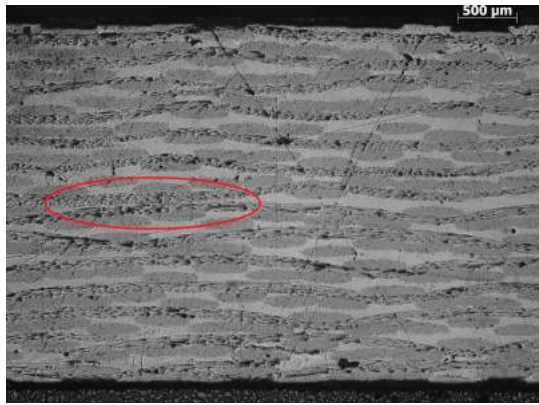


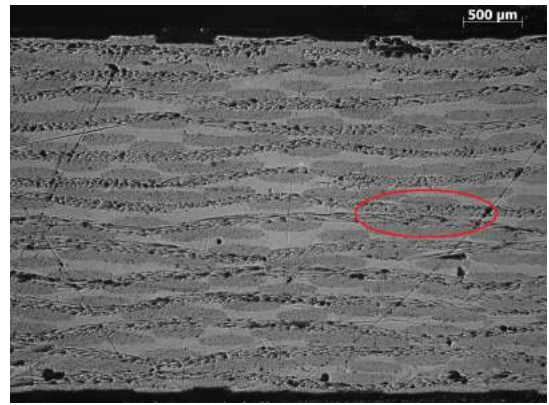
Figure 5.15: Thickness results for preconsolidated and co-consolidated laminates

This increase in thickness is translated into less regions with fibre-fibre contact and more resin pockets at the delamination interface. This is clearly visible by comparing cross-sections of co-consolidated laminates at 270°C and cross-sections of preconsolidated laminates (see Figures 5.16 and 5.17). Figure 5.18 shows cross-sections of co-consolidated laminates at 300°C and although it is not clearly evident, it is believed that there are slightly less regions of fibre-fibre contact regions than preconsolidated laminates due to the slightly higher thickness of the former. In resin pocket regions large plastic deformations can occur, thereby increasing the fracture toughness. However, in the regions of fibre-fibre contact the effect of resin pockets is reduced and the fracture toughness is lowered [72]. Therefore, as co-consolidated laminates have less regions of fibre-fibre contact and more resin pocket regions, the  $G_{IC}$  AVG increases.

Higher thicknesses may also have a positive effect on  $G_{IC}$  VIS. In thicker laminates, the fibre-network is not fully compacted, so the resin pocket region at the crack tip may be slightly larger, thus increasing the distance between adjacent fibres. As a result, higher plastic deformations ahead of the crack tip may occur, thereby delaying the onset of crack growth.

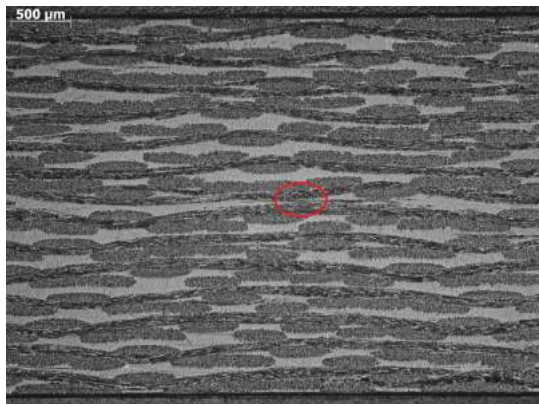


(a) Cross section of preconsolidated laminate (1)

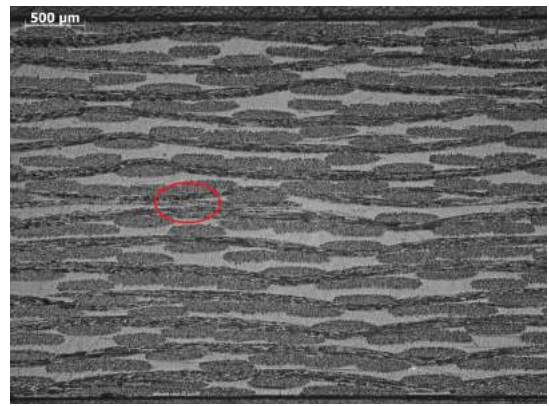


(b) Cross section of preconsolidated laminate (2)

Figure 5.16: Microscopy cross-sections of 14-ply preconsolidated laminate at 320°C with large areas of fibre-fibre contact at the midplane interface (2.5x magnification)

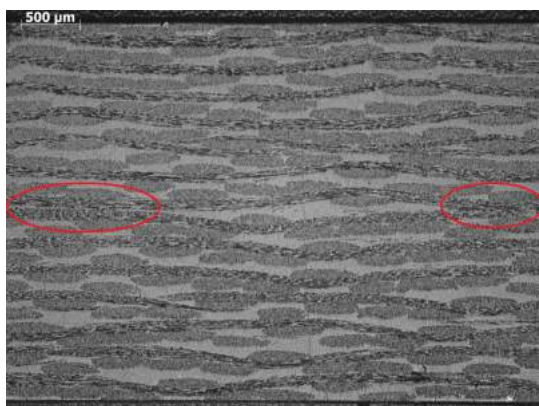


(a) Cross section of co-consolidated laminate in run n°5 (1)



(b) Cross section of co-consolidated laminate in run n°5 (2)

Figure 5.17: Microscopy cross-sections of 14-ply co-consolidated laminate at 270°C with small areas of fibre-fibre contact at the midplane interface (2.5x magnification)



(a) Cross section of co-consolidated laminate in run n°6 (1)



(b) Cross section of co-consolidated laminate in run n°6 (2)

Figure 5.18: Microscopy cross-sections of 14-ply co-consolidated laminate at 300°C with large areas of fibre-fibre contact at the midplane interface (2.5x magnification), but possibly lower than preconsolidated laminates'

In conclusion, high  $G_{IC}$  VIS and  $G_{IC}$  AVG values in co-consolidated laminates is a relevant feature towards the feasibility proof of the multiple step forming approach for thermoplastic composites. This result indicates that the weakest or most critical areas in multiple step formed parts may not occur at the co-consolidated regions. Moreover, results suggest that in order to achieve the same or higher  $G_{IC}$  as preconsolidated laminates, mould temperatures may not necessarily have to be as high as the temperature applied in the consolidation cycle of preconsolidated laminates (320°C). This is particularly relevant from a manufacturing viewpoint, as lower mould temperatures are translated into lower energy costs. Another point of interest from a manufacturing standpoint is the fact that in combination with a temperature of 270°C, 5 minutes co-consolidation time is enough to produce strong bonds. This suggests that the co-consolidation stage in a multiple step forming process may be relatively short if fast cooling mechanisms are also employed.

### 5.3.2. ANOM results

Results of the ANOM are presented in Figures 5.19 and 5.20:

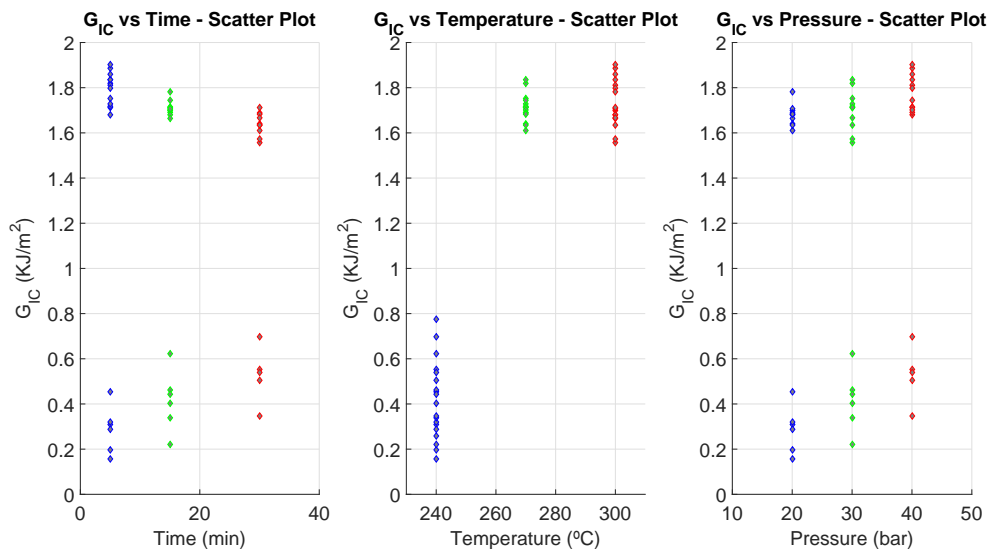


Figure 5.19:  $G_{IC}$  VIS vs Time, Temperature and Pressure scatter plots

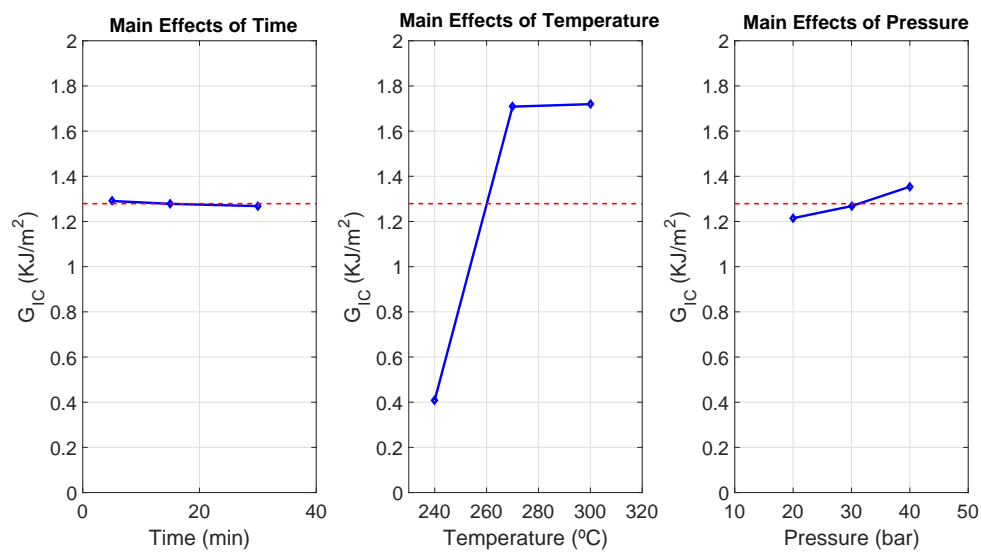


Figure 5.20: Main effects plots for  $G_{IC}$  VIS output

According to Figure 5.19, the  $G_{IC}$  VIS vs Time scatter plot indicates the existence of an interaction. For lower temperatures (i.e. 240°C), an increase in co-consolidation time increases  $G_{IC}$ , whereas for higher temperatures (i.e. 270°C and 300°C), an increase in co-consolidation time leads to the reduction of  $G_{IC}$ . This difference in trends makes the influence of time on  $G_{IC}$  VIS more difficult to quantify. This is seen in the time main effect plot depicted in Figure 5.20, where the curve is practically flat. The curve flattens because the opposite trends "cancel each other out". Hereupon, despite the main effect plot indicating no influence of time on  $G_{IC}$  VIS, it is more accurate to conclude that longer times tend to negatively affect  $G_{IC}$  VIS at higher temperatures (270°C and 300°C) but they create a positive effect at lower temperatures (240°C).

The temperature main effect plot clearly indicates a strong effect of temperature on  $G_{IC}$  VIS. The curve shows a steep increase between 240°C and 270°C, thus suggesting that the feasible process window starts somewhere in between. The temperature at which the feasible process window begins should be determined in future research. Followed by the steep increase, the curve seems to have a plateau, thus indicating that an increase of temperature beyond 270°C doesn't improve  $G_{IC}$  VIS. This result is particularly interesting from a manufacturing viewpoint since lower mould temperatures may be used without compromising on co-consolidation quality between formed laminates.

Finally, pressure seems to have a moderate effect on  $G_{IC}$  VIS. The slope of the curve depicted in the pressure main effect plot in Figure 5.20 is small and indicates that higher pressures are beneficial in achieving higher  $G_{IC}$ . Its correspondent scatter plot presented in Figure 5.19 also shows the same trend for both high and low temperatures.

### 5.3.3. ANOVA results

Results from the ANOVA are summarized in Table 5.3:

Table 5.3: ANOVA results for  $G_{IC}$  VIS output

Input parameter	DOF	SS	% Contribution	$F_{prac}$	$F_{table}$	Significance
Time	2	0.0007742	0.02238 %	0.03294	19	NO
Temperature	2	3.405	98.44 %	144.9	19	YES
Pressure	2	0.02965	0.8572 %	1.262	19	NO
Error	2	0.02351	0.6795 %	1	N/A	N/A
Total	8	3.459	100 %	N/A	N/A	N/A

The tabulated F-ratio,  $F_{table}$ , corresponds to a risk value,  $\alpha$ , of 0.05 (see Appendix B.2 for further details).

Results presented in Table 5.3 show that only temperature has a significant effect on the fracture toughness of co-consolidated GF/PEI composite laminates. The effect of temperature, however, is only significant in the range between 240°C and 270°C. In the range between 270°C and 300°C,  $G_{IC}$  VIS remains unchanged.

The ANOVA reveals that time has no effect on  $G_{IC}$  VIS. This result was expected given the almost horizontal curve obtained from the ANOM (see Figure 5.20). However, as explained in the previous section, scatter plots indicate the existence of an interaction between temperature and time, which cannot be captured by the ANOVA.

Finally, despite the ANOM indicating a moderate effect of pressure on  $G_{IC}$  VIS (see Figure 5.20), results from the ANOVA reveal that the effect of this factor just slightly outweighs the effect of experimental error ( $F_{prac} = 1.262$ ).  $F_{prac}$  is much lower than the tabulated value for  $\alpha = 0.05$  and also lower than  $F_{table}$  when  $\alpha = 0.1$  ( $F_{table_{\alpha=0.1}} = 9$ ). As a result, it is not possible to statistically prove that the effect of pressure on  $G_{IC}$  VIS is significant.

### 5.3.4. Interaction plots

The number of degrees of freedom (see Appendix A - Equation A.2) required to describe a two-way interaction is given by:

$$DOF_{two-way\ interaction} = (n^{o}levels - 1)(n^{o}levels - 1) = (3 - 1)(3 - 1) = 4 \quad (5.5)$$

Since there are three two way interactions (i.e. Temperature x Time, Temperature x Pressure and Time x Pressure), the total number of degrees of freedom required in the experiment to evaluate control factor effects and study all the two-way interactions is:

$$DOF_{required} = n^{o}factors * DOF_f + n^{o}factors * DOF_{two-way\ interaction} = 3 * 2 + 3 * 4 = 18 \quad (5.6)$$

This experiment, however, has only 8 degrees of freedom (see result of Equation A.2). Therefore, it is not possible to fully characterize the three two-way interactions. To do so, the designed experiment would need to have more degrees of freedom, which would only be possible if a full factorial array experiment with 27 runs (i.e. 26 degrees of freedom) would have been performed. As a result, interaction plots presented in this section are mainly meant to provide an idea of possible trends and to support some of the hypotheses presented in this chapter.

Temperature vs Pressure and Temperature vs Time interaction plots are presented in Figure 5.21:

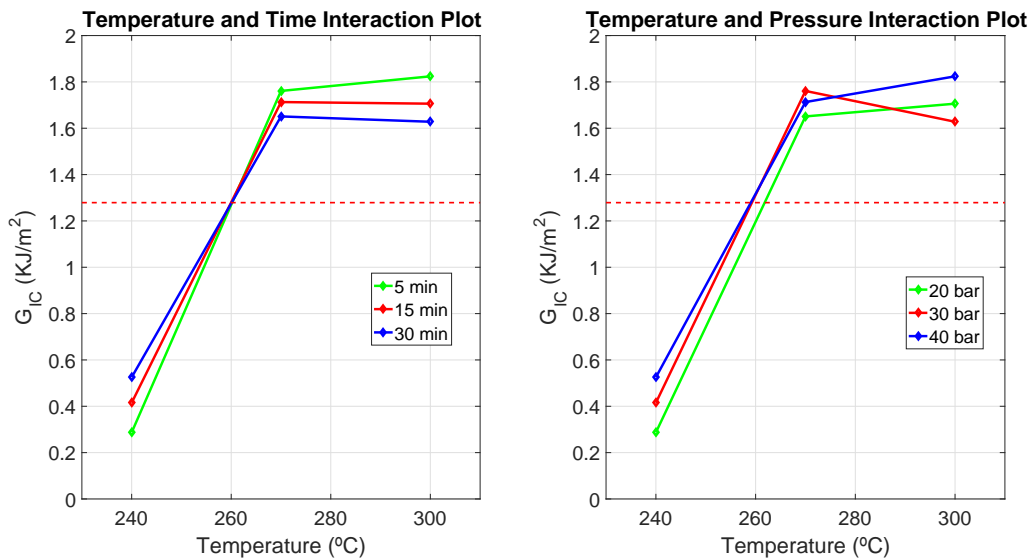


Figure 5.21: Interaction plots for  $G_{IC}$  VIS output

The first plot is in agreement with the trends found in  $G_{IC}$  VIS vs Time scatter plot presented in Figure 5.19. At 240°C, a longer co-consolidation time results in a higher  $G_{IC}$ , but from 270°C, the trend changes. Furthermore, comparing the (300°C, 30min) and (300°C, 15min) data points, it seems like the higher pressure in the former (30 bar) was not able to produce a higher  $G_{IC}$  VIS. The same applies to the (270°C, 15min) and (270°C, 5min) data points, where despite the higher pressure in the former (40 bar), a lower  $G_{IC}$  VIS was obtained. These two cases suggest that time effects may possibly be stronger compared to pressure effects, even though the F-ratio calculated for the time factor in the ANOVA was much lower.

The Temperature x Pressure interaction plot shows that the 40 bar curve is always above the 20 bar curve, thus in agreement with the premise that higher pressures are beneficial at achieving higher  $G_{IC}$  VIS. However, the 30 bar curve is not consistent with this trend. This behaviour can be explained by the fact that the time effect is actually playing a role on  $G_{IC}$  VIS.

Notice, for instance, the data points at the 240°C level. At this level, the 40 bar data point is above the 30 bar, which is in turn above the 20 bar data point. If we check the time values assigned to the (240°C, 40bar), (240°C, 30bar) and (240°C, 20bar) data points we can see that these are 30min, 15min and 5min, respectively. This supports the hypothesis presented previously, that longer times result in higher  $G_{IC}$  VIS for low temperatures, even though not completely since it was also concluded from the ANOM that higher pressures also tend to give higher  $G_{IC}$  VIS.

It is, however, in the 270°C and 300°C temperature levels of the Temperature x Pressure interaction plot that we can see the relevant role that time plays on  $G_{IC}$  VIS. The (270°C, 20bar), (270°C, 30bar) and (270°C, 40bar) data points had assigned co-consolidation times of 30min, 5min and 15min, respectively. Thus, the fact that the 30 bar curve is the highest, followed by the 40 and 20 bar curves, is compatible with the hypothesis that reduced co-consolidation times result in higher  $G_{IC}$  VIS. The same also applies for data points at the 300°C level, where the 40 bar data point (the highest) corresponds to a co-consolidation time of 5 min, the 30 bar data point (the lowest) to 30 min and the 20 bar to 15 min. This leads to the conclusion that time effects may even be stronger compared to pressure effects, even though they could not be captured neither in the ANOM nor the ANOVA due to unrepresented interaction effects.

Lower  $G_{IC}$  VIS values for longer co-consolidation times at high temperatures (270°C and 300°C) may be related to lower specimen thicknesses. The following ANOM and ANOVA results show how the thickness is reduced when co-consolidation time and temperature is increased:

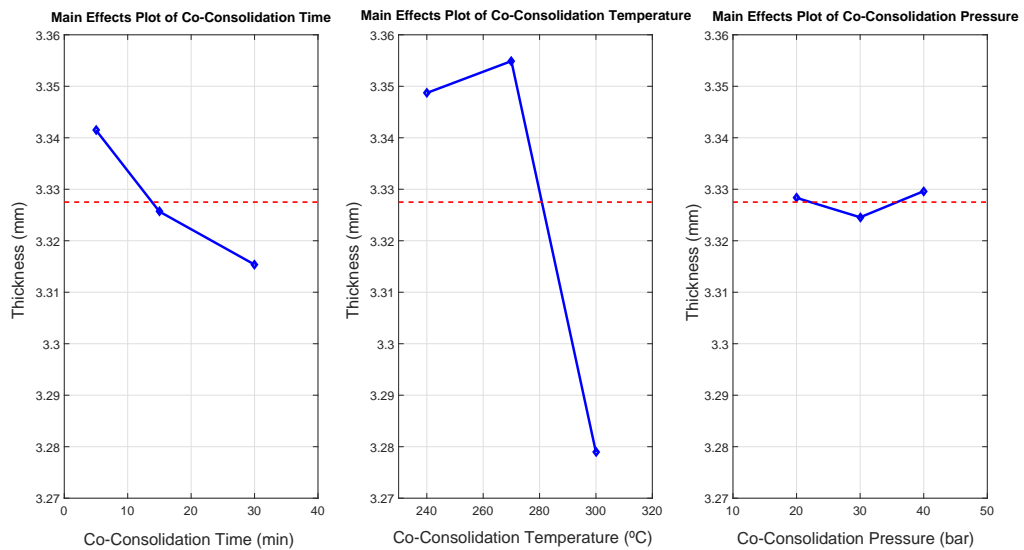


Figure 5.22: Main effects plots for thickness output

Table 5.4: ANOVA results for thickness output

Input parameter	DOF	SS	% Contribution	$F_{prac}$	$F_{table}$	Significance
Time	2	0.0010379	8.8164 %	67.425	19	YES
Temperature	2	0.010678	90.699 %	693.63	19	YES
Pressure	2	4.1698e <sup>-5</sup>	0.3542 %	2.7088	19	NO
Error	2	1.5394e <sup>-5</sup>	0.13076 %	1	N/A	N/A
Total	8	0.011773	100 %	N/A	N/A	N/A

Prel et al [69] reported that thicker specimens have higher strain rates (or crack tip opening rates) than thin specimens. Higher strain rates lead to an increase in the matrix yield strength,  $\sigma_y$ . An increase in yield strength leads to a reduction in the plastic zone size,  $r_p$ , which is inversely proportional to the yield strength squared [73]:

$$r_p \propto \frac{1}{\sigma_y^2} \quad (5.7)$$

A smaller damaged zone means that there is a tendency for the matrix alone, rather than the adjacent plies, to be loaded at the crack tip. As a result, the  $G_{IC}$  VIS of thicker specimens will tend toward

the pure matrix values, which are considerably higher than the composite's, and hence the slight increase of  $G_{IC}$  VIS for thicker specimens.

According to temperature main effects plot in Figure 5.22, higher temperatures reduce the thickness of co-consolidated laminates significantly, with an even stronger effect than longer co-consolidation times. However,  $G_{IC}$  VIS does not reduce when temperature is changed from 270°C to 300°C, thus not being consistent with the hypothesis presented previously. Nevertheless, it is possible that the lower thickness of co-consolidated laminates at very high temperatures (i.e. 300°C) is counteracted by a higher degree of molecular diffusion, and therefore a higher inherent interlaminar strength. As a result, the two effects balance each other and ultimately lead to equal  $G_{IC}$  VIS at temperatures of 270°C and 300°C.

## 5.4. Summary

The mode I interlaminar fracture toughness,  $G_{IC}$ , of preconsolidated and co-consolidated GF/PEI woven composites was determined and compared. Laminates co-consolidated at temperatures of 270°C and 300°C have approximately the same  $G_{IC}$  initiation values ( $G_{IC}$  VIS) as preconsolidated laminates, but substantially higher  $G_{IC}$  propagation values ( $G_{IC}$  AVG). Within the range of values studied, results show that temperature's effects on  $G_{IC}$  VIS are the strongest and clearly significant. Trends observed in interaction and scatter plots suggest that longer times decrease  $G_{IC}$  VIS within the feasible processing window. Indication that higher pressures increase  $G_{IC}$  VIS is also noticeable from main effects plots. Finally, good quality co-consolidated bonds can be achieved at relatively low temperatures (270°C) and short times (5 minutes), thus showing great potential for the manufacturing of multiple step formed shapes. This result will be used in the next chapter, where multiple step formed shapes will be post-consolidated with this parameter setting in order to obtain good quality bonds between formed and co-consolidated laminates.



# 6

## Multiple step forming and post-consolidation of GF/PEI composite laminates

Results presented in Chapter 5 showed that co-consolidation temperatures in the range of 270°C - 300°C are able to produce co-consolidated bonds between GF/PEI composites with a high  $G_{IC}$ . Based on this result, the potential for proving the feasibility of the multiple step forming approach for thermoplastic composites is evident. This range of co-consolidation temperatures, however, cannot be achieved in the designed experimental setup due to the 240°C limit at which the metal mould can be heated. As a result, the feasibility of the multiple step forming concept needs to be proven through a different method. The method consists of multiple step forming two laminates using a mould temperature of 240°C, the minimum required to produce sufficient bonding between two co-consolidated laminates, and then perform a post-consolidation step. In this step the multiple step formed shape is submitted to a temperature and pressure cycle in a hot press with a parameter setting able to increase the  $G_{IC}$  of co-consolidated laminates. A schematic representation of the production sequence is depicted in the following figure:

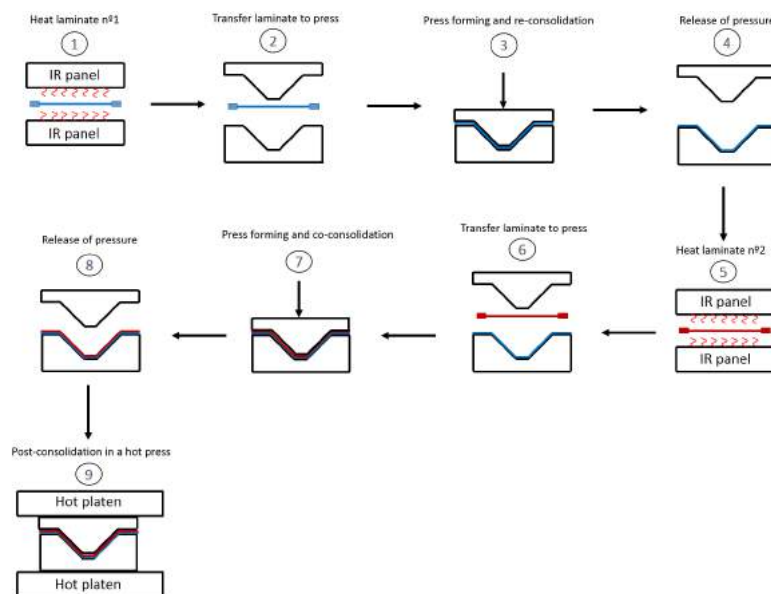


Figure 6.1: Multiple step forming process followed by a post-consolidation step

This method is applied in this experimental study. DCB test specimens are then taken from post-consolidated shapes and tested to determine  $G_{IC}$ . Results are then compared to the  $G_{IC}$  of preconsolidated laminates. Based on the results, final conclusions regarding the feasibility of the multiple step forming approach for thermoplastic composites are drawn.

Herewith, the following research question is aimed to be answered at the end of this chapter:

1. Can multiple step formed shapes be submitted to a post-consolidation process and achieve similar  $G_{IC}$  values as the ones obtained for preconsolidated laminates?

## 6.1. Experimental Procedure

### 6.1.1. Materials and blank preparation

The material used in this study was the same GF/PEI woven composite specified in section 4.1.1, but it came from a different roll. The roll used here was manufactured in 2016, while the roll used in the previous chapter was supplied in 2012. Due to this difference, DCB tests were also performed in preconsolidated laminates in order to provide a fair comparison with the  $G_{IC}$  obtained in formed and post-consolidated laminates. The procedure used for producing preconsolidated DCB test specimens was the same as the one described in section 5.1.

For the multiple step forming process followed by a post-consolidation step, laminates with a  $[(0/90)]_7$  stacking sequence were produced by cutting, laying up and consolidating 580x580 mm stacks of pre-preg according to the cycle shown in Figure 4.2. 7-ply laminates were laid up according to the layout presented in Figure 5.5a so that 14-ply co-consolidated and multiple step formed laminates could be produced according to the layout presented in Figure 5.5b. 335x180 mm blanks were then cut using a Darley guillotine according to the following layout:

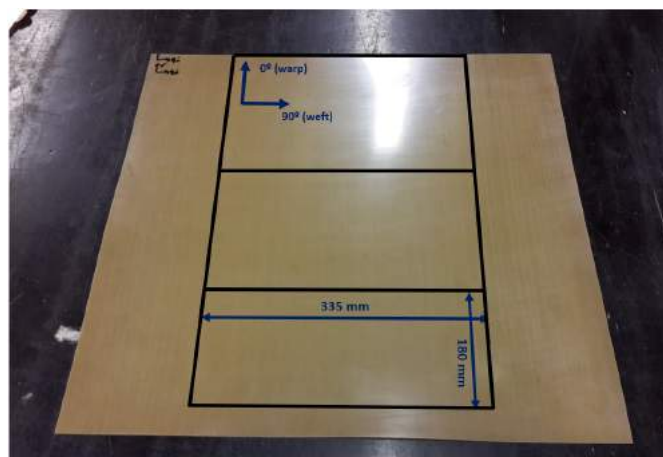


Figure 6.2: Blank cutting layout

Blanks were then sanded using P800 grinding paper and water to remove release agent residue, followed by degreasing with isopropanol and drying at 130°C for 3 hours to remove absorbed moisture.

### 6.1.2. Multiple step forming process

Three multiple step forming cycles were performed so that six specimens for mode I interlaminar fracture toughness testing could be cut from the sidewalls of the formed shapes (i.e. two specimens per formed shape). The parameters used in the multiple step forming cycles are summarized in Table 6.1:

Table 6.1: Multiple step forming process parameters

Step n°	Mould Temperature (°C)	Pressure (bar)	(Co) Consolidation time (min)	Blank dimensions (mm)	Blank layup
Step 1	240	40	5	335x180	[(0/90)] <sub>7</sub>
Step 2	240	40	7.5	335x180	[(0/90)] <sub>7</sub>

No cooling under pressure was applied in the multiple step forming runs. After the 7.5 minute co-consolidation stage of the process at 240°C, pressure was released and multiple step formed shapes were removed from the mould. In order to take DCB test specimens from the formed shapes, 84x53 mm and 50  $\mu\text{m}$  thick Kapton films were placed on the sidewalls of the laminate formed in the first forming step, as shown in Figure 6.3:

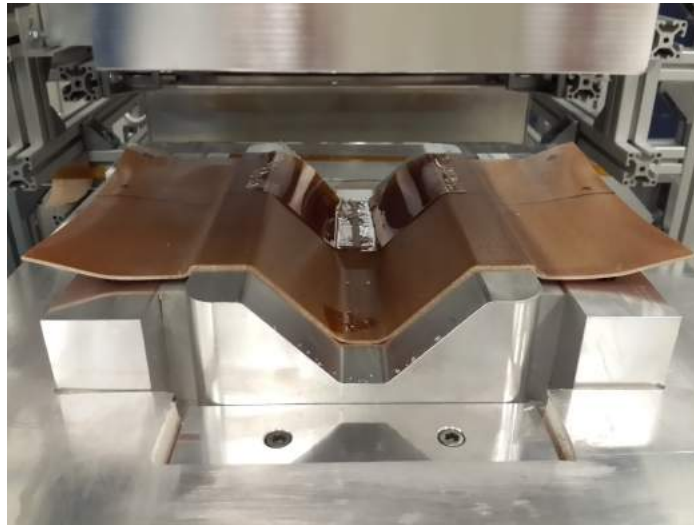


Figure 6.3: Kapton films placed on the sidewalls of the laminate formed in the first step in order to create a crack and enable the production of specimens for DCB testing

In one of the multiple step forming cycles, a thermocouple was also introduced at the laminate-laminate interface in order to monitor the temperature during the post-consolidation step.

### 6.1.3. Post-consolidation process

After the multiple step forming process, the edges of the formed blanks were trimmed using a diamond blade. Trimmed shapes were then submitted to a post-consolidation process in a hot press. The tool set was transferred from the forming press to the hot press, which contains two heated platens that can be heated to high temperatures (above 300°C). Trimmed shapes were placed and fixed on the metal mould before the rubber mould was placed over the former, as shown in Figure 6.4:



(a) Formed shape fixed on the metal mould



(b) Closed moulds

Figure 6.4: (a) Formed shape placed and fixed on the metal mould and then (b) submitted to a post-consolidation process by closing the moulds and applying temperature and pressure

The post-consolidation process was carried using the same parameter setting as run n°2 in the orthogonal array experiment performed in Chapter 5 (see Table 5.1). A post-consolidation temperature of 270°C was applied, in combination with a pressure of 30 bar and a holding time of 5 minutes. The main reasons for employing this parameter setting in the post-consolidation process were:

1. A 270°C temperature revealed to be sufficient in achieving high  $G_{IC}$  in co-consolidated laminates
2. Temperatures higher than 270°C could potentially lead to significant damage in the rubber mould
3. Since that ANOVA results presented in Table 5.3 indicate a very moderate effect of pressure on  $G_{IC}$ , a 30 bar pressure was applied. A 40 bar pressure was not applied in order to prevent significant damage in the rubber mould
4. An holding time of 5 minutes was applied because shorter consolidation times tend to increase  $G_{IC}$  at higher temperatures (i.e. 270°C - 300°C)

The programmed post-consolidation temperature and pressure cycle, and the measured temperature curves during the process are provided in Figures 6.5 and 6.6, respectively:

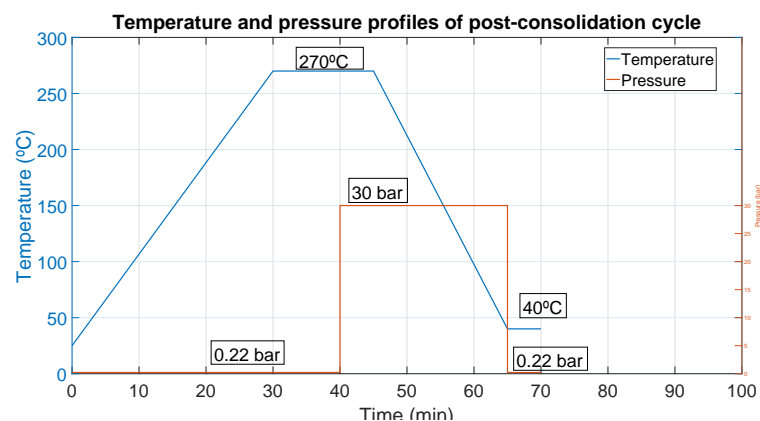


Figure 6.5: Post-consolidation process - Programmed temperature, pressure and time profiles

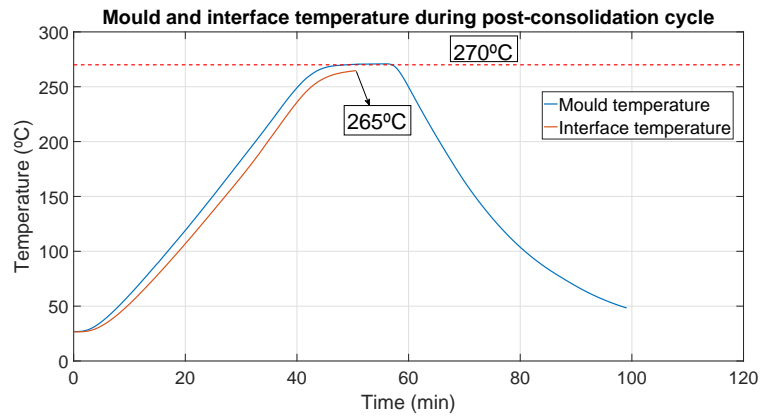


Figure 6.6: Measured temperature curves during the post-consolidation process

Note that after the setpoint temperature of 270°C was reached, there was a holding time of 10 minutes in order to give time for the metal mould and the formed laminate to reach this temperature. Only after 10 minutes, 30 bar consolidation pressure was applied. Moreover, contrarily to the co-consolidation runs performed in Chapter 5 (see Figure 5.6), an initial pressure of 0.22 bar was applied during the heat-up stage of the process. This pressure was applied in order to increase the heat-up rate of the laminate and ensure that the 270°C temperature was achieved at the laminate-laminate-interface.

Measured temperature curves show that the metal mould achieved the target temperature of 270°C. On the other hand, the interface temperature was 265°C at the moment the 30 bar pressure was applied. After applying pressure the thermocouple snapped and temperatures stopped being recorded. Nevertheless, based on the temperature curves obtained in Chapter 4, it is safe to assume that the interface temperature eventually increased after applying pressure and most likely reached a temperature of 270°C.

#### 6.1.4. Specimen preparation

After the post-consolidation process, specimens for DCB testing were cut from the sidewalls of the formed shapes using a high precision diamond cutting blade according to the following layout:

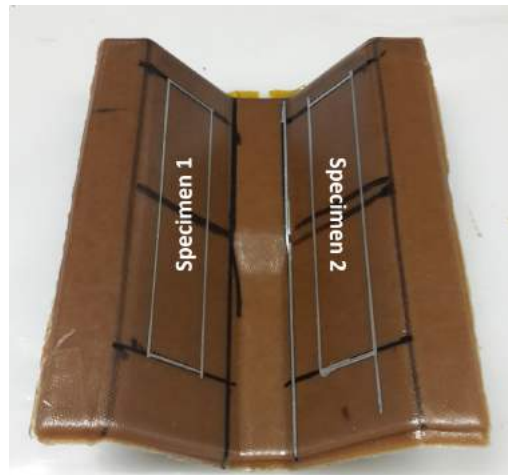


Figure 6.7: Specimen cutting layout from post-consolidated formed shape

After cutting, specimens were prepared according to the procedure described in section 5.1.3. DCB tests were then performed using the same methodology described in section 5.2.2.

## 6.2. Results and Discussion

### 6.2.1. DCB test results

$G_{IC}$  VIS and  $G_{IC}$  AVG results for preconsolidated and co-consolidated laminates are presented in Figure 6.8:

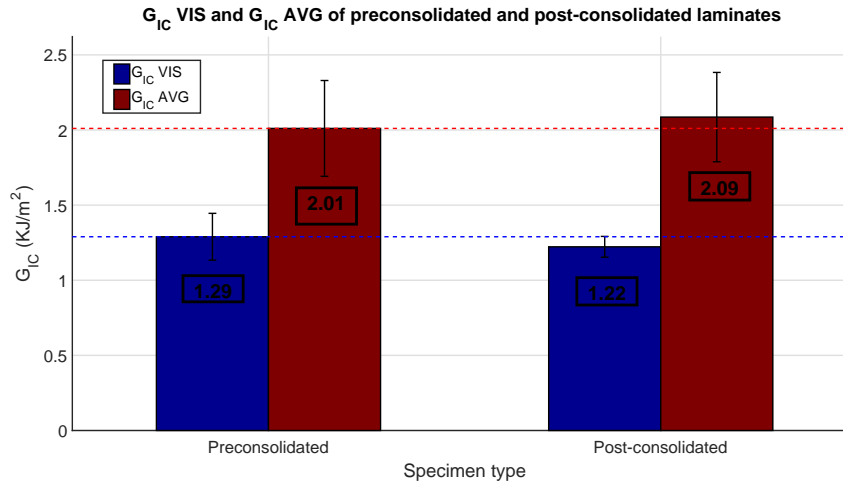


Figure 6.8: DCB test results of preconsolidated and post-consolidated laminates

$G_{IC}$  VIS and  $G_{IC}$  AVG of multiple step formed and post-consolidated laminates are very similar to the ones obtained for preconsolidated laminates. This result strongly supports the feasibility of the multiple step forming approach for thermoplastic composites. It proves that multiple step formed parts can be produced without compromising on the mode I interlaminar fracture toughness property in co-consolidated regions.

Note that the values obtained for this material are lower compared to the ones obtained for the material used in Chapter 5 (see Figure 5.14). Despite the material used in this experimental study being from the same supplier and having the same specifications as the material used in Chapter 5, it was retrieved from a roll produced 4 years later. As a result, the material may have been submitted to different manufacturing and chemical processes, which subsequently led to differences in the molecular structure of the PEI matrix and to a decrease in toughness. It is also possible that long-time storage of the material used in Chapter 5 led to higher moisture intakes. Higher moisture content may have increased matrix ductility and contributed to an increase in  $G_{IC}$ . This phenomenon has been reported in carbon/epoxy composites [68].

The thicknesses of the two types of specimens were also very similar, as suggested by the bar chart presented in Figure 6.9, even though the post-consolidation step was carried at a much lower temperature than the preconsolidation cycle (320°C). This most likely stemmed from the 0.22 bar pressure applied during the heat-up stage of the post-consolidation process, thus not 0 bar as the co-consolidation cycles presented in Chapter 5 which eventually resulted in higher thickness for co-consolidated laminates.

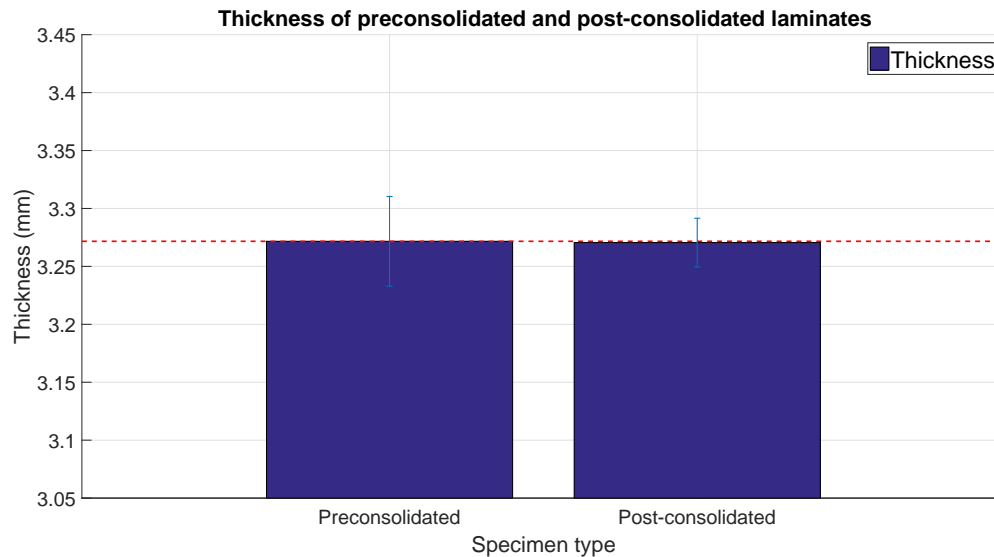


Figure 6.9: Thickness of preconsolidated and press formed post-consolidated laminates

The similar thicknesses of the two types of specimens supports the hypothesis presented in section 5.3.4, which states that different thicknesses lead to different crack opening rates and therefore different  $G_{IC}$  initiation values. As the thicknesses in this case were very similar, so as the  $G_{IC}$  VIS values, as shown in Figure 6.8. Moreover, similar thicknesses are also translated into similar amount of fibre-fibre contact areas. This, in turn, contributes to similar  $G_{IC}$  propagation values, as the distance between alternating resin pockets, which tend to increase the fracture toughness, remains the same. Therefore, similar  $G_{IC}$  AVG values are also evident in Figure 6.8.

### 6.2.2. Qualitative analysis of post-consolidated formed shape

After the post-consolidation process, significant differences in shape's details were observed with respect to the shape before post-consolidation, as depicted in Figure 6.10:



(a) Formed shape before post-consolidation process



(b) Formed shape after post-consolidation process

Figure 6.10: Formed shape (a) before and (b) after performing a post-consolidation process

Shape's details became much better reproduced after the post-consolidation process at 270°C. The

large corner radii regions, stemming from lack of pressure during the multiple step forming process (see Figure 6.10a), were completely suppressed during the post-consolidation step. The lower matrix viscosity at 270°C allowed the rubber mould to force the material into the metal mould's shape at the corners, thereby generating pressure in these regions and improving the dimensional accuracy.

The formed shape after the post-consolidation process (see Figure 6.10b) had, therefore, a much smoother surface at the corners and at the joggle compared to the non post-consolidated shape. Furthermore, the color of the two formed shapes, before and after post-consolidation, also differed substantially. The formed shape acquired a much darker color after post-consolidation. This may be related to the fact that in the multiple step forming process no cooling under pressure took place, opposed to the post-consolidation process. The lighter color is therefore obtained when the material is not fully re-consolidated after being heated above  $T_g$ . Thus, cooling under pressure is necessary to fully re-consolidate the composite material and is therefore recommended.

In conclusion, in order to feasibly employ multiple step forming processes for GF/PEI composites without the aid of an additional post-consolidation step, the use of higher mould temperatures in combination with active cooling mechanisms is strongly recommended. The higher mould temperature not only promotes a better bonding in co-consolidated regions, but also improves the forming behaviour, as details can be much better reproduced. The use of active cooling mechanisms is also essential in guaranteeing faster production cycles and enabling cooling under pressure, which promotes the full re-consolidation of the material.

### 6.3. Summary

GF/PEI composite laminates were press formed in two steps with a mould temperature of 240°C and no cooling under pressure. Formed shapes were then submitted to a post-consolidation step at 270°C in order to increase the degree of bonding between the two laminates formed in different steps. Specimens were then cut from post-consolidated shapes to perform DCB tests and determine the mode I interlaminar fracture toughness. Results show that it is possible to achieve a high  $G_{IC}$  between laminates formed in different steps.  $G_{IC}$  VIS and  $G_{IC}$  AVG of multiple press formed and post-consolidated laminates are the same as preconsolidated laminates'. The feasibility of the multiple step forming approach for thermoplastic composites is therefore proven. In order to reduce process cycle times, a post-consolidation process can potentially be avoided by performing the co-consolidation stage in the forming press. For thermoplastic composite materials with a PEI matrix, this requires the use of higher mould temperatures (e.g. 270°C) and the use of active cooling mechanisms which are able to increase the cooling rate.

# 7

## Conclusions and Recommendations

### *Conclusions*

The work carried out in this thesis aimed at providing an answer to the research question established in Chapter 1 and formulated as: *Is the multiple step forming approach feasible and could it potentially be applied in an industrial environment?*. Based on the findings presented in Chapters 4-6, we can conclude that the multiple step forming approach is feasible, but further work must be developed to implement it in an industrial environment.

The research sub-questions formulated in Chapter 1 can then be answered as follows:

- Q: Is it possible to form laminates in different steps into three-dimensional shapes without visual forming defects?

*A: Yes, laminates can be formed in multiple steps into three-dimensional shapes without visual forming defects. The blankholder developed in this thesis effectively prevents defects associated with the inability of two laminates to slip with respect to each other. Herein, the multiple step forming approach is feasible from a formability standpoint.*

- Q: Is it possible to achieve a good quality bond between formed and co-consolidated laminates in different steps? If so, what temperatures are needed?

*A: Yes, it is possible to achieve good quality bonds between formed and co-consolidated laminates in different steps. The process is only feasible within a certain temperature range, which for PEI matrix systems is 270°C - 300°C. Within this temperature range, high  $G_{IC}$  values can be obtained in GF/PEI formed and co-consolidated laminates.*

- Q: What is the influence of co-consolidation temperature, pressure and time on the bond quality of co-consolidated laminates?

*A: Temperature has a large influence on bond quality of co-consolidated laminates. For GF/PEI composites, the  $G_{IC}$  steeply increases from 240°C to 270°C and then reaches a plateau. Co-consolidation pressure and time do not affect bond quality significantly. Trends suggest that, within the feasible processing window, shorter times and higher pressures slightly increase the  $G_{IC}$  of co-consolidated laminates.*

## Recommendations

The multiple step forming approach for thermoplastic composites is feasible both from a formability and structural integrity standpoint, but future work must be developed to apply this approach in an industrial environment. The introduction of a post-consolidation step and the inability to actively cool down the metal mould increases production cycle times significantly. Therefore, it is with a view on applying the concept in an industrial environment that the following recommendations are outlined:

1. Increasing the maximum temperature limit of the metal mould and incorporating active cooling mechanisms is the first priority. Cooling of a metal mould may be achieved through a mechanical heat sink, which absorbs the heat from the mould after mechanical contact. Then, a production cycle would potentially look as follows:

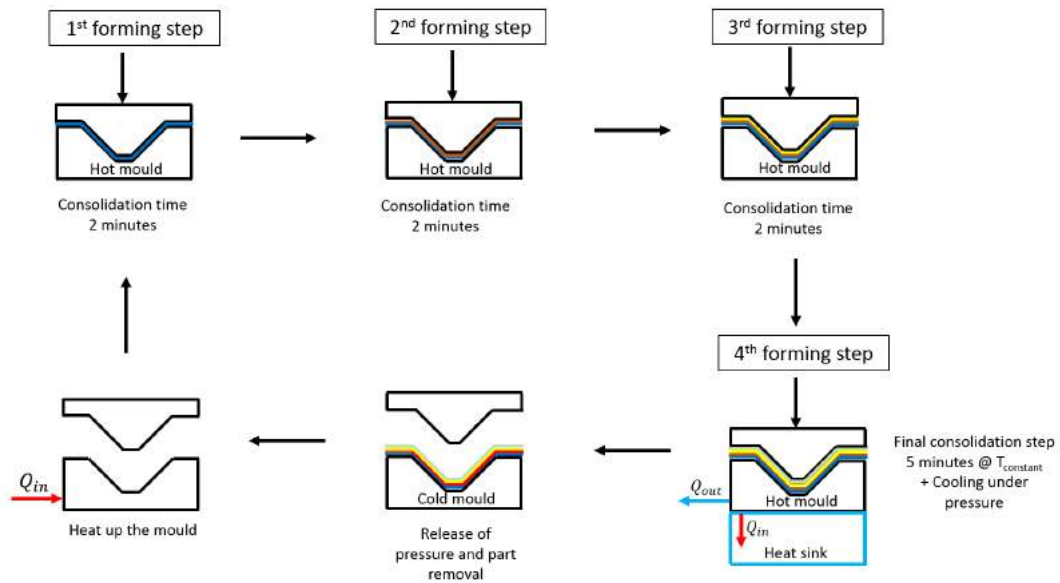


Figure 7.1: Potential multiple step forming production cycle, with short consolidation times in each forming step, and a final consolidation step with cooling under pressure

2. Actively cooling down the metal mould in each production cycle requires heating it up for the next production cycle. As a result, fast heating mechanisms should also be incorporated in order to reduce time gaps in between production cycles. In a more sophisticated system, multiple metal moulds can cycle through each other. Thus, when one mould is cooled down, another one already heated is ready to replace it. This would constitute a moving tool system.
3. An alternative solution for fast cooling and heating rates may be achieved by designing a mould comprised of two materials. One material is thin-walled and heated to high temperatures, while the second material has a large volume and its primary function is to cool down the first material. The two may be connected through springs or pneumatic pistons so that at the final consolidation step the mechanism allows the two materials to make contact with each other, thereby cooling down the part being manufactured. Once the part is removed, the two materials separate from each other and the thin-walled material can be quickly heated due to its small volume. A schematic representation of such a system is depicted below:

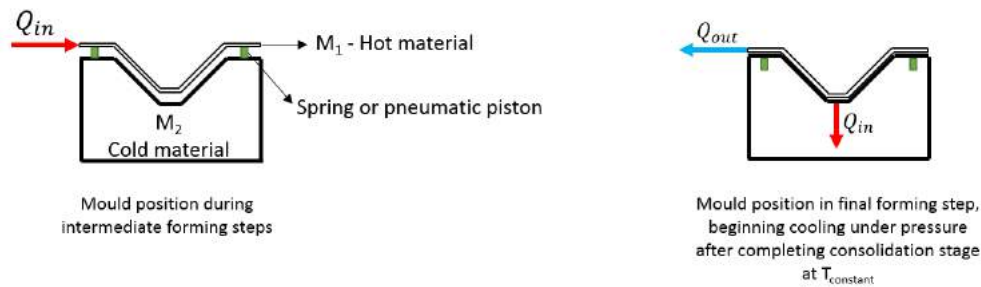
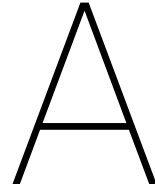


Figure 7.2: Mould concept with two materials connected through springs or pneumatic pistons, allowing fast cooling and heating rates

4. The co-consolidation time parameter may be optimized. With reduced co-consolidation times (e.g. less than 5 minutes), an overall decrease in production cycle times may be achieved.
5. Investigate the mode II and mixed-mode (mode I and II) critical strain-energy release rates of co-consolidated laminates, compare it preconsolidated laminates and determine how they are influenced by processing temperature, time and pressure. These results may provide a better insight on the delamination resistance of multiple step formed parts under different loading conditions.
6. Using different tooling materials with low ability to remove heat from laminates. To co-consolidate thermoplastic composite laminates, temperatures must be kept at high temperatures. Therefore, a mould which is capable of maintaining laminates' temperatures as high as possible for longer periods of time may improve the efficiency of the process.
7. Forming and co-consolidating laminates with dissimilar materials should also be studied. In such an approach, a GF/PEI woven composite laminate could be formed in the first step and a CF/PEEK unidirectional composite laminate formed in the second step. With such a method, hybrid parts may be manufactured, thus giving more room for design optimization.





## Designing an orthogonal array experiment

In order to determine the effect of control factors on the quality of a certain process, it is common to perform a set of experimental runs where these parameters are set at various values. These parameters vary within a certain range, whose boundaries are referred to as the *experimental design space* [74].

One of the approaches to study a specific design space is the full factorial experiment. In a full factorial experiment, all possible combinations of all factor values are investigated. Therefore, in a case where we have three control factors (temperature, pressure and time) varied at three values each, the total number of combinations would be given as:

$$n^{\circ} \text{ combinations} = y^x = 3^3 = 27 \quad (\text{A.1})$$

Where  $x$  is the number of factors and  $y$  is the number of values. A total number of 27 combinations would have to be investigated, which means that 27 co-consolidation cycles would have to be performed. The large number of experiments used for the amount of information needed to understand the influence of factor effects in the process is, therefore, the biggest weakness of this approach.

As a result, statistical techniques that can generate enough information from a small number of tests are required in order to understand what the optimum values for the control factors are and to determine what is the influence of each control factor on the response (i.e. increasing time causes an increase, decrease or no difference in the fracture toughness of GF/PEI co-consolidated laminates?).

This leads to another approach, called the orthogonal array experiment, to study a specific design space. The orthogonal array is a method that only requires a fraction of the full factorial combinations to extract the amount of information needed to determine the influence of each control factor on a certain response. In an orthogonal array, no factor is given more or less weight in the experiment than the other factors, thus creating a balance of the various combinations. Moreover, the effect of each factor can be assessed independently of the effects of the other factors.

Through this method, the influence of time, pressure and temperature on the mode I interlaminar fracture toughness of GF/PEI co-consolidated laminates could be determined by performing the following orthogonal array experiment:

Table A.1: Co-consolidation L9 orthogonal array experiment

Run	Time (min)	Temperature (°C)	Pressure (bar)
1	5	240	20
2	5	270	30
3	5	300	40
4	15	240	30
5	15	270	40
6	15	300	20
7	30	240	40
8	30	270	20
9	30	300	30

Note that from the 27 combinations in the full factorial experiment, the experiment is now reduced to only 9 combinations.

The orthogonality concept can be illustrated in this table through some properties. First, all three different values of each parameter occur the same number of times in each column of the array. Furthermore, for the three rows with level 5min in the first column, one row has level 240°C, another 270°C and the other 300°C in the second column. The same can be said for the three rows with the levels 15min and 30min in column 1. In fact, the same balance of factor levels can be found for every pair of columns in the array.

The concept of *degrees of freedom* is also used to describe how big an experiment must be and how much information can be extracted. The number of degrees of freedom in a matrix experiment is given by the number of runs in the experiment minus 1:

$$DOF_{exp} = n^{\circ} \text{ runs} - 1 \quad (\text{A.2})$$

The degrees of freedom needed to describe a factor effect is equal to the number of levels tested for that factor minus 1:

$$DOF_f = n^{\circ} \text{ levels} - 1 \quad (\text{A.3})$$

And therefore the total number of degrees of freedom required to describe every factor effect is:

$$\text{Total } DOF_f = (n^{\circ} \text{ factors}) * DOF_f \quad (\text{A.4})$$

Hereby, for the present case, where 3 factors at 3 levels are investigated in 9 experimental runs, the following results are obtained:

$$DOF_{exp} = 8$$

$$DOF_f = 2$$

$$\text{Total } DOF_f = 6$$

The number of degrees of freedom of the matrix experiment is higher than the required number of degrees of freedom to describe every factor effect. This means that more information will be generated than we actually need and that the effects of all control factors can be described. The extra degrees of freedom can be used to calculate the variance due to experimental error.

# B

## Statistical methods - Analysis of Means and Analysis of Variance

To better demonstrate the statistical methods and equations used in both the Analysis of Means (ANOM) and Analysis of Variance (ANOVA), the following  $G_{IC}$  VIS results obtained in DCB tests are provided:

Table B.1:  $G_{IC}$  VIS results

Run	Time (min)	Temperature (°C)	Pressure (bar)	$G_{IC}$ VIS (KJ/m <sup>2</sup> )
1	5	240	20	0.287
2	5	270	30	1.761
3	5	300	40	1.824
4	15	240	30	0.415
5	15	270	40	1.713
6	15	300	20	1.706
7	30	240	40	0.525
8	30	270	20	1.651
9	30	300	30	1.628

### B.1. Analysis of means (ANOM)

In an analysis of means (ANOM), the average effect of each control factor on  $G_{IC}$  VIS is determined. It starts by taking the  $G_{IC}$  VIS averages that correspond with the factor levels. So, for the present case we obtain:

$$\overline{G_{IC(5min)}} = (R_1 + R_2 + R_3)/3 = (0.287 + 1.761 + 1.824)/3 = 1.291 \quad [KJ/m^2]$$

$$\overline{G_{IC(15min)}} = (R_4 + R_5 + R_6)/3 = (0.415 + 1.713 + 1.706)/3 = 1.278 \quad [KJ/m^2]$$

$$\overline{G_{IC(30min)}} = (R_7 + R_8 + R_9)/3 = (0.525 + 1.651 + 1.628)/3 = 1.268 \quad [KJ/m^2]$$

$$\overline{G_{IC(240^\circ C)}} = (R_1 + R_4 + R_7)/3 = (0.287 + 0.415 + 0.525)/3 = 0.409 \quad [KJ/m^2]$$

$$\overline{G_{IC(270^\circ C)}} = (R_2 + R_5 + R_8)/3 = (1.761 + 1.713 + 1.651)/3 = 1.708 \quad [KJ/m^2]$$

$$\overline{G_{IC(300^\circ C)}} = (R_3 + R_6 + R_9)/3 = (1.824 + 1.706 + 1.628)/3 = 1.719 \quad [KJ/m^2]$$

$$\overline{G_{IC(20bar)}} = (R_1 + R_6 + R_8)/3 = (0.287 + 1.706 + 1.651)/3 = 1.215 \quad [KJ/m^2]$$

$$\overline{G_{IC(30bar)}} = (R_2 + R_4 + R_9)/3 = (1.761 + 0.415 + 1.628)/3 = 1.268 \quad [KJ/m^2]$$

$$\overline{G_{IC(40bar)}} = (R_3 + R_5 + R_7)/3 = (1.824 + 1.713 + 0.525)/3 = 1.354 \quad [KJ/m^2]$$

## B.2. Analysis of variance (ANOVA)

This technique uses the *sum of squares* to quantitatively determine the deviation of the control factor effect response averages from the experimental mean response [74]. The significance of each control factor is then quantified by comparing the variance between the control factor effects against the variance due to random experimental error and the effects of unrepresented interactions. Thus, the ratio in Equation B.1, referred to as the *F-ratio*, can be calculated by dividing the control factor effect variance by the experimental error variance. If this ratio is lower than 1, the experimental error outweighs the control factor effect and therefore the control factor is insignificant to the global response. If  $F_{prac} \approx 2$ , the control factor only has a moderate effect compared to experimental error [74]. If  $F_{prac} > 4$  the control factor effect is strong compared to experimental error and is clearly significant [74]. In addition to these comparisons, the F-ratio can also be compared to tabulated values. Thereby, if  $F_{prac} > F_{table}$ , we can conclude that the control factor effect is significant to the response and outweighs the effects of unrepresented interactions and random experimental error.

$$F_{prac} = \frac{\text{mean square due to a control factor}}{\text{mean square due to experimental error}} \quad (B.1)$$

As explained in Appendix A, the total number of degrees of freedom in this L9 orthogonal array designed experiment is equal to 8. The number of degrees of freedom used, however, is 6 (2 for each control factor). This means that the 2 extra degrees of freedom can be used to calculate the variance due to experimental error, thus not having the need to resort to replicate experiments. This process will be more thoroughly explained later in this section.

The ANOVA, hereby, starts by first calculating the overall mean of the experimental runs, from which all the variances are calculated. The overall mean is given by:

$$\overline{G_{IC}} = \frac{1}{9}(0.287 + 1.761 + \dots + 1.628) = 1.279 \quad (B.2)$$

Then, the grand total sum of squares (GTSS) is calculated through the following expression:

$$GTSS = \sum_{i=1}^9 (G_{IC})^2 = 0.287^2 + 1.761^2 + \dots + 1.628^2 = 18.18 \quad (B.3)$$

The GTSS can be decomposed into two parts:

1. The sum of squares due to the overall mean:

$$SS \text{ due to mean} = (n^\circ \text{ experiments}) * (\overline{G_{IC}})^2 = 9 * 1.279^2 = 14.72 \quad (B.4)$$

2. The total sum of squares:

$$\text{Total SS} = \sum_{i=1}^9 (G_{IC_i} - \overline{G_{IC}})^2 = 3.459 \quad (B.5)$$

Note that the  $GTSS = \text{total SS} + SS \text{ due to mean}$ .

The ANOVA technique now uses the sum of squares to define the contribution of each control factor within the total sum of squares. The method numerically quantifies the variation induced by the control factor effects around the overall experimental mean, hence the name *analysis of variance*. Variances are used to quantify the strength of the control factor effects [74].

Therefore, for the time factor, the sum of squares due to variation about the mean is:

$$\begin{aligned}
SS_{time} &= (n^{\circ} \text{ exp. at 5 min})(\overline{G_{IC(5min)}} - \overline{G_{IC}})^2 + (n^{\circ} \text{ exp. at 15 min})(\overline{G_{IC(15min)}} - \overline{G_{IC}})^2 \\
&+ (n^{\circ} \text{ exp. at 30 min})(\overline{G_{IC((30min)}} - \overline{G_{IC}})^2 \\
&= 3(1.291 - 1.279)^2 + 3(1.278 - 1.279)^2 + 3(1.268 - 1.279)^2 \\
&= 0.0007742
\end{aligned} \tag{B.6}$$

The procedure can be repeated for the temperature and pressure factors as well, thus yielding in the following results:

$$SS_{temperature} = 3.405$$

$$SS_{pressure} = 0.02965$$

The calculated values represent the relative importance of each factor in controlling the measured response, in this case,  $G_{IC}$ . When the components are added, a very similar value as the total SS is obtained:

$$SS_{time} + SS_{temperature} + SS_{pressure} = 0.0007742 + 3.405 + 0.02965 = 3.436$$

The reason for this value not being the same as the total SS is precisely due to the fact that not all of the experiment's degrees of freedom were used. If we recall the results from Equations A.2 and A.4, the experiment has 8 degrees of freedom while only 6 were being used. The extra 2 degrees of freedom result in this small discrepancy between the total SS and the sum of the 3 sums of squares depicted in the expression above. As a result, the sum of squares due to experimental error and unrepresented interactions is given as follows:

$$\begin{aligned}
SS_{error} &= Total\ SS - (SS_{time} + SS_{temperature} + SS_{pressure}) \\
&= 3.459 - 3.436 \\
&= 0.02351
\end{aligned} \tag{B.7}$$

With these results, the percentage contribution of each control factor on the measured property can be calculated as follows:

$$Percentage\ contribution = \frac{SS_{factor}}{Total\ SS} * 100 \tag{B.8}$$

Thus yielding in the following results:

$$Time : 0.02238\%$$

$$Temperature : 98.44\%$$

$$Pressure : 0.8572\%$$

$$Error : 0.6795\%$$

Finally, to conclude the analysis of variance, the F-ratios of each control factor can be calculated through Equation B.1. For the time parameter, the expression yields in the following result:

$$F_{prac(time)} = \frac{SS_{time}}{SS_{error}} = \frac{0.0007742}{0.02351} = 0.03294 \tag{B.9}$$

Repeating the procedure for the other two factors we obtain:

$$F_{prac(temperature)} = 144.9$$

$$F_{prac(pressure)} = 1.262$$

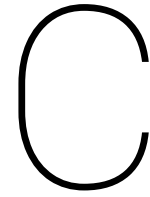
The results obtained above can then be summarized in the following table:

Table B.2: ANOVA results for  $G_{IC}$  output

Input parameter	DOF	SS	% Contribution	$F_{prac}$	$F_{table}$	Significance
Time	2	0.0007742	0.02238 %	0.03294	19	NO
Temperature	2	3.405	98.44 %	144.9	19	YES
Pressure	2	0.02965	0.8572 %	1.262	19	NO
Error	2	0.02351	0.6795 %	1	N/A	N/A
Total	8	3.459	100 %	N/A	N/A	N/A

The significance of each parameter is determined by comparing the practical F-ratio, calculated using Equation B.9 ( $F_{prac}$ ), to the theoretical F-ratio given in Fisher-Snedecor tables ( $F_{table}$ ) using a risk value,  $\alpha$ , of 0.05.

The  $\alpha$  level represents the probability of rejecting a null hypothesis when it is true (Type I error). So, for instance, in this case the null hypothesis can be formulated as: "*Temperature does not have an effect on  $G_{IC}$* ". A type I error would then be to reject the fact that temperature does not have an effect on  $G_{IC}$  when it actually doesn't have an effect on  $G_{IC}$ . A type II error would be not to reject the null hypothesis when it is false. So, if  $\alpha$  is very small, the probability of making a type I error is very small, but at the same time, the probability of making a type II error increases. As a result, an  $\alpha$  level of 0.05 (i.e. 5%) is a good balance between the two issues and it was therefore chosen in this analysis.

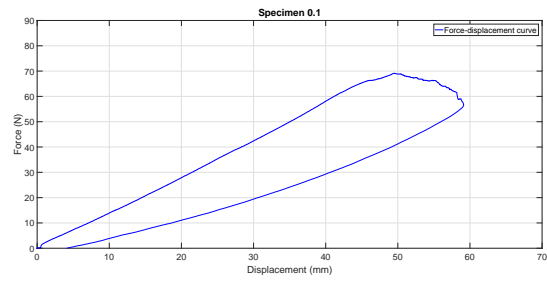


# Double Cantilever Beam Test Data and Load-Displacement Curves

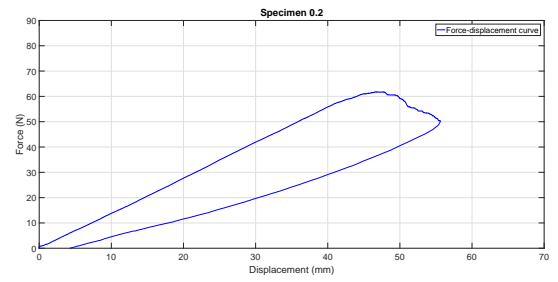
## C.1. Preconsolidated Specimens

Table C.1: DCB test results of preconsolidated specimens

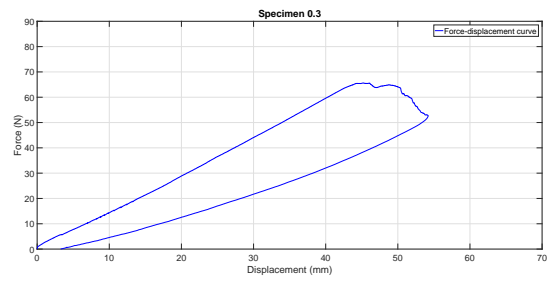
Specimen n°	$a_0$	$\delta$	P	$\delta/a_0$	b	h	t	F	L	$G_{IC}$	MBT
Specimen 1	52.4	41.92	61.86	0.8	24.85	3.14	11.0342	0.555	132	<b>VIS</b>	1.6588
	N/A	N/A	N/A	N/A	24.85	3.14	N/A	N/A	132	<b>Avg</b>	2.3447
Specimen 2	52.4	40.32	56.24	0.7695	24.76	3.19	11.0467	0.5791	132	<b>VIS</b>	1.5181
	N/A	N/A	N/A	N/A	24.76	3.19	N/A	N/A	132	<b>Avg</b>	2.0779
Specimen 3	52.4	43.06	64.17	0.8218	24.81	3.27	11.0675	0.5371	132	<b>VIS</b>	1.7123
	N/A	N/A	N/A	N/A	24.81	3.27	N/A	N/A	132	<b>Avg</b>	2.1113
Specimen 4	53	41.39	60.46	0.7809	24.88	3.30	11.0758	0.5722	132	<b>VIS</b>	1.6289
	N/A	N/A	N/A	N/A	24.88	3.30	N/A	N/A	132	<b>Avg</b>	2.1412
Specimen 5	53	40.69	59.24	0.7677	24.93	3.27	11.0667	0.5827	132	<b>VIS</b>	1.5946
	N/A	N/A	N/A	N/A	N/A	N/A	N/A	N/A	N/A	<b>Avg</b>	N/A



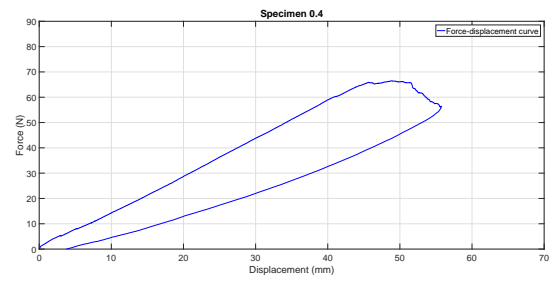
(a) Load-displacement curve specimen 1



(b) Load-displacement curve specimen 2



(c) Load-displacement curve specimen 3



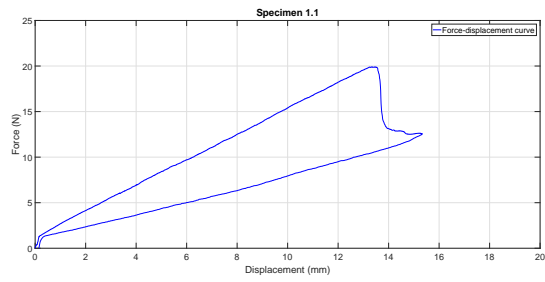
(d) Load-displacement curve specimen 4

Figure C.1: Load-displacement curves of preconsolidated specimens

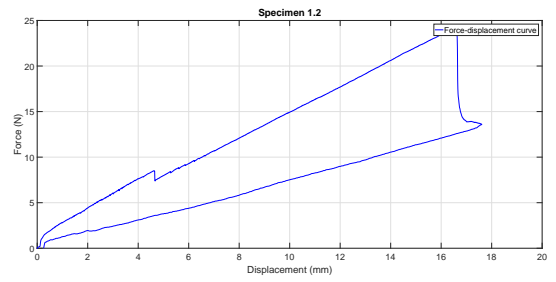
## C.2. Co-consolidated Specimens Run 1

Table C.2: DCB test results of co-consolidated specimens run 1

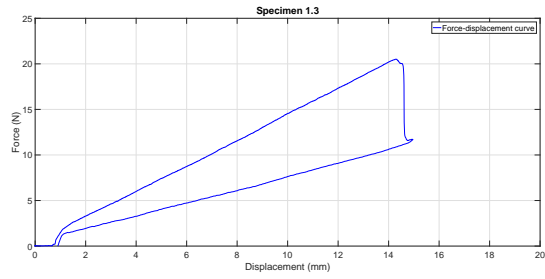
Specimen n°	$a_0$	$\delta$	P	$\delta/a_0$	b	h	t	F	L	G <sub>IC</sub>	MBT
Specimen 1	52.75	13.518	19.872	0.25627	24.77	3.34	11.085	N/A	132	<b>VIS</b>	0.2489
	N/A	N/A	N/A	N/A	24.77	3.34	N/A	N/A	132	<b>Avg</b>	0.2469
Specimen 2	52.75	16.53	23.925	0.31336	24.79	3.35	11.0867	N/A	132	<b>VIS</b>	0.4536
	N/A	N/A	N/A	N/A	24.79	3.35	N/A	N/A	132	<b>Avg</b>	0.3591
Specimen 3	52.75	13.64	20.51	0.2586	24.88	3.40	11.10	N/A	132	<b>VIS</b>	0.31974
	N/A	N/A	N/A	N/A	24.88	3.40	N/A	N/A	132	<b>Avg</b>	0.2608
Specimen 4	52	9.77	13.827	0.18788	24.84	3.34	11.0842	N/A	132	<b>VIS</b>	0.156877
	N/A	N/A	N/A	N/A	24.84	3.34	N/A	N/A	132	<b>Avg</b>	0.2270
Specimen 5	52.25	10.53	16.26	0.20153	24.89	3.36	11.090	N/A	132	<b>VIS</b>	0.197483
	N/A	N/A	N/A	N/A	24.89	3.36	N/A	N/A	132	<b>Avg</b>	0.1127
Specimen 6	52.25	12.90	19.27	0.2469	24.85	3.39	11.0967	N/A	132	<b>VIS</b>	0.2872
	N/A	N/A	N/A	N/A	24.85	3.39	N/A	N/A	132	<b>Avg</b>	0.2160



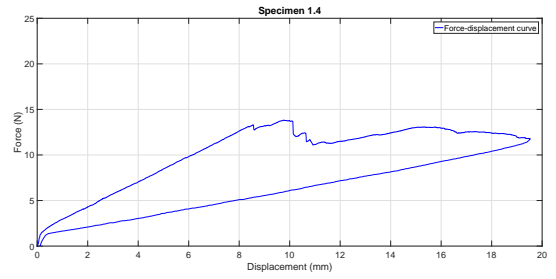
(a) Load-displacement curve specimen 1



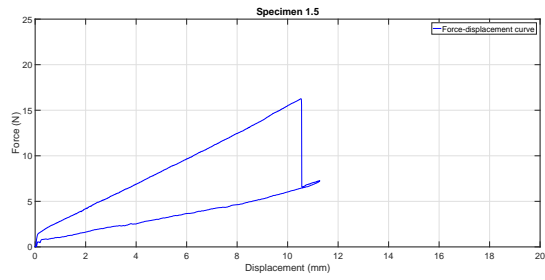
(b) Load-displacement curve specimen 2



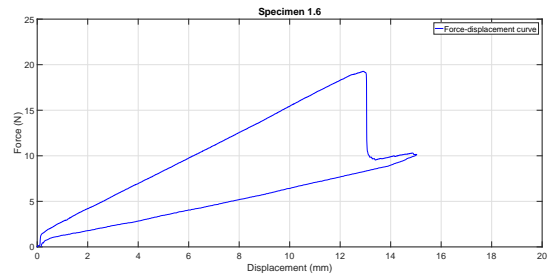
(c) Load-displacement curve specimen 3



(d) Load-displacement curve specimen 4



(e) Load-displacement curve specimen 5



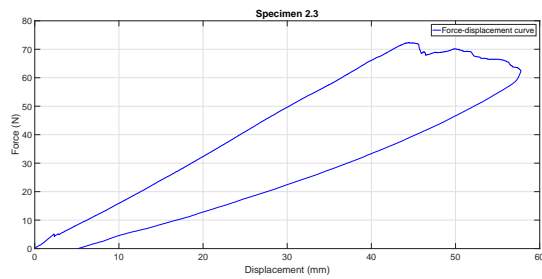
(f) Load-displacement curve specimen 6

Figure C.2: Load-displacement curves of co-consolidated specimens run 1

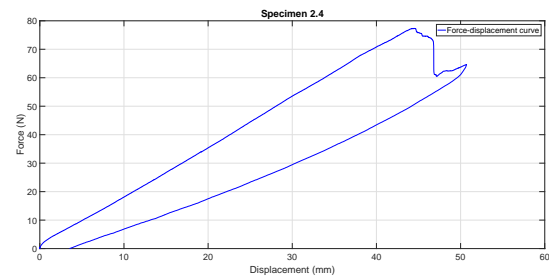
## C.3. Co-consolidated Specimens Run 2

Table C.3: DCB test results of co-consolidated specimens run 2

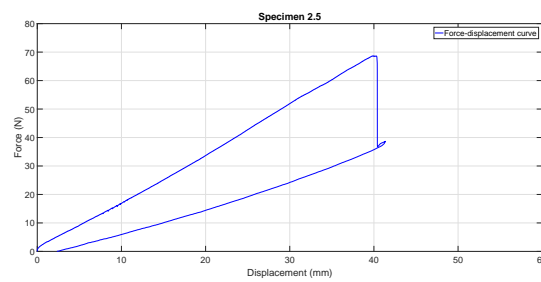
Specimen n°	$a_0$	$\delta$	P	$\delta/a_0$	b	h	t	F	L	$G_{IC}$	MBT
Specimen 1	50	41.84	69.1	0.8368	24.70	3.32	11.08	0.5118	132	VIS	1.8182
	N/A	N/A	N/A	N/A	N/A	N/A	N/A	N/A	N/A	Avg	N/A
Specimen 2	50	38.71	65.01	0.7742	24.82	3.38	11.095	0.5625	132	VIS	1.71096
	N/A	N/A	N/A	N/A	N/A	N/A	N/A	N/A	N/A	Avg	N/A
Specimen 3	50	41.13	67.66	0.8226	24.92	3.36	11.0908	0.5233	132	VIS	1.7531
	N/A	N/A	N/A	N/A	24.92	3.36	N/A	N/A	132	Avg	2.8987
Specimen 4	50	39.41	69.87	0.7882	24.81	3.37	11.0933	0.55131	132	VIS	1.8356
	N/A	N/A	N/A	N/A	24.81	3.37	N/A	N/A	132	Avg	3.1250
Specimen 5	50	37.75	65.17	0.755	24.84	3.39	11.0967	0.57765	132	VIS	1.71633
	N/A	N/A	N/A	N/A	24.84	3.39	N/A	N/A	132	Avg	2.1469
Specimen 6	50	38.28	64.55	0.7656	24.41	3.38	11.0942	0.56935	132	VIS	1.72901
	N/A	N/A	N/A	N/A	N/A	N/A	N/A	N/A	N/A	Avg	N/A



(a) Load-displacement curve specimen 3



(b) Load-displacement curve specimen 4



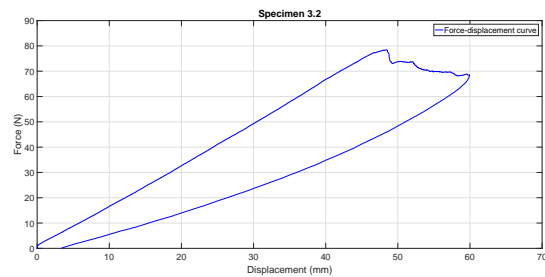
(c) Load-displacement curve specimen 5

Figure C.3: Load-displacement curves of co-consolidated specimens run 2

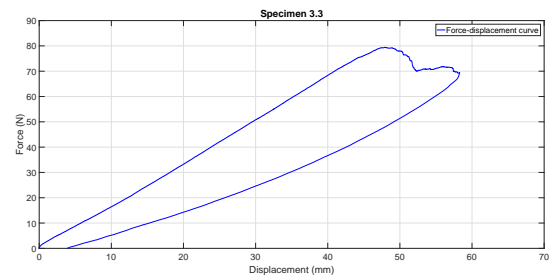
### C.4. Co-Consolidated Specimens Run 3

Table C.4: DCB test results of co-consolidated specimens run 3

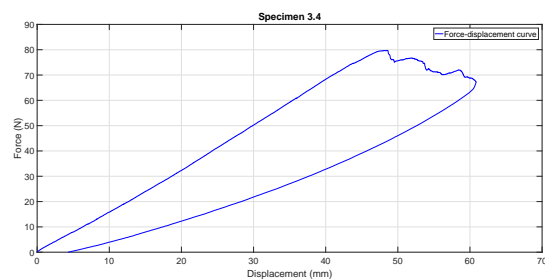
Specimen n°	$a_0$	$\delta$	P	$\delta/a_0$	b	h	t	F	L	$G_{IC}$	MBT
Specimen 1	51	41.81	63.96	0.8198	24.90	3.25	11.0617	0.5317	132	<b>VIS</b>	1.67936
	N/A	N/A	N/A	N/A	N/A	N/A	N/A	N/A	N/A	<b>Avg</b>	N/A
Specimen 2	50.5	42.54	70.87	0.84238	24.91	3.27	11.0675	0.5102	132	<b>VIS</b>	1.8341
	N/A	N/A	N/A	N/A	24.91	3.27	N/A	N/A	132	<b>Avg</b>	2.8337
Specimen 3	51	41.83	71.45	0.8202	24.76	3.29	11.0733	0.5311	132	<b>VIS</b>	1.8854
	N/A	N/A	N/A	N/A	24.76	3.29	N/A	N/A	132	<b>Avg</b>	2.4856
Specimen 4	51	41.24	70.43	0.8086	24.82	3.32	11.080	0.54032	132	<b>VIS</b>	1.8597
	N/A	N/A	N/A	N/A	24.82	3.32	N/A	N/A	132	<b>Avg</b>	3.2840
Specimen 5	51	42.49	69.09	0.8331	24.80	3.32	11.080	0.52026	132	<b>VIS</b>	1.8113
	N/A	N/A	N/A	N/A	N/A	N/A	N/A	N/A	N/A	<b>Avg</b>	N/A
Specimen 6	51	44.24	69.82	0.8675	24.83	3.27	11.0817	0.49153	132	<b>VIS</b>	1.79841
	N/A	N/A	N/A	N/A	24.83	3.27	N/A	N/A	132	<b>Avg</b>	2.9138
Specimen 7	50.5	44.11	74.86	0.87347	24.92	3.35	11.0875	0.4835	132	<b>VIS</b>	1.90282
	N/A	N/A	N/A	N/A	N/A	N/A	N/A	N/A	N/A	<b>Avg</b>	N/A



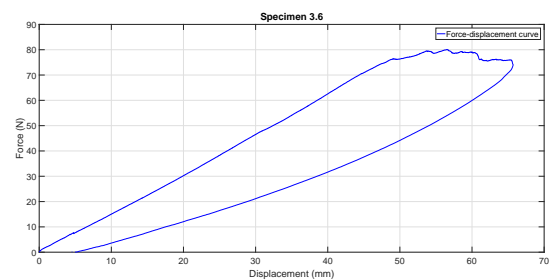
(a) Load-displacement curve specimen 2



(b) Load-displacement curve specimen 3



(c) Load-displacement curve specimen 4



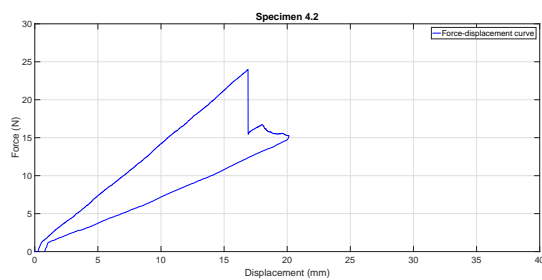
(d) Load-displacement curve specimen 6

Figure C.4: Load-displacement curves of co-consolidated specimens run 3

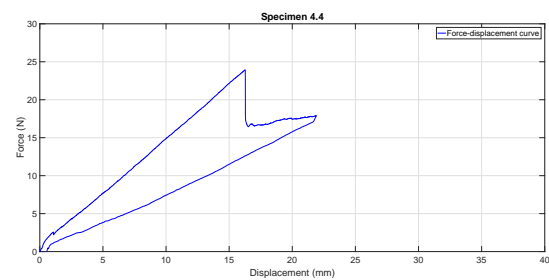
## C.5. Co-Consolidated Specimens Run 4

Table C.5: DCB test results of co-consolidated specimens run 4

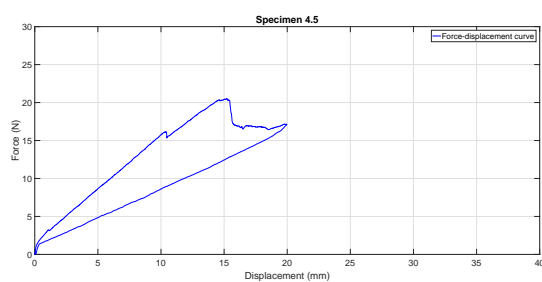
Specimen n°	$a_0$	$\delta$	P	$\delta/a_0$	b	h	t	F	L	$G_{IC}$	MBT
Specimen 1	53	11.1	17.5	0.2094	24.85	3.34	11.0685	N/A	132	VIS	0.2212
	N/A	N/A	N/A	N/A	N/A	N/A	N/A	N/A	N/A	Avg	N/A
Specimen 2	53	16.89	24.00	0.3187	24.82	3.35	11.0883	N/A	132	VIS	0.4622
	N/A	N/A	N/A	N/A	24.82	3.35	N/A	N/A	132	Avg	0.3739
Specimen 3	53	15.34	23.00	0.2894	24.79	3.35	11.0867	N/A	132	VIS	0.4028
	N/A	N/A	N/A	N/A	N/A	N/A	N/A	N/A	N/A	Avg	N/A
Specimen 4	53	16.27	23.94	0.307	24.81	3.34	11.0842	N/A	132	VIS	0.4443
	N/A	N/A	N/A	N/A	24.81	3.34	N/A	N/A	132	Avg	0.4010
Specimen 5	53	14.58	20.35	0.2751	24.80	3.35	11.0867	N/A	132	VIS	0.3386
	N/A	N/A	N/A	N/A	24.80	3.35	N/A	N/A	132	Avg	0.3633
Specimen 6	52	21.1	30.92	0.40577	24.81	3.35	11.0867	0.82084	132	VIS	0.6226
	N/A	N/A	N/A	N/A	24.81	3.35	N/A	N/A	132	Avg	0.5460



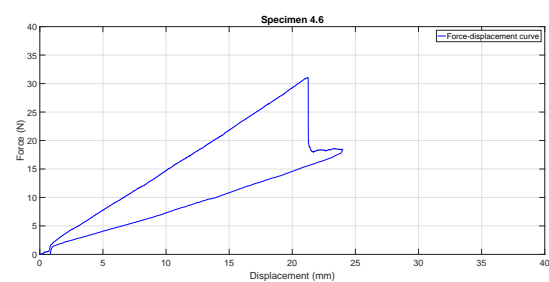
(a) Load-displacement curve specimen 2



(b) Load-displacement curve specimen 4



(c) Load-displacement curve specimen 5



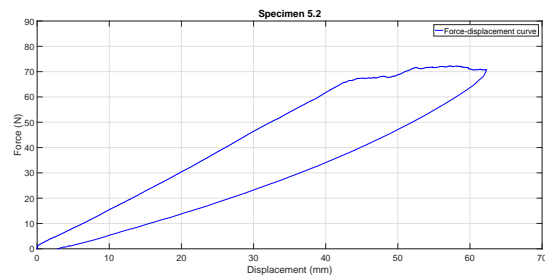
(d) Load-displacement curve specimen 6

Figure C.5: Load-displacement curves of co-consolidated specimens run 4

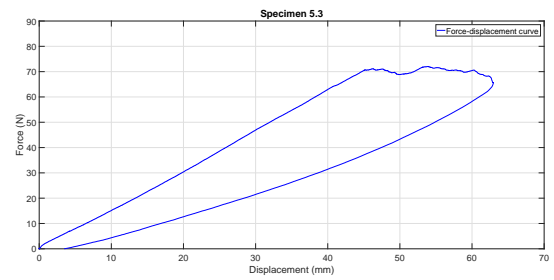
## C.6. Co-Consolidated Specimens Run 5

Table C.6: DCB test results of co-consolidated specimens run 5

Specimen n°	$a_0$	$\delta$	P	$\delta/a_0$	b	h	t	F	L	$G_{IC}$	MBT
Specimen 1	52.5	41.92	65.06	0.7985	24.83	3.36	11.0908	0.5557	132	<b>VIS</b>	1.7440
	N/A	N/A	N/A	N/A	N/A	N/A	N/A	N/A	N/A	<b>Avg</b>	N/A
Specimen 2	52	40.99	63.34	0.7883	24.87	3.36	11.0908	0.5614	132	<b>VIS</b>	1.6906
	N/A	N/A	N/A	N/A	24.87	3.36	N/A	N/A	132	<b>Avg</b>	2.2914
Specimen 3	52	40.86	64.28	0.7858	24.88	3.34	11.0858	0.5635	132	<b>VIS</b>	1.7159
	N/A	N/A	N/A	N/A	24.88	3.34	N/A	N/A	132	<b>Avg</b>	3.0808
Specimen 4	52.5	41.38	63.77	0.7882	24.85	3.35	11.0867	0.5640	132	<b>VIS</b>	1.7110
	N/A	N/A	N/A	N/A	N/A	N/A	N/A	N/A	N/A	<b>Avg</b>	N/A
Specimen 5	53	42.31	63.06	0.7983	24.76	3.35	11.0875	0.5583	132	<b>VIS</b>	1.7027
	N/A	N/A	N/A	N/A	N/A	N/A	N/A	N/A	N/A	<b>Avg</b>	N/A



(a) Load-displacement curve specimen 2



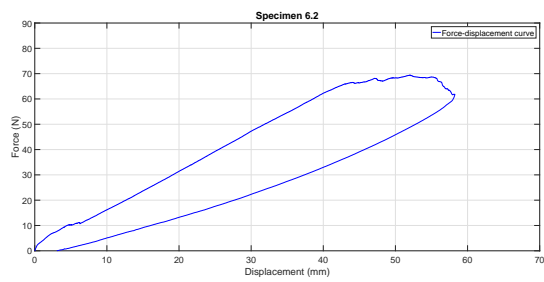
(b) Load-displacement curve specimen 3

Figure C.6: Load-displacement curves of co-consolidated specimens run 5

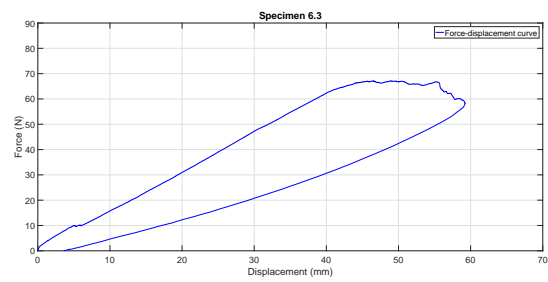
## C.7. Co-Consolidated Specimens Run 6

Table C.7: DCB test results of co-consolidated specimens run 6

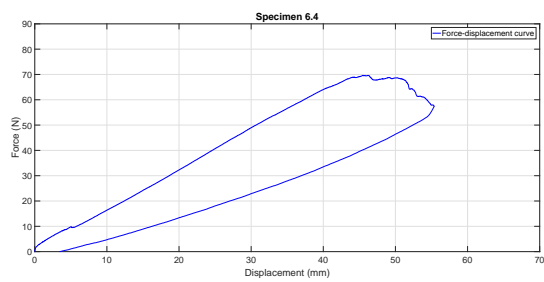
Specimen n°	$a_0$	$\delta$	P	$\delta/a_0$	b	h	t	F	L	$G_{IC}$	MBT
Specimen 1	51	42.85	68.07	0.8402	24.80	3.24	11.068	0.5149	132	<b>VIS</b>	1.7811
	N/A	N/A	N/A	N/A	N/A	N/A	N/A	N/A	N/A	<b>Avg</b>	N/A
Specimen 2	51	41.83	64.58	0.8202	24.85	3.26	11.0650	0.5313	132	<b>VIS</b>	1.6986
	N/A	N/A	N/A	N/A	24.85	3.26	N/A	N/A	132	<b>Avg</b>	2.7923
Specimen 3	51	41.23	63.81	0.8084	24.92	3.29	11.0717	0.5407	132	<b>VIS</b>	1.6789
	N/A	N/A	N/A	N/A	24.92	3.29	N/A	N/A	132	<b>Avg</b>	3.1341
Specimen 4	51	40.54	64.69	0.7949	24.91	3.29	11.0717	0.5516	132	<b>VIS</b>	1.708
	N/A	N/A	N/A	N/A	24.91	3.29	N/A	N/A	132	<b>Avg</b>	2.9476
Specimen 5	51.5	39.34	62.28	0.7639	24.82	3.32	11.0792	0.5784	132	<b>VIS</b>	1.6631
	N/A	N/A	N/A	N/A	24.82	3.32	N/A	N/A	132	<b>Avg</b>	3.0647



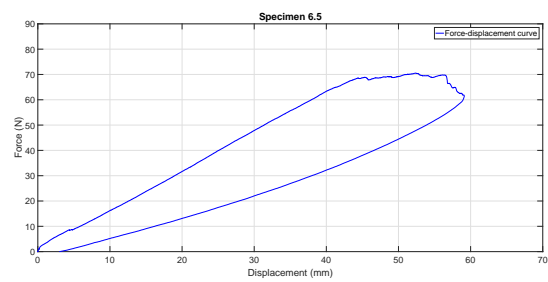
(a) Load-displacement curve specimen 2



(b) Load-displacement curve specimen 3



(c) Load-displacement curve specimen 4



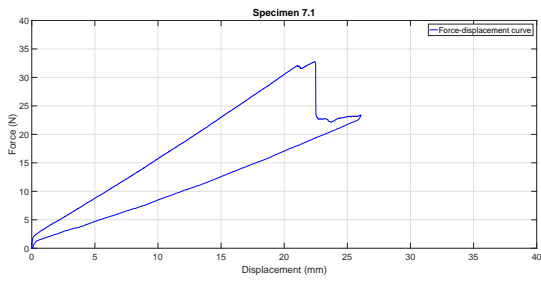
(d) Load-displacement curve specimen 5

Figure C.7: Load-displacement curves of co-consolidated specimens run 6

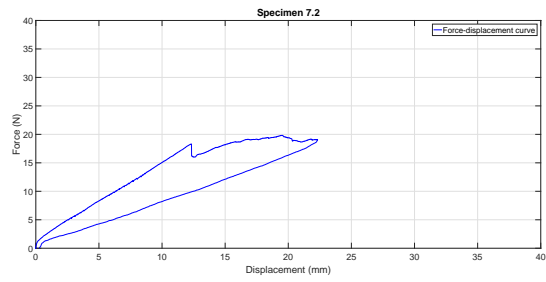
## C.8. Co-Consolidated Specimens Run 7

Table C.8: DCB test results of co-consolidated specimens run 7

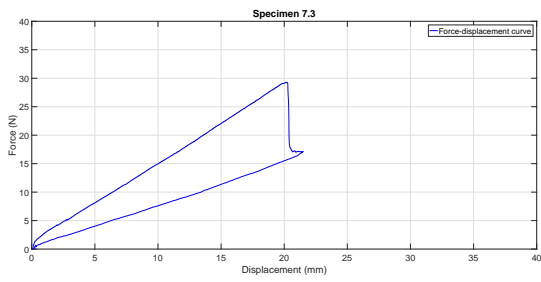
Specimen n°	$a_0$	$\delta$	P	$\delta/a_0$	b	h	t	F	L	$G_{IC}$	MBT
Specimen 1	53	21.18	31.95	0.3996	24.72	3.36	11.0908	N/A	132	<b>VIS</b>	0.7748
	N/A	N/A	N/A	N/A	24.72	3.36	N/A	N/A	132	<b>Avg</b>	0.7056
Specimen 2	53	12.33	18.32	0.23264	24.79	3.37	11.0917	N/A	132	<b>VIS</b>	0.2579
	N/A	N/A	N/A	N/A	24.79	3.37	N/A	N/A	132	<b>Avg</b>	0.3769
Specimen 3	51	20.19	29.23	0.39588	24.86	3.35	11.0867	N/A	132	<b>VIS</b>	0.6982
	N/A	N/A	N/A	N/A	24.86	3.35	N/A	N/A	132	<b>Avg</b>	0.6595
Specimen 4	53	14.49	20.14	0.2841	24.81	3.33	11.0825	N/A	132	<b>VIS</b>	0.346
	N/A	N/A	N/A	N/A	N/A	N/A	N/A	N/A	N/A	<b>Avg</b>	N/A
Specimen 5	51	17.54	24.18	0.3439	24.76	3.32	11.080	N/A	132	<b>VIS</b>	0.5038
	N/A	N/A	N/A	N/A	24.76	3.32	N/A	N/A	132	<b>Avg</b>	0.5215
Specimen 6	51	19.09	24.47	0.3743	24.81	3.31	11.0775	0.83601	132	<b>VIS</b>	0.5538
	N/A	N/A	N/A	N/A	24.81	3.31	N/A	N/A	132	<b>Avg</b>	0.4800
Specimen 7	53	18.27	26.00	0.3447	24.86	3.31	11.0775	0.85628	132	<b>VIS</b>	0.5408
	N/A	N/A	N/A	N/A	24.86	3.31	N/A	N/A	132	<b>Avg</b>	0.4416



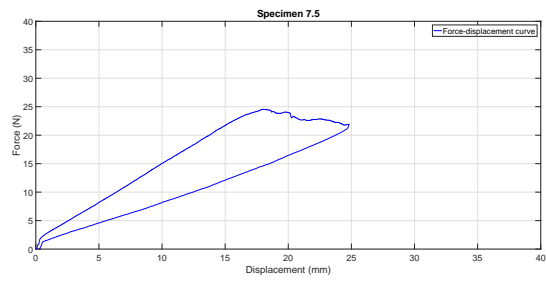
(a) Load-displacement curve specimen 1



(b) Load-displacement curve specimen 2



(c) Load-displacement curve specimen 3



(d) Load-displacement curve specimen 5



(e) Load-displacement curve specimen 6



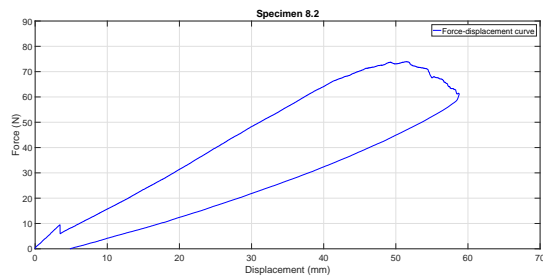
(f) Load-displacement curve specimen 7

Figure C.8: Load-displacement curves of co-consolidated specimens run 7

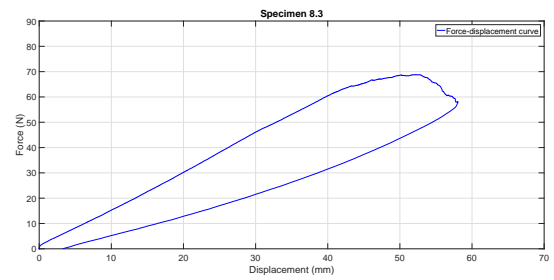
## C.9. Co-Consolidated Specimens Run 8

Table C.9: DCB test results of co-consolidated specimens run 8

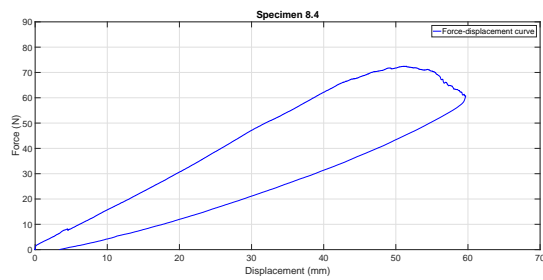
Specimen n°	$a_0$	$\delta$	P	$\delta/a_0$	b	h	t	F	L	$G_{IC}$	MBT
Specimen 1	52.5	39.97	61.01	0.7613	24.85	3.35	11.0875	0.5849	132	<b>VIS</b>	1.6400
	N/A	N/A	N/A	N/A	N/A	N/A	N/A	N/A	N/A	<b>Avg</b>	N/A
Specimen 2	52.5	39.06	62.77	0.744	24.84	3.34	11.0850	0.5983	132	<b>VIS</b>	1.6873
	N/A	N/A	N/A	N/A	24.84	3.34	N/A	N/A	132	<b>Avg</b>	3.1832
Specimen 3	52.5	39.59	59.86	0.7541	24.83	3.34	11.0842	0.5906	132	<b>VIS</b>	1.6105
	N/A	N/A	N/A	N/A	24.83	3.34	N/A	N/A	132	<b>Avg</b>	2.9428
Specimen 4	52.5	39.09	60.75	0.7446	24.81	3.35	11.0875	0.5978	132	<b>VIS</b>	1.6349
	N/A	N/A	N/A	N/A	24.81	3.35	N/A	N/A	132	<b>Avg</b>	2.8593
Specimen 5	52.5	40.64	62.63	0.7741	24.85	3.35	11.0867	0.5750	132	<b>VIS</b>	1.6828
	N/A	N/A	N/A	N/A	24.85	3.35	N/A	N/A	132	<b>Avg</b>	3.2421



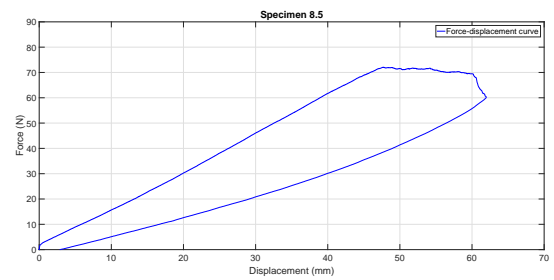
(a) Load-displacement curve specimen 2



(b) Load-displacement curve specimen 3



(c) Load-displacement curve specimen 4



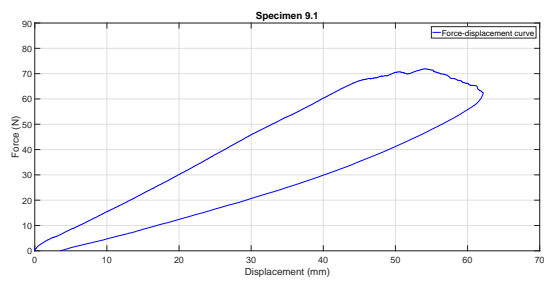
(d) Load-displacement curve specimen 5

Figure C.9: Load-displacement curves of co-consolidated specimens run 8

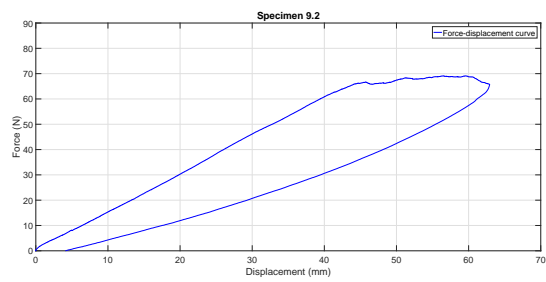
### C.10. Co-Consolidated Specimens Run 9

Table C.10: DCB test results of co-consolidated specimens run 9

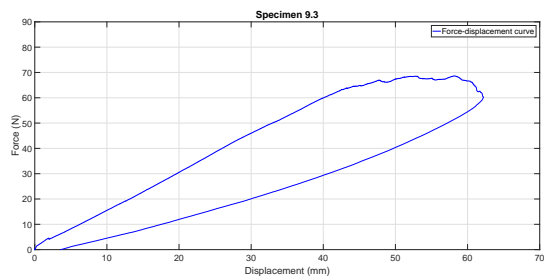
Specimen n°	$a_0$	$\delta$	P	$\delta/a_0$	b	h	t	F	L	$G_{IC}$	MBT
Specimen 1	52	42.82	64.43	0.8235	24.82	3.28	11.0692	0.5336	132	VIS	1.7111
	N/A	N/A	N/A	N/A	24.82	3.28	N/A	N/A	132	Avg	2.8749
Specimen 2	51.5	41.49	62.75	0.8056	24.84	3.28	11.070	0.5455	132	VIS	1.6654
	N/A	N/A	N/A	N/A	24.84	3.28	N/A	N/A	132	Avg	2.7749
Specimen 3	51.5	38.71	58.2	0.7517	24.81	3.26	11.0658	0.5883	132	VIS	1.5558
	N/A	N/A	N/A	N/A	24.81	3.26	N/A	N/A	132	Avg	2.9813
Specimen 4	51.5	39.10	59.00	0.74592	24.87	3.25	11.0633	0.5824	132	VIS	1.5735
	N/A	N/A	N/A	N/A	N/A	N/A	N/A	N/A	N/A	Avg	N/A
Specimen 5	51.5	40.58	61.41	0.7880	24.86	3.24	11.0592	0.5599	132	VIS	1.6348
	N/A	N/A	N/A	N/A	24.86	3.24	N/A	N/A	132	Avg	2.4449



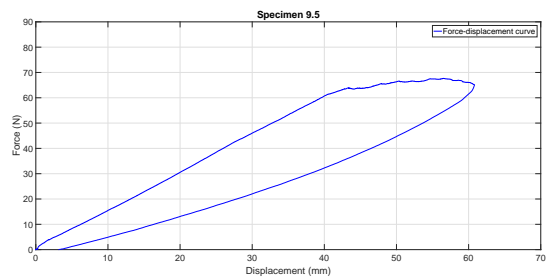
(a) Load-displacement curve specimen 2



(b) Load-displacement curve specimen 2



(c) Load-displacement curve specimen 3



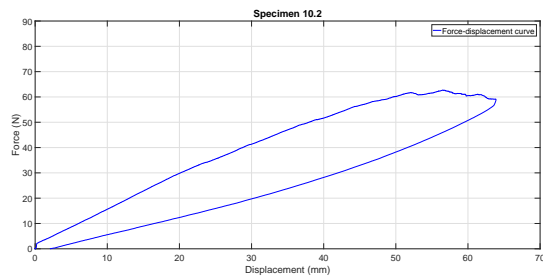
(d) Load-displacement curve specimen 5

Figure C.10: Load-displacement curves of co-consolidated specimens run 9

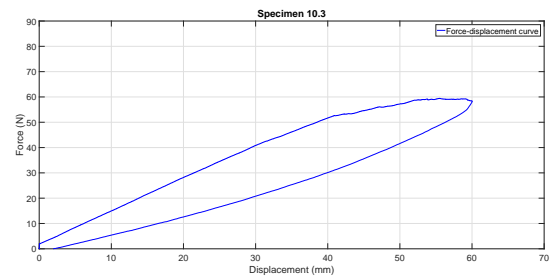
## C.11. Post-consolidated specimens from multiple step formed shape

Table C.11: DCB test results of specimens taken from post-consolidated multiple step formed shape

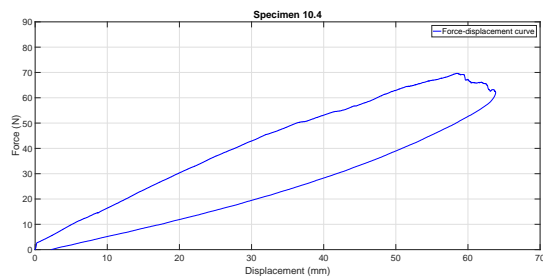
Specimen n°	$a_0$	$\delta$	P	$\delta/a_0$	b	h	t	F	L	$G_{IC}$	MBT
Specimen 1	53	39.64	47.77	0.7479	25.09	3.28	11.07	0.5979	132	VIS	1.2770
	N/A	N/A	N/A	N/A	N/A	N/A	N/A	N/A	N/A	Avg	N/A
Specimen 2	52	37.23	49.3	0.7159	25.02	3.30	11.075	0.6175	132	VIS	1.3067
	N/A	N/A	N/A	N/A	25.02	3.30	N/A	N/A	132	Avg	1.9701
Specimen 3	52.5	33.28	44.26	0.6339	25.02	3.28	11.0692	0.67897	132	VIS	1.1421
	N/A	N/A	N/A	N/A	25.02	3.28	N/A	N/A	132	Avg	1.9679
Specimen 4	51	32.64	45.64	0.64	25.00	3.27	11.0667	0.6688	132	VIS	1.1721
	N/A	N/A	N/A	N/A	25.00	3.27	N/A	N/A	132	Avg	2.5271
Specimen 5	54	35.72	46.15	0.6615	25.07	3.26	11.0658	0.6654	132	VIS	1.215
	N/A	N/A	N/A	N/A	25.07	3.26	N/A	N/A	132	Avg	1.8787



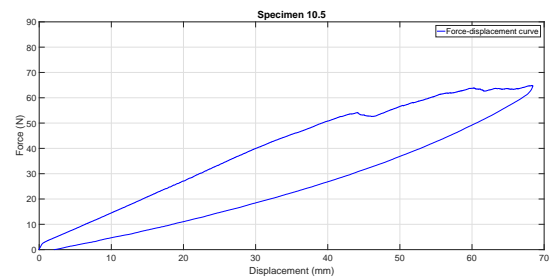
(a) Load-displacement curve specimen 2



(b) Load-displacement curve specimen 3



(c) Load-displacement curve specimen 4



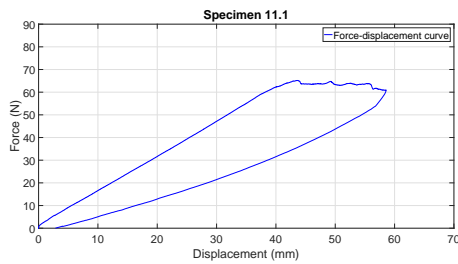
(d) Load-displacement curve specimen 5

Figure C.11: Load-displacement curves of specimens taken from post-consolidated multiple step formed shape

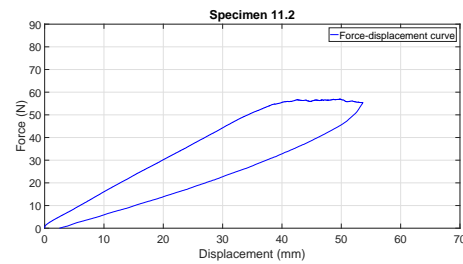
## C.12. Preconsolidated specimens from new material

Table C.12: DCB test results of preconsolidated specimens from new material roll

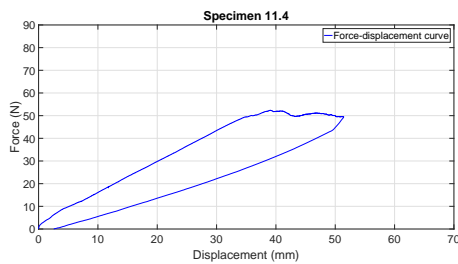
Specimen n°	$a_0$	$\delta$	P	$\delta/a_0$	b	h	t	F	L	$G_{IC}$	MBT
Specimen 1	51	35.82	56.4	0.7024	25.01	3.31	11.0775	0.6232	132	VIS	1.4806
	N/A	N/A	N/A	N/A	25.01	3.31	N/A	N/A	N/A	Avg	2.5469
Specimen 2	51	36.94	53.02	0.7243	25.06	3.30	11.075	0.6067	132	VIS	1.3945
	N/A	N/A	N/A	N/A	25.06	3.30	N/A	N/A	132	Avg	1.8090
Specimen 3	51.5	30.38	43.95	0.5957	25.04	3.28	11.07	0.6996	132	VIS	1.0972
	N/A	N/A	N/A	N/A	25.04	3.28	N/A	N/A	132	Avg	1.9313
Specimen 4	51	32.71	46.22	0.6414	25.05	3.24	11.06	0.6414	132	VIS	1.1857
	N/A	N/A	N/A	N/A	25.05	3.24	N/A	N/A	132	Avg	1.7428
Specimen 5	52	35.94	47.31	0.6912	25.13	3.22	11.055	0.6363	132	VIS	1.2419
	N/A	N/A	N/A	N/A	25.13	3.22	N/A	N/A	132	Avg	2.0232



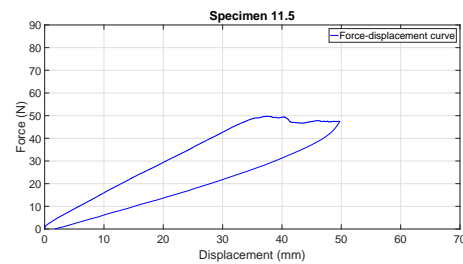
(a) Load-displacement curve specimen 1



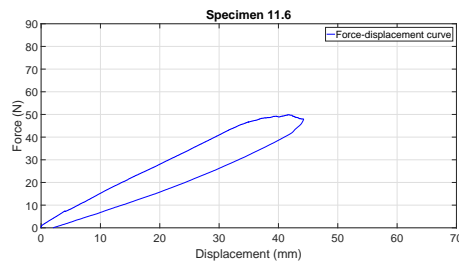
(b) Load-displacement curve specimen 2



(c) Load-displacement curve specimen 3



(d) Load-displacement curve specimen 4



(e) Load-displacement curve specimen 5

Figure C.12: Load-displacement curves of preconsolidated specimens from new material roll



# Bibliography

- [1] Justin Hale. Boeing 787 from the Ground Up. <http://www.boeing.com/commercial/aeromagazine/articles/qtr{ }4{ }06/article{ }04{ }2.html>.
- [2] The A350 XWB: an Xtra revenue generator. <http://www.a350xwb.com/cost-effectiveness/>.
- [3] F. L. Matthews and R. D. Rawlings. Chapter 7 - Polymer matrix composites. In Flake C Campbell Jr, editor, *Manufacturing Technology for Aerospace Structural Materials*. Elsevier, 2011.
- [4] John D Muzzy and Ancil O. Kays. Thermoplastic vs. thermosetting structural composites. *Polymer Composites*, 5(3):169–172, 1984.
- [5] Arnt R. Offringa. Thermoplastic applications composites-rapid processing applications. *Composites : Part A*, 27(A):329–336, 1996.
- [6] Dutch Thermoplastic Composites: Aerospace Structures. <http://www.composites.nl/products/aerospace-structures/>.
- [7] Amir Abbas Zadpoor, Jos Sinke, and Rinze Benedictus. The mechanical behavior of adhesively bonded tailor-made blanks. *International Journal of Adhesion and Adhesives*, 29(5):558–571, 2009.
- [8] Mohammed A. Omar. Chapter 2 - Stamping and Metal Forming Processes. In Mohammed A. OMAR, editor, *The Automotive Body Manufacturing Systems and Processes*, chapter 2, pages 15–105. John Wiley & Sons, 2011. ISBN 9780470976333.
- [9] Patrick J. Mallon and Conchur M. Obradaigh. Chapter 2.26 - Compliant Mold Techniques for Thermoplastic Composites. In *Comprehensive Composite Materials*, chapter 2.26 - Com, pages 873–913. 2000.
- [10] Andrew Craig Long, editor. *Composites Forming Technologies*. Elsevier, 2014. ISBN 9781855736078.
- [11] D. Thomas Campbell and David R Cramer. Hybrid Thermoplastic Composite Ballistic Fabrication Study. *Advancement of Materials & Process Engineering*, 2008.
- [12] L.M.J. Robroek. *The Development of Rubber Forming as a Rapid Thermoforming Technique for Continuous Fibre Reinforced Thermoplastic Composites*. PhD thesis, TU Delft, 1994.
- [13] P. Harrison, M. J. Clifford, and A. C. Long. Shear characterisation of viscous woven textile composites: A comparison between picture frame and bias extension experiments. *Composites Science and Technology*, 64(10-11):1453–1465, 2004.
- [14] R. Akkerman, B. Rietman, S. Haanappel, and U. Sachs. Towards Design for Thermoplastic Composites Manufacturing Using Process Simulation. Technical report, Thermoplastic Composites Research Cente & University of Twente, 2012.
- [15] S. P. Haanappel and R. Akkerman. Shear characterisation of uni-directional fibre reinforced thermoplastic melts by means of torsion. *Composites Part A: Applied Science and Manufacturing*, 56: 8–26, 2014.
- [16] R. Scherer and K. Friedrich. Inter- and intraply-slip flow processes during thermoforming of cf/pp-laminates. *Composites Manufacturing*, 2(2):92–96, 1991.
- [17] S. R. Morris and C. T. Sun. An investigation of interply slip behaviour in AS4/PEEK at forming temperatures. *Composites Manufacturing*, 5(4):217–224, 1994.

- [18] Gilbert Lebrun, Martin N. Bureau, and Johanne Denault. Thermoforming-Stamping of Continuous Glass Fiber/Polypropylene Composites: Interlaminar and Tool-Laminate Shear Properties. *Journal of Thermoplastic Composite Materials*, 17(2):137–165, 2004.
- [19] Adrian M. Murtagh, John J. Lennon, and Patrick J. Mallon. Surface friction effects related to pressforming of continuous fibre thermoplastic composites. *Composites Manufacturing*, 6(3-4):169–175, 1995.
- [20] M. Hou and K. Friedrich. 3-D stamp forming of thermoplastic matrix composites. *Applied Composite Materials*, 1(2):135–153, 1994.
- [21] M. Hou. Stamp forming of continuous glass fibre reinforced polypropylene. *Composites Part A: Applied Science and Manufacturing*, 28(8):695–702, 1997.
- [22] M. Hou. Stamp forming of fabric reinforced thermoplastic composites. *Polymer Composites*, 17(4):596–603, 1996.
- [23] M. Hou, K. Friedrich, and R. Scherer. Optimization of stamp forming of thermoplastic composite bends. *Composite Structures*, 27(1-2):157–167, 1994.
- [24] M. Hou, L. Ye, H. J. Leeb, and Y. W. Maib. Manufacture of a carbon-fabric-reinforced polyetherimide (CF/PEI) composite material. *Composites science and technology*, 58(2):181–190, 1998.
- [25] M. Hou, L. Ye, and Y. W. Mai. Manufacturing Process and Mechanical Properties of Thermoplastic Composite Components. *Journal of Materials Processing Technology*, 63(1):334–338, 1997.
- [26] M. Hou, L. Ye, and Y. W. Mai. Manufacturing of an aileron rib with advanced thermoplastic composites. *Journal of Thermoplastic Composite Materials*, 10(2):185–195, 1997.
- [27] Valeria Antonelli. *Improvements of thermoforming of thermoplastic composites using a collection of rubber particles as a soft mould half*. Phd thesis, TU Delft, 2014.
- [28] Conchur O’Bradaigh, Byron Pipes, and Patrick Mallon. Issues in Diaphragm Forming of Continuous Fiber Reinforced Thermoplastic Composites. *Polymer Composites*, 12(4), 1991.
- [29] P.J. Mallon, C.M. O’Brádaigh, and R.B. Pipes. Polymeric diaphragm forming of complex-curvature thermoplastic composite parts. *Composites*, 20(1):48–56, 1989.
- [30] A Keane and J Mallon. Investigation of the effects of varying the processing parameters in diaphragm forming of advanced thermoplastic composite laminates. *Composites Manufacturing*, 6(3):145–152, 1995.
- [31] P. de Luca, P. Lefébure, and A.K. Pickett. Numerical and experimental investigation of some press forming parameters of two fibre reinforced thermoplastics: APC2-AS4 and PEI-CETEX. *Composites Part A: Applied Science and Manufacturing*, 29(1-2):101–110, 1998.
- [32] S P Haanappel, R. Ten Thije, and R Akkerman. Forming Predictions of UD Reinforced Thermoplastic Laminates. *14th European Conference on Composite Materials*, pages 1–10, 2010.
- [33] Sebastiaan P. Haanappel, Ulrich Sachs, Rene H.W. ten Thije, Bert Rietman, and Remko Akkerman. Forming of Thermoplastic Composites. *Key Engineering Materials*, 504-506:237–242, 2012.
- [34] Sebastiaan Haanappel. *Forming of UD fibre reinforced thermoplastics*. Phd thesis, University of Twente, 2013.
- [35] S. P. Haanappel, R. H. W. Ten Thije, U. Sachs, B. Rietman, and R. Akkerman. Formability analyses of uni-directional and textile reinforced thermoplastics. *Composites Part A: Applied Science and Manufacturing*, 56:80–92, 2014.
- [36] N. Zahlan and J. M. O’Neill. Design and fabrication of composite components; the spring-forward phenomenon. *Composites*, 20(1):77–81, 1989.

- [37] Lalit K. Jain, Meng Hou, Lin Ye, and Yiu-Wing Mai. Spring-in study of the aileron rib manufactured from advanced thermoplastic composite. *Composites Part A: Applied Science and Manufacturing*, 29(8):973–979, 1998.
- [38] A. Salomi, T. Garstka, K. Potter, A. Greco, and A. Maffezzoli. Spring-in angle as molding distortion for thermoplastic matrix composite. *Composites Science and Technology*, 68(14):3047–3054, 2008.
- [39] P. Han, J. Butterfield, S. Buchanan, R. McCool, Z. Jiang, M. Price, and A. Murphy. The prediction of process-induced deformation in a thermoplastic composite in support of manufacturing simulation. *Proceedings of the Institution of Mechanical Engineers, Part B: Journal of Engineering Manufacture*, 227(10):1417–1429, 2013.
- [40] C. Brauner, C. Peters, F. Brandwein, and A. S. Herrmann. Analysis of process-induced deformations in thermoplastic composite materials. *Journal of Composite Materials*, 48(22):2779–2791, 2014.
- [41] L. K. Jain and Yiu-Wing Mai. Stresses and deformations induced during manufacturing. Part I theoretical analysis of composite cylinders and shells. *Journal of Composite Materials*, 31(7):672–695, 1997.
- [42] L. K. Jain, B. G. Lutton, Yiu-Wing Mai, and R. Paton. Stresses and deformations induced during manufacturing. Part II a study of the spring-in phenomenon. *Journal of Composite Materials*, 31(7):696–719, 1997.
- [43] D. W. Radford and T. S. Rennick. Separating sources of manufacturing distortion in laminated composites. *Journal of Composite Materials*, 19(8):621–641, 2000.
- [44] C.M. O’Brádaigh and P.J. Mallon. Effect of forming temperature on the properties of polymeric diaphragm formed thermoplastic composites. *Composites Science and Technology*, 35(3):235–255, 1989.
- [45] Jan-anders E Manson, Terry L Schneider, and James C Seferis. Press-Forming of Continuous-Fiber-Reinforced Thermoplastic Composites. *Polymer composites*, 11(2):114–120, 1990.
- [46] P.-Y.B. Jar, R. Mulone, P. Davies, and H.-H. Kausch. A study of the effect of forming temperature on the mechanical behaviour of carbon-fibre/peek composites. *Composites Science and Technology*, 46(1):7–19, 1993.
- [47] Lin Ye and Andrew Beehag. Role of cooling pressure on interlaminar fracture properties of comingled CF/PEEK composites. *Composites Part A: Applied Science and Manufacturing*, 27(3):175–182, 1996.
- [48] M D Wakeman and P Blanchard. Void Evolution During Stamp-Forming of Thermoplastic Composites. In *15th International Conference on Composite Materials (ICCM-15)*, 2005.
- [49] K. Friedrich and M. Hou. On stamp forming of curved and flexible geometry components from continuous glass fiber/polypropylene composites. *Composites Part A: Applied Science and Manufacturing*, 29(3):217–226, 1998.
- [50] P. Harrison, R. Gomes, and N. Curado-Correia. Press forming a 0/90 cross-ply advanced thermoplastic composite using the double-dome benchmark geometry. *Composites Part A: Applied Science and Manufacturing*, 54:56–69, 2013.
- [51] W. I. Lee, M. F. Talbott, G. S. Springer, and L. A. Berglund. Effects of Cooling Rate on the Crystallinity and Mechanical Properties of Thermoplastic Composites. *Journal of Reinforced Plastics and Composites*, 6(1):2–12, 1987.
- [52] M. F. Talbott, G. S. Springer, and L. A. Berglund. The Effects of Crystallinity on the Mechanical Properties of PEEK Polymer and Graphite Fiber Reinforced PEEK. *Journal of Composite Materials*, 21(11):1056–1081, 1987.

- [53] Hugues Lessard, Gilbert Lebrun, Abdelhaq Benkaddour, and Xuan Tan Pham. Influence of process parameters on the thermostamping of a [0/90]<sub>12</sub> carbon/polyether ether ketone laminate. *Composites Part A: Applied Science and Manufacturing*, 70, 2015.
- [54] P. O. Hagstrand, F. Bonjour, and J. A E Manson. The influence of void content on the structural flexural performance of unidirectional glass fibre reinforced polypropylene composites. *Composites Part A: Applied Science and Manufacturing*, 36(5):705–714, 2005.
- [55] R. McCool, A. Murphy, R. Wilson, Z. Jiang, M. Price, J. Butterfield, and P. Hornsby. Thermoforming carbon fibre-reinforced thermoplastic composites. *Proceedings of the Institution of Mechanical Engineers, Part L: Journal of Materials: Design and Applications*, 226(2):91–102, 2012.
- [56] A. Dutta, M. Niemeyer, and M. Cakmak. Thermoforming of Advanced Thermoplastic Composites I: Single Curvature Parts. *Polymer Composites*, 12(4):257–272, 1991.
- [57] C Ageorges, L Ye, and M Hou. Advances in fusion bonding techniques for joining thermoplastics materials composites: a review. 32(2001), 2006.
- [58] Woo Il Lee and George S. Springer. A Model of the Manufacturing Process of Thermoplastic Matrix Composites. *Journal of Composite Materials*, 21(11):1017–1055, 1987. doi: 10.1177/002199838702101103.
- [59] Young Hwa Kim and Richard P. Wool. A theory of healing at a polymer-polymer interface. *Macromolecules*, 16(7):1115–1120, 1983.
- [60] Christos Kassapoglou. *Modeling the Effect of Damage in Composite Structures*. Wiley, 1 edition, 2015. ISBN 9781119013211.
- [61] ASTM. Standard Test Method for Short-Beam Strength of Polymer Matrix Composite Materials. pages 1–8, .
- [62] EN ISO. Fibre-reinforced plastic composites — Determination of apparent interlaminar shear strength by short-beam method.
- [63] ASTM. D5528-01 2001. Standard Test Method for Mode I Interlaminar Fracture Toughness of Unidirectional Fiber-Reinforced Polymer Matrix Composites. .
- [64] R. Akkerman, P. E. Reed, K. Y. Huang, and L. Warnet. Comparison of fracture toughness (GIC) values of polyetherimide (PEI) and a carbon-fibre/PEI composite: an experimental and theoretical study. *European Structural Integrity Society*, 27(C):3–14, 2000. doi: 10.1016/S1566-1369(00)80003-5.
- [65] J. W. Gillespie, L. A. Carlsson, and A. J. Smiley. Rate-dependent mode I interlaminar crack growth mechanisms in graphite/epoxy and graphite/PEEK. *Composites Science and Technology*, 28(1):1–15, 1987. doi: 10.1016/0266-3538(87)90058-3.
- [66] Ki-young Kim, L I N Ye, and Kim-meng Phoa. Interlaminar Fracture Toughness of CF / PEI and GF / PEI Composites at Elevated Temperatures. *Applied Composite Materials*, 11:173–190, 2004.
- [67] J.W. He, M Y; Hutchinson. Interlaminar fracture toughness and toughening of laminated composite materials : a review. *Journal of Applied Mechanics*, 111(5):270–78, 1989. doi: 10.1016/0010-4361(89)90211-5.
- [68] R. Selzer and K. Friedrich. Mechanical properties and failure behaviour of carbon fibre-reinforced polymer composites under the influence of moisture. *Composites Part A: Applied Science and Manufacturing*, 28(6):595–604, 1997. doi: 10.1016/S1359-835X(96)00154-6.
- [69] Y. J. Prel, P. Davies, M. L. Benzeggagh, and F.-X. Charentenay. Mode I and Mode II Delamination of Thermosetting and Thermoplastic Composites. *Composite materials: Fatigue and Fracture*, 2:251–269, 1989. doi: 10.1520/STP10419S.
- [70] W S Johnson and P D Mangalgi. Influence of the Resin on Interlaminar Mixed-Mode Fracture. pages 295–315, 1987.

- [71] B. Vieille, W. Albouy, L. Chevalier, and L. Taleb. About the influence of stamping on thermoplastic-based composites for aeronautical applications. *Composites Part B: Engineering*, 45 (1):821–834, 2013.
- [72] W. J B Groupe, L. L. Warnet, B. Rietman, H. A. Visser, and R. Akkerman. Optimization of the tape placement process parameters for carbon-PPS composites. *Composites Part A: Applied Science and Manufacturing*, 50, 2013. doi: 10.1016/j.compositesa.2013.03.003.
- [73] R.B. Pipes A.J. Smiley. Rate Effects on Mode I Interlaminar Fracture Toughness in Composite Materials. *Journal of Composite Materials*, 21(7):670–687, 1987. doi: 10.1177/002199838702100706.
- [74] William Y. Fowlkes and Clyde M. Creveling. *Engineering Methods for Robust Product Design - Using Taguchi Methods in Technology and Product Development*. Engineering Process Improvement Series, 1 edition, 1995. ISBN 0-201-63367-1.